11 Spatial and Temporal Features of Multisensory Processes: Bridging between Animal and Human Studies

Diana K. Sarko, Aaron R. Nidiffer, Albert R. Powers III, Dipanwita Ghose, Andrea Hillock-Dunn, Matthew C. Fister, Juliane Krueger, and Mark T. Wallace

CONTENTS

11.1 Introduction 190
11.2 Neurophysiological Studies in Animal Models: Integrative Principles as a Foundation for Understanding Multisensory Interactions 190
11.3 Neurophysiological Studies in Animal Models: New Insights into Interdependence of Integrative Principles 191
11.3.1 Spatial Receptive Field Heterogeneity and Its Implications for Multisensory Interactions 191
11.3.2 Spatiotemporal Dynamics of Multisensory Processing 195
11.4 Studying Multisensory Integration in an Awake and Behaving Setting: New Insights into Utility of Multisensory Processes 197
11.5 Human Behavioral and Perceptual Studies of Multisensory Processing: Building Bridges between Neurophysiological and Behavioral and Perceptual Levels of Analysis 199
11.5.1 Defining the "Temporal Window" of Multisensory Integration 199
11.5.2 Stimulus-Dependent Effects on the Size of the Multisensory Temporal Window 200
11.5.3 Can "Higher-Order" Processes Affect Multisensory Temporal Window? 201
11.6 Adult Plasticity in Multisensory Temporal Processes: Psychophysical and Neuroimaging Evidence 201
11.7 Developmental Plasticity in Multisensory Representations: Insights from Animal and Human Studies 203
11.7.1 Neurophysiological Studies into Development of Multisensory Circuits 203
11.7.2 Development of Integrative Principles 205
11.7.3 Experientially based Plasticity in Multisensory Circuits 205
11.7.4 Development of Human Multisensory Temporal Perception 206
11.8 Conclusions and Future Directions 208
References 208

11.1 INTRODUCTION

Multisensory processing is a pervasive and critical aspect of our behavioral and perceptual repertoires, facilitating and enriching a wealth of processes including target identification, signal detection, speech comprehension, spatial navigation, and flavor perception to name but a few. The adaptive advantages that multisensory integration confers are critical to survival, with effective acquisition and use of multisensory information enabling the generation of appropriate behavioral responses under circumstances in which one sense is inadequate. In the behavioral domain, a number of studies have illustrated the strong benefits conferred under multisensory circumstances, with the most salient examples including enhanced orientation discrimination (Stein et al. 1988, 1989), improved target detection (Frassinetti et al. 2002; Lovelace et al. 2003), and speeded responses (Hershenson 1962; Hughes et al. 1994; Frens et al. 1995; Harrington and Peck 1998; Corneil et al. 2002; Forster et al. 2002; Molholm et al. 2002; Amlot et al. 2003; Diederich et al. 2003; Calvert and Thesen 2004).

Along with these behavioral examples, there are myriad perceptual illustrations of the power of multisensory interactions. For example, the intensity of a light is perceived as greater when presented with a sound (Stein et al. 1996) and judgments of stimulus features such as speed and orientation are often more accurate when combined with information available from another sense (Soto-Faraco et al. 2003; Manabe and Riquimaroux 2000; Clark and Graybiel 1966; Wade and Day 1968). One of the most compelling examples of multisensory-mediated perceptual gains can be seen in the speech realm, where the intelligibility of a spoken signal can be greatly enhanced when the listener can see the speaker's face (Sumby and Pollack 1954). In fact, this bimodal gain may be a principal factor in the improvements in speech comprehension seen in those with significant hearing loss after visual training (Schorr et al. 2005; Rouger et al. 2007). Regardless of whether the benefits are seen in the behavioral or perceptual domains, they typically exceed those that are predicted on the basis of responses to each of the component unisensory stimuli (Hughes et al. 1994, 1998; Corneil and Munoz 1996; Harrington and Peck 1998). Such deviations from simple additive models provide important insights into the neural bases for these multisensory interactions in that they strongly argue for a convergence and active integration of the different sensory inputs within the brain.

11.2 NEUROPHYSIOLOGICAL STUDIES IN ANIMAL MODELS: INTEGRATIVE PRINCIPLES AS A FOUNDATION FOR UNDERSTANDING MULTISENSORY INTERACTIONS

Information from multiple sensory modalities converges at many sites within the central nervous system, providing the necessary anatomical framework for multisensory interactions (Calvert and Thesen 2004; Stein and Meredith 1993). Multisensory convergence at the level of the single neuron commonly results in an integrated output such that the multisensory response is typically distinct from the component responses, and often from their predicted addition as well. Seminal studies of multisensory processing initially focused on a midbrain structure, the superior colliculus (SC), because of its high incidence of multisensory neurons, its known spatiotopic organization, and its well-defined role in controlling orientation movements of the eyes, pinnae, and head (Sparks 1986; Stein and Meredith 1993; Sparks and Groh 1995; Hall and Moschovakis 2004; King 2004).

These foundational studies of the SC of cats (later reaffirmed by work in nonhuman primate models, see Wallace and Stein 1996, 2001; Wallace et al. 1996) provided an essential understanding of the organization of multisensory neurons and the manner in which they integrate their different sensory inputs. In addition to characterizing the striking nonlinearities that frequently define the responses of these neurons under conditions of multisensory stimulation, these studies established a series of fundamental principles that identified key stimulus features that govern multisensory interactions (Meredith and Stein 1983, 1985, 1986; Meredith et al. 1987). The *spatial principle* deals

with the physical location of the paired stimuli, and illustrates the importance of spatial proximity in driving the largest proportionate gains in response. Similarly, the *temporal principle* captures the fact that the largest gains are typically seen when stimuli are presented close together in time, and that the magnitude of the interaction declines as the stimuli become increasingly separated in time. Finally, the *principle of inverse effectiveness* reflects the fact that the largest gains are generally seen to the pairing of two weakly effective stimuli. As individual stimuli become increasingly effective in driving neuronal responses, the size of the interactions seen to the pairing declines. Together, these principles have provided an essential predictive outline for understanding multisensory integration at the neuronal level, as well as for understanding the behavioral and perceptual consequences of multisensory pairings. However, it is important to point out that these principles, although widely instructive, fail to capture the complete integrative profile of any individual neuron. The reason for this is that space, time, and effectiveness are intimately intertwined in naturalistic stimuli, and manipulating one has a consequent effect on the others. Recent studies, described in the next section, have sought to better understand the strong interdependence between these factors, with the hope of better elucidating the complex spatiotemporal architecture of multisensory interactions.

Please verify if the changes made here are OK.

11.3 NEUROPHYSIOLOGICAL STUDIES IN ANIMAL MODELS: NEW INSIGHTS INTO INTERDEPENDENCE OF INTEGRATIVE PRINCIPLES

11.3.1 Spatial Receptive Field Heterogeneity and Its Implications for Multisensory Interactions

Early observations during the establishment of the neural principles of multisensory integration hinted at a complexity not captured by integrative "rules" or constructs. For example, in structuring experiments to test the spatial principle, it was clear that stimulus location not only played a key role in the magnitude of the multisensory interaction, but also that the individual sensory responses were strongly modulated by stimulus location. Such an observation suggested an interaction between the spatial and inverse effectiveness principles, and one that might possibly be mediated by differences in unisensory responses as a function of location within the neuron's receptive field. Recently, this concept has been tested by experiments specifically designed to characterize the microarchitecture of multisensory receptive fields.

In these experiments, stimuli from each of the effective modalities were presented at a series of locations within and outside the classically defined excitatory receptive field of individual multisensory neurons (Figure 11.1). Studies were conducted in both subcortical (i.e., SC) and cortical [i.e., the anterior ectosylvian sulcus (AES)] multisensory domains in the cat, in which prior work had illustrated that the receptive fields of multisensory neurons are quite large (Stein and Meredith 1993; Benedek et al. 2004; Furukawa and Middlebrooks 2002; Middlebrooks and Knudsen 1984; Middlebrooks et al. 1998; Xu et al. 1999; Wallace and Stein 1996, 1997; Nagy et al. 2003). In this manner, spatial receptive field (SRFs) can be created for each of the effective modalities, as well as for the multisensory combination. It is important to point out that in these studies, the stimuli are identical (e.g., same luminance, loudness, and spectral composition) except for their location. The results of these analyses have revealed a marked degree of heterogeneity to the SRFs of both SC and AES multisensory neurons (Carriere et al. 2008; Royal et al. 2009). This response heterogeneity is typically characterized by regions of high response (i.e., hot spots) surrounded by regions of substantially weaker response. Studies are ongoing to determine whether features such as the number or size of these hot spots differ between subcortical and cortical areas.

Although these SRF analyses have revealed a previously uncharacterized feature of multisensory neurons, perhaps the more important consequence of this SRF heterogeneity is the implication that this has for multisensory interactions. At least three competing hypotheses can be envisioned for the role of receptive field heterogeneity in multisensory integration—each with strikingly different

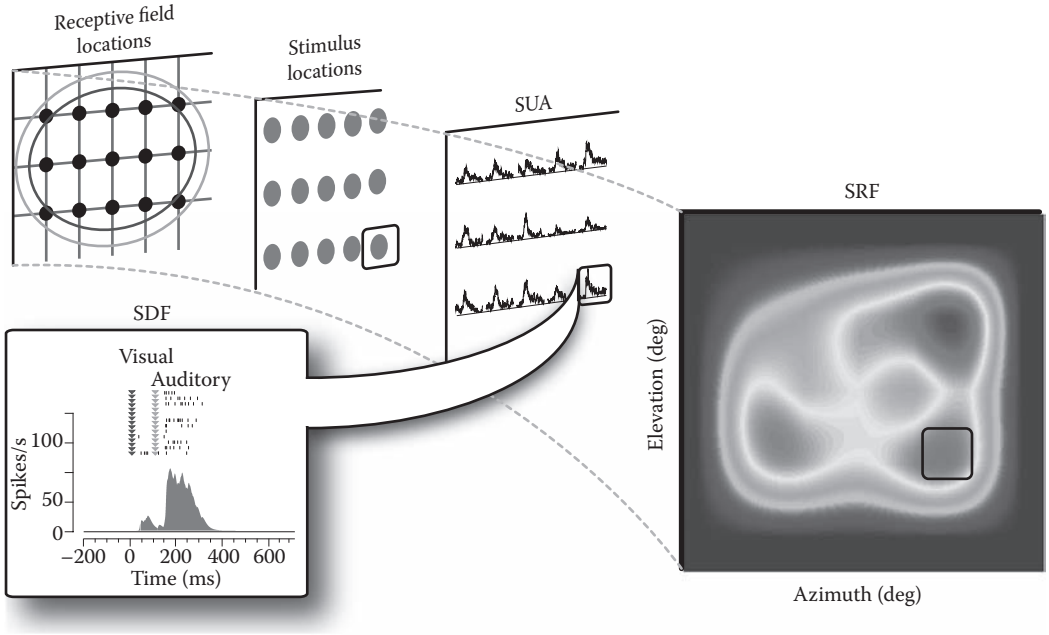

FIGURE 11.1 Construction of an SRF for an individual multisensory neuron. Each stimulus location (green dots) tested within receptive field (red and blue circles) generates a response that is then compiled into a single unit activity (SUA) plot. SUA plot at one location is shown in detail to illustrate how spike density function (SDF) is derived. Finally, SDF/SUA data are transformed into a pseudocolor SRF plot in which normalized evoked response is shown relative to azimuth and elevation. Evoked responses are scaled to maximal response, with warmer colors representing higher firing rates. (Adapted from Carriere et al., *J. Neurophysiol.,* 99, 2357–2368, 2008.)

Color notations (green dots; red and blue circles) were found in figure caption. Note that art is in gray scale. Please revise caption accordingly

predictions. The first is that spatial location takes precedence and that the resultant interactions would be completely a function of the spatial disparity between the paired stimuli. In this scenario, the largest interactions would be seen when the stimuli were presented at the same location, and the magnitude of the interaction would decline as spatial disparity increased. Although this would seem to be a strict interpretation of the spatial principle, in fact, even the early characterization of this principle focused not on location or disparity, but rather on the presence or absence of stimuli within the receptive field (Meredith and Stein 1986), hinting at the relative lack of importance of absolute location. The second hypothesis is that stimulus effectiveness would be the dominant factor, and that the interaction would be dictated not by spatial location but rather by the magnitude of the individual sensory response (which would be modulated by changes in spatial location). The final hypothesis is that there is an interaction between stimulus location and effectiveness, such that both would play a role in shaping the resultant interaction. If this were the case, studies would seek to identify the relative weighting of these two stimulus dimensions to gain a better mechanistic view into these interactions.

The first foray into this question focused on cortical area AES (Carriere et al. 2008). Here, it was found that SRF architecture played an essential deterministic role in the observed multisensory interactions, and most intriguingly, in a manner consistent with the second hypothesis outlined above. Thus, and as illustrated in Figure 11.2, SRF architecture resulted in changes in stimulus

a-d panels were not labeled in the illustration; please check if the caption corresponds with the artwork provided.

FIGURE 11.2 **(See color insert.)** Multisensory interactions in AES neurons differ based on location of paired stimuli. (a) Visual, auditory, and multisensory SRFs are shown with highlighted locations (b, d) illustrating response suppression (left column), response enhancement (middle column), and no significant interaction (right column). (c) Shaded areas depict classically defined receptive fields for visual (blue) and auditory (green) stimuli.

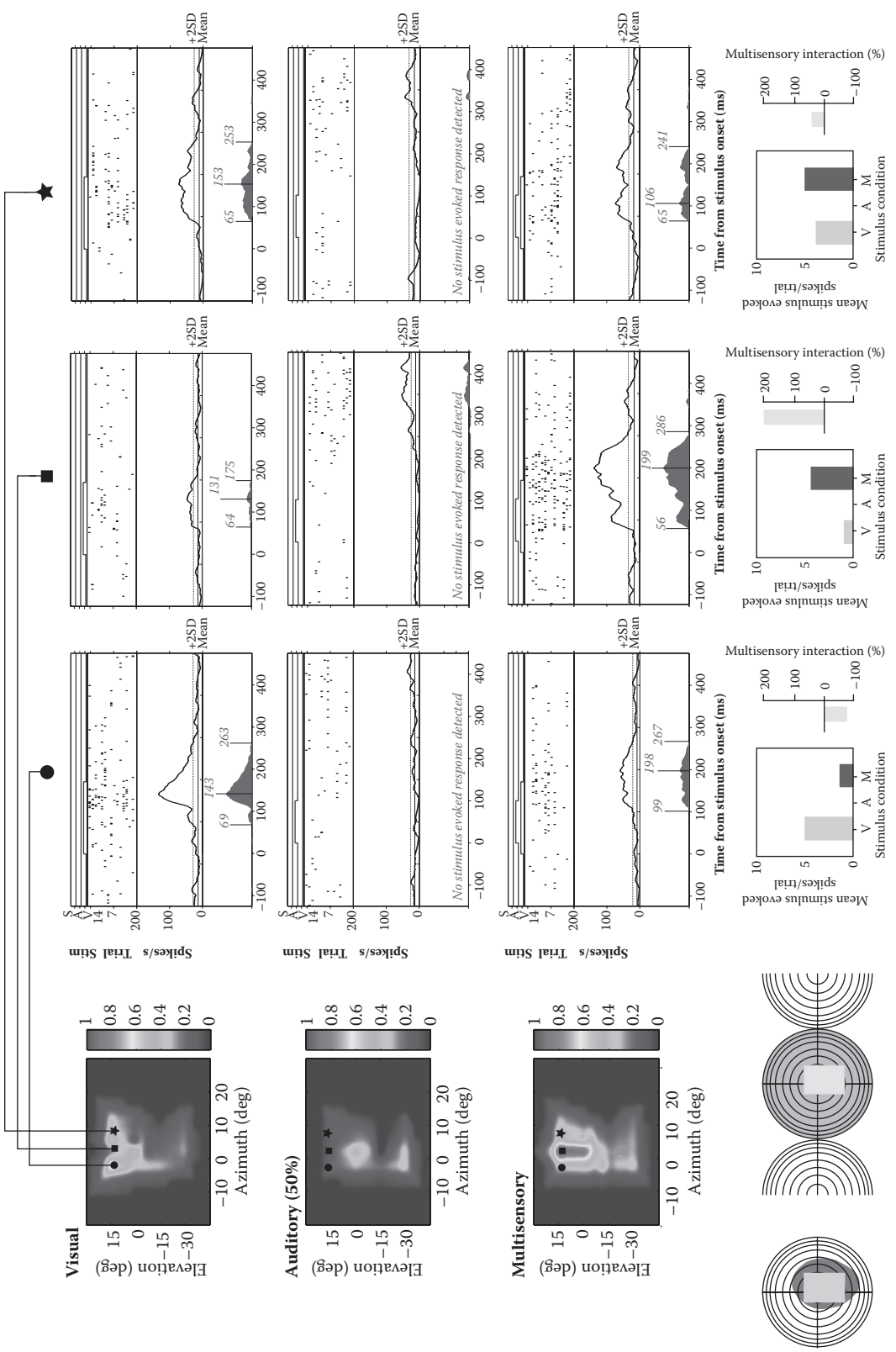
Visual
Auditory (50%)
Multisensory
Elevation (deg)
Azimuth (deg)
Spikes/s Trial Stim
+2SD Mean
Time from stimulus onset (ms)
No stimulus evoked response detected
Multisensory interaction (%)
Mean stimulus evoked spikes/trial
Stimulus condition
V A M

effectiveness that formed the basis for the multisensory interaction. In the neuron shown, if the stimuli were presented in a region of strong response within the SRF, a response depression would result (Figure 11.2b, left column). In contrast, if the stimuli were moved to a location of weak response, their pairing resulted in a large enhancement (Figure 11.2b, center column). Intermediate regions of response resulted in either weak or no interactions (Figure 11.2b, right column). In addition to this traditional measure of multisensory gain (relative to the best unisensory response), these same interactions can also be examined and quantified relative to the predicted summation of the unisensory responses (Wallace et al. 1992; Wallace and Stein 1996; Stein and Wallace 1996; Stanford et al. 2005; Royal et al. 2009; Carriere et al. 2008). In these comparisons, strongly effective pairings typically result in subadditive interactions, weakly effective pairings result in superadditive interactions, and intermediate pairings result in additive interactions. Visualization of these different categories of interactions relative to additive models can be captured in pseudocolor representations such as that shown in Figure 11.3, in which the actual multisensory SRF is contrasted against that predicted on the basis of additive modeling. Together, these results clearly illustrate the primacy of stimulus efficacy in dictating multisensory interactions, and that the role of space per se appears to be a relatively minor factor in governing these integrative processes.

Parallel studies are now beginning to focus on the SC, and provide an excellent comparative framework from which to view multisensory interactive mechanisms across brain structures. In this work, Krueger et al. (2009) reported that the SRF architecture of multisensory neurons in the SC is not only similar to that of cortical neurons, but also that stimulus effectiveness appears to once again be the key factor in dictating the multisensory response. Thus, stimulus pairings within regions of weak unisensory response often resulted in superadditive interactions (Figure 11.4b–c, square), whereas pairings at locations of strong unisensory responses typically exhibited subadditive interactions (Figure 11.4b–c, circle). Overall, such an organization presumably boosts signals within weakly effective regions of the unisensory SRFs during multisensory stimulus presentations and yields more reliable activation for each stimulus presentation.

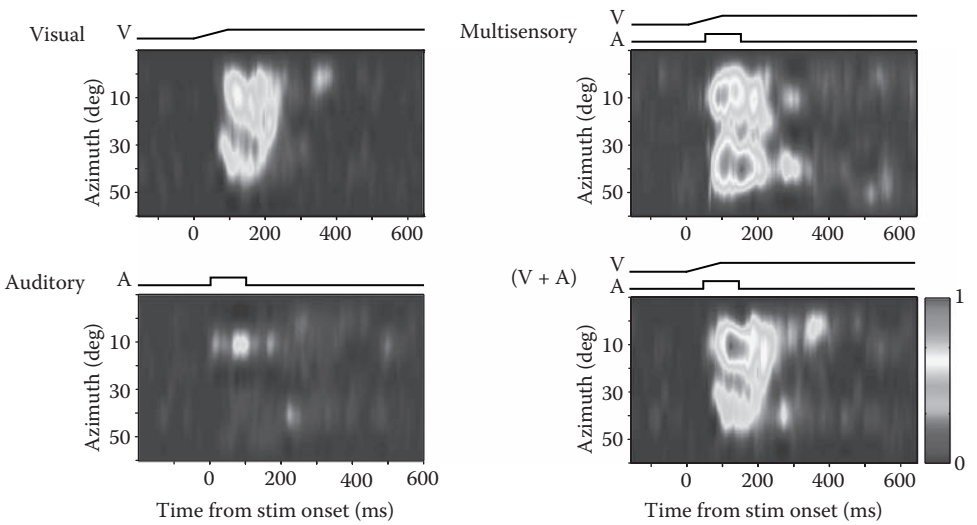

FIGURE 11.3 Multisensory interactions relative to additive prediction models. Visual, auditory, and multisensory (VA) SRFs are shown for an individual multisensory neuron of AES. True multisensory responses can be contrasted with those predicted by an additive model (V + A) and reveal a richer integrative microarchitecture than predicted by simple linear summation of unisensory response profiles. (Adapted from Carriere et al., Spatial heterogeneity of cortical receptive fields and its impact on multisensory interactions., *J. Neurophysiol.,* 99, 2357–2368, 2008.)

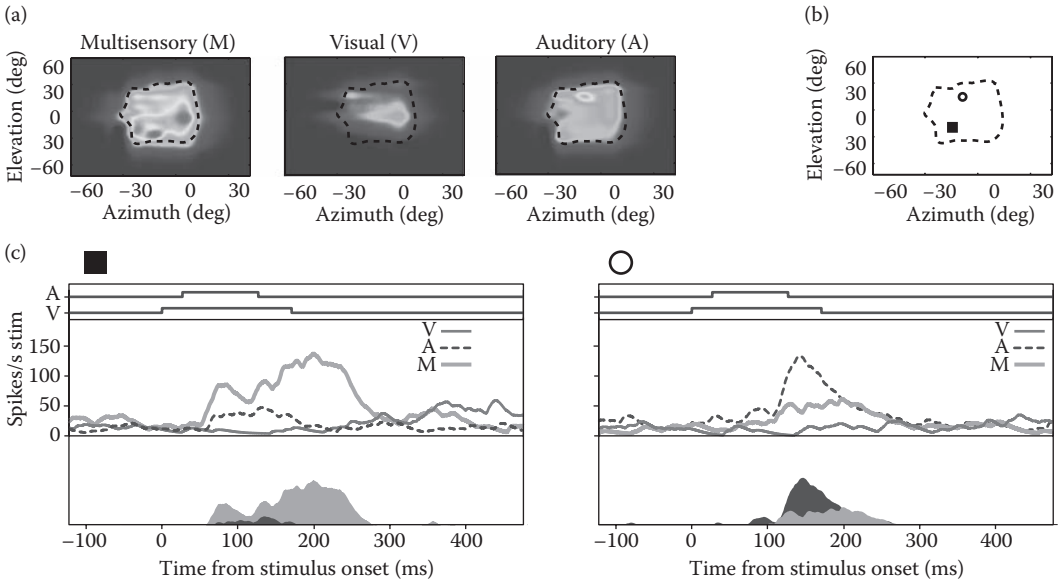

FIGURE 11.4 Multisensory interactions in SC neurons differ based on location of paired stimuli. (a) Visual, auditory, and multisensory SRFs are shown as a function of azimuth (*x* axis) and elevation (*y* axis). Specific locations within receptive field (b) are illustrated in detail (c) to show evoked responses for visual, auditory, and multisensory conditions. Weakly effective locations (square) result in response enhancement, whereas conditions evoking a strong unisensory response (circle) result in response suppression.

Although SRF architecture appears similar in both cortical and subcortical multisensory brain regions, there are also subtle differences that may provide important insights into both the underlying mechanistic operations and the different behavioral and perceptual roles of AES and SC. For example, when the SRFs of a multisensory neuron in the SC are compared under different sensory conditions, there appears to be a global similarity in the structure of each SRF with respect to both the number and location of hot spots. This might indicate that the overall structure of the SRF is dependent on fixed anatomical and/or biophysical constraints such as the extent of dendritic arbors. However, these characteristics are far less pronounced in cortical SRFs (Carriere et al. 2008), possibly due to the respective differences in the inputs to these two structures (the cortex receiving more heterogeneous inputs) and/or due to less spatiotopic order in the cortex. Future work will seek to better clarify these intriguing differences across structures.

11.3.2 Spatiotemporal Dynamics of Multisensory Processing

In addition to the clear interactions between space and effectiveness captured by the aforementioned SRF analyses, an additional stimulus dimension that needs to be included is time. For example, and returning to the initial outlining of the interactive principles, changing stimulus location impacts not only stimulus effectiveness, but also the temporal dynamics of each of the unisensory (and multisensory) responses. Thus, dependent on the location of the individual stimuli, responses will have very different temporal patterns of activation.

More recently, the importance of changes in temporal response profiles has been highlighted by findings that the multisensory responses of SC neurons show shortened latencies when compared with the component unisensory responses (Rowland et al. 2007), a result likely underlying the behavioral finding of the speeding of saccadic eye movements under multisensory conditions (Frens and Van Opstal 1998; Frens et al. 1995; Hughes et al. 1998; Amlot et al. 2003; Bell et al. 2005).

Additional work focused on the temporal dimension of multisensory responses has extended the original characterization of the temporal principle to nonhuman primate cortex, where Kayser and colleagues (2008) have found that audiovisual interactions in the superior temporal plane of rhesus monkey neocortex are maximal when a visual stimulus precedes an auditory stimulus by 20 to 80 ms. Along with these unitary changes, recent work had also shown that the timing of sensory inputs with respect to ongoing neural oscillations in the neocortex has a significant impact on whether neuronal responses are enhanced or suppressed. For instance, in macaque primary auditory cortex, properly timed somatosensory input has been found to reset ongoing oscillations to an optimal excitability phase that enhances the response to temporally correlated auditory input. In contrast, somatosensory input delivered during suboptimal, low-excitability oscillatory periods depresses the auditory response (Lakatos et al. 2007).

Although clearly illustrating the importance of stimulus timing in shaping multisensory interactions, these prior studies have yet to characterize the interactions between time, space, and effectiveness in the generation of a multisensory response. To do this, recent studies from our laboratory have extended the SRF analyses described above to include time, resulting in the creation of spatiotemporal receptive field (STRF) plots. It is important to point out that such analyses are not a unique construct to multisensory systems, but rather stem from both spatiotemporal and spectrotemporal receptive field studies within individual sensory systems (David et al. 2004; Machens et al. 2004; Haider et al. 2010; Ye et al. 2010). Rather, the power of the STRF here is its application

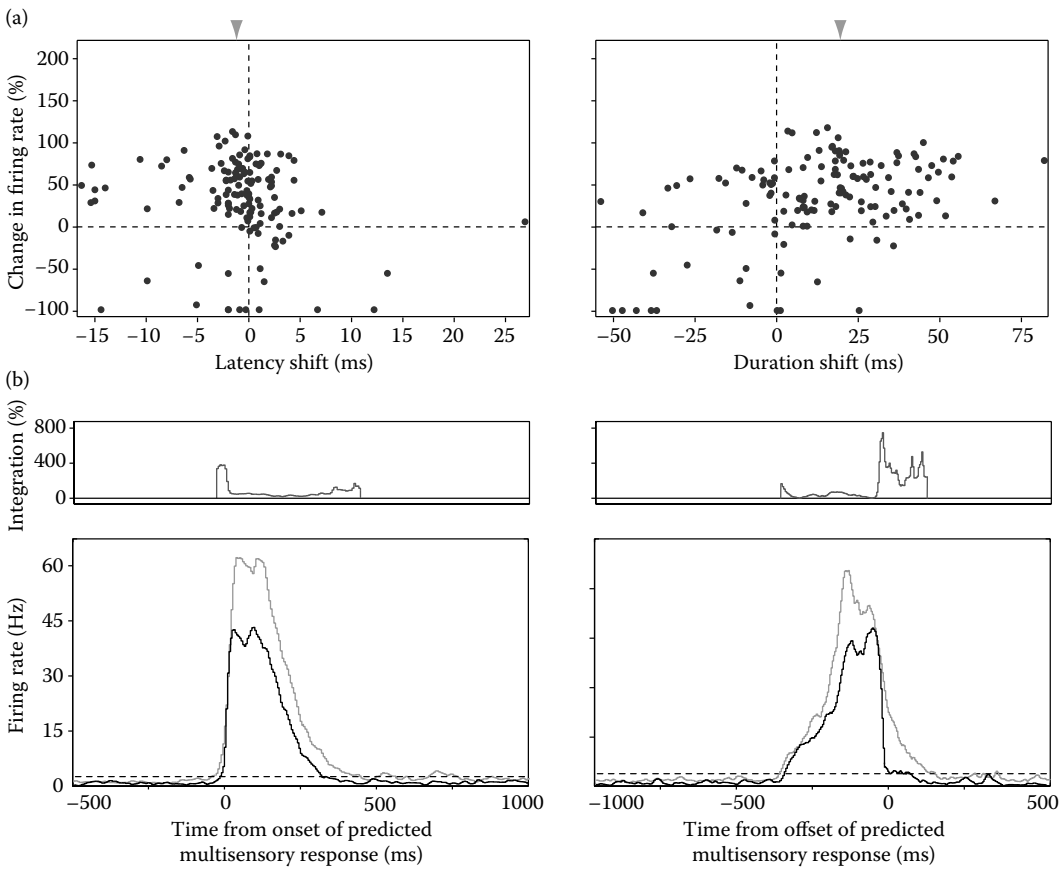

FIGURE 11.5 Spatiotemporal response dynamics in multisensory AES neurons. A reduced response latency (a) and increased response duration (b) characterized spatiotemporal dynamics of paired multisensory stimuli.

to multisensory systems as a modeling framework from which important mechanistic insights can be gained about the integrative process.

The creation of STRFs for cortical multisensory neurons has revealed interesting features about the temporal dynamics of multisensory interactions and the evolution of the multisensory response (Royal et al. 2009). Most importantly, these analyses, when contrasted with simple additive models based on the temporal architecture of the unisensory responses, identified two critical epochs in the multisensory response not readily captured by additive processes (Figure 11.5). The first of these, presaged by the Rowland et al. study described above, revealed an early phase of superadditive multisensory responses that manifest as a speeding of response (i.e., reduced latency) under multisensory conditions. The second of these happens late in the response epoch, where the multisensory response continues beyond the truncation of the unisensory responses, effectively increasing response duration under multisensory circumstances. It has been postulated that these two distinct epochs of multisensory integration may ultimately be linked to very different behavioral and/or perceptual roles (Royal et al. 2009). Whereas reduced latencies may speed target detection and identification, extended response duration may facilitate perceptual analysis of the object or area of interest. One interesting hypothesis is that the early speeding of responses will be more prominent in SC multisensory neurons given their important role in saccadic (and head) movements, and that the extended duration will be seen more in cortical networks engaged in perceptual analyses. Future work, now in progress in our laboratory (see below), will seek to clarify the behavioral/perceptual roles of these integrative processes by directly examining the links at the neurophysiological and behavioral levels.

11.4 STUDYING MULTISENSORY INTEGRATION IN AN AWAKE AND BEHAVING SETTING: NEW INSIGHTS INTO UTILITY OF MULTISENSORY PROCESSES

As research on the neural substrates of multisensory integration progresses, and as the behavioral and perceptual consequences of multisensory combinations become increasingly apparent, contemporary neuroscience is faced with the challenge of bridging between the level of the single neuron and whole animal behavior and perception. To date, much of the characterization of multisensory integration at the cellular level has been conducted in anesthetized animals, which offer a variety of practical advantages. However, given that anesthesia could have substantial effects on neural encoding, limiting the interpretation of results within the broader construct of perceptual abilities (Populin 2005; Wang et al. 2005; Ter-Mikaelian et al. 2007), the field must now turn toward awake preparations in which direct correlations can be drawn between neurons and behavior/perception.

Currently, in our laboratory, we are using operant conditioning methods to train animals to fixate on a single location while audiovisual stimuli are presented in order to study SRF architecture in this setting (and compare these SRFs with those generated in anesthetized animals). In addition to providing a more naturalistic view into receptive field organization, these studies can then be extended in order to begin to address the relationships between the neural and behavioral levels. One example of this is the use of a delayed saccade task, which has been used in prior work to parse sensory from motor responses in the SC (where many neurons have both sensory and motor activity; Munoz et al. 1991a, 1991b; Munoz and Guitton 1991; Guitton and Munoz 1991). In this task, an animal is operantly conditioned to fixate on a simple visual stimulus (a light-emitting diode or LED), and to hold fixation for the duration of the LED. While maintaining fixation, a peripheral LED illuminates, resulting in a sensory (i.e., visual) response in the SC. A short time later (usually on the order of 100–200 ms), the fixation LED is shut off, cueing the animal to generate a motor response to the location at which the target was previously presented. The "delay" allows the sensory response to be dissociated from the motor response, thus providing insight into the nature of the sensory–motor transform. Although such delayed saccade tasks have been heavily employed in

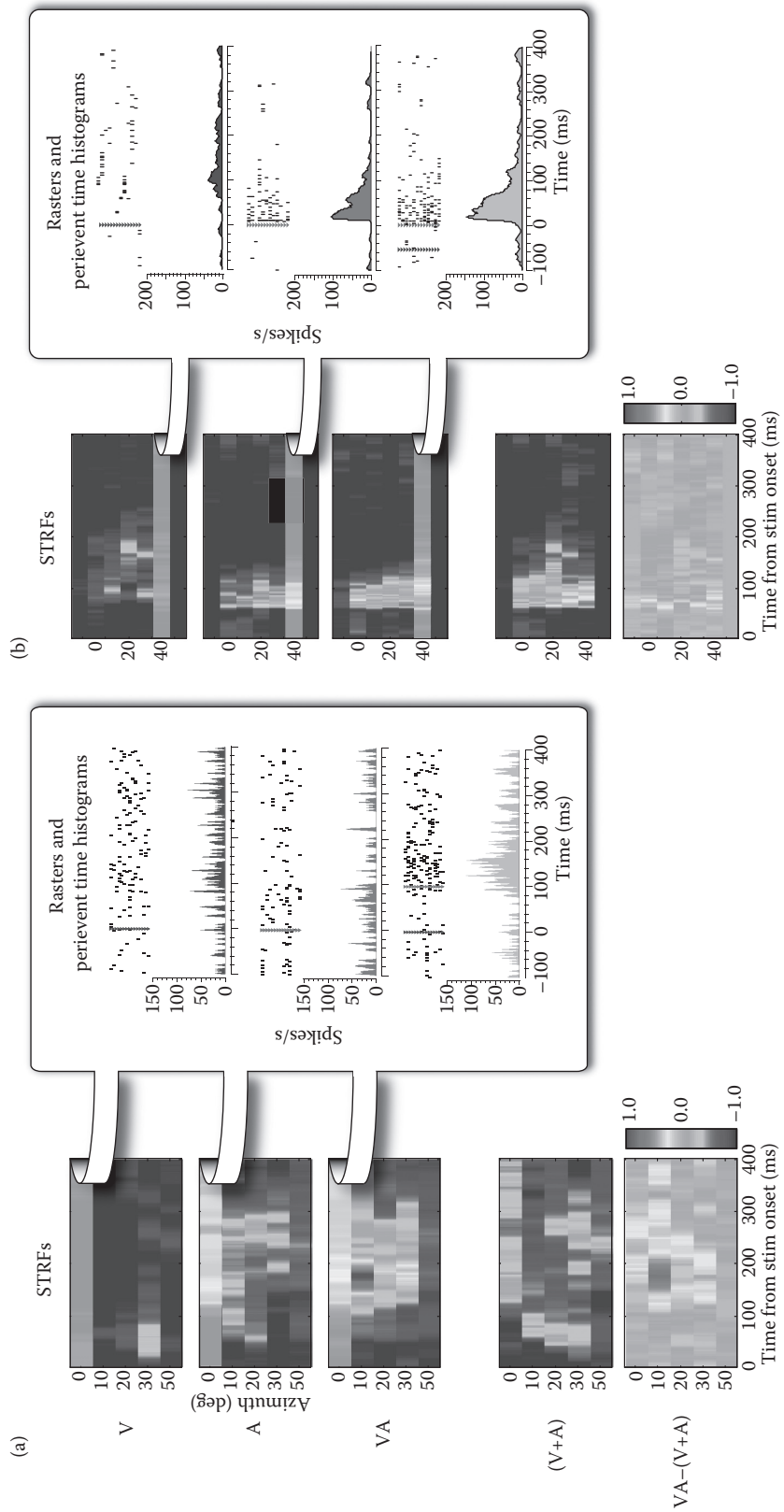

FIGURE 11.6 (See color insert.) Representative STRF from awake (a) versus anesthetized (b) recordings from cat SC using simple audiovisual stimulus presentations (an LED paired with broadband noise). In awake animals, superadditive interactions occurred over multiple time points in multisensory condition (VA) when compared to what would be predicted based on a linear summation of unisensory responses (V + A; see contrast, VA – [V + A]). This differs from anesthetized recordings from SC in which multisensory interactions are limited to earliest temporal phase of multisensory response.

both the cat and monkey, they are typically used to eliminate "confounding" sensory influences on the motor responses.

Another advantage afforded by the awake preparation is the ability to study how space, time, and effectiveness interact in a state more reflective of normal brain function, and which is likely to reveal important links between multisensory neuronal interactions and behavioral/perceptual enhancements such as speeded responses, increased detection, and accuracy gains. Ideally, these analyses could be structured to allow direct neurometric–psychometric comparisons, providing fundamental insights into how individual neurons and neuronal assemblies impact whole organismic processes.

Preliminary studies have already identified that multisensory neurons in the SC of the awake cat demonstrate extended response durations, as well as superadditive interactions over multiple time scales, when compared to anesthetized animals in which multisensory interactions are typically limited to the early phases of the response (Figure 11.6; Krueger et al. 2008). These findings remain to be tested in multisensory regions of the cortex, or extended beyond simple stimuli (LEDs paired with white noise) to more complex, ethologically relevant cues that might better address multisensory perceptual capabilities. Responses to naturalistic stimuli in cats have primarily been examined in unisensory cortices, demonstrating that simplification of natural sounds (bird chirps) results in significant alteration of neuronal responses (Bar-Yosef et al. 2002) and that firing rates differ for natural versus time-reversed conspecific vocalizations (Qin et al. 2008) in the primary auditory cortex. Furthermore, multisensory studies in primates have shown that multisensory enhancement in the primary auditory cortex of awake monkeys was reduced when a mismatched pair of naturalistic audiovisual stimuli was presented (Kayser et al. 2010).

11.5 HUMAN BEHAVIORAL AND PERCEPTUAL STUDIES OF MULTISENSORY PROCESSING: BUILDING BRIDGES BETWEEN NEUROPHYSIOLOGICAL AND BEHAVIORAL AND PERCEPTUAL LEVELS OF ANALYSIS

As should be clear from the above description, the ultimate goal of neurophysiological studies is to provide a more informed view into the encoding processes that give rise to our behaviors and perceptions. Indeed, these seminal findings in the animal model can be used as important instruction sets for the design of experiments in human subjects to bridge between these domains. Recently, our laboratory has embarked on such experiments with a focus on better characterizing how stimulus timing influences multisensory perceptual processes, with a design shaped by our knowledge of the temporal principle.

11.5.1 Defining the "Temporal Window" of Multisensory Integration

In addition to emphasizing the importance of stimulus onset asynchrony (SOA) in determining the outcome of a given multisensory pairing, experiments in both SC and AES cortex of the cat showed that the span of time over which response enhancements are generally seen in these neurons is on the order of several hundred milliseconds (Meredith et al. 1987; Wallace and Stein 1996; Wallace et al. 1992, 1996). Behavioral studies have followed up on these analyses to illustrate the temporal constraints of multisensory combinations on human performance, and have found that the presentation of cross-modal stimulus pairs in close temporal proximity results in shortened saccadic reaction times (Colonius and Diederich 2004; Colonius and Arndt 2001; Frens et al. 1995), heightened accuracy in understanding speech in noise (McGrath and Summerfield 1985; Pandey et al. 1986; van Wassenhove et al. 2007), as well as playing an important role in multisensory illusions such as the McGurk effect (Munhall et al. 1996), the sound-induced flash illusion (Shams et al. 2000, 2002), the parchment skin illusion (Guest et al. 2002), and the stream-bounce illusion (Sekuler et al. 1997). Moreover, multisensory interactions as demonstrated using population-based functional imaging methods (Dhamala et al. 2007; Kavounoudias et al. 2008; Macaluso et al. 2004; Noesselt

et al. 2007) have been shown to be greatest during synchronous presentation of stimulus pairs. Perhaps even more important than synchrony in these studies was the general finding that multisensory interactions were typically preserved over an extended window of time (i.e., several hundred milliseconds) surrounding simultaneity, giving rise to the term "temporal window" for describing the critical period for these interactions (Colonius and Diederich 2004; van Wassenhove et al. 2007; Dixon and Spitz 1980). The concept of such a window makes good ethological sense, in that it provides a buffer for the latency differences that characterize the propagation times of energies in the different senses. Most illustrative here are the differences between the propagation times of light and sound in our environment, which differ by many orders of magnitude. As a simple example of this difference, take an audiovisual event happening at a distance of 1 m, where the incident energies will arrive at the retina almost instantaneously and at the cochlea about 3 ms later (the speed of sound is approximately 330 m/s). Now, if we move that same audiovisual source to a distance of 20 m, the difference in arrival times expands to 60 ms. Hence, having a window of tolerance for these audiovisual delays represents an effective means to continue to bind stimuli across modalities even without absolute correspondence in their incident arrival times.

Because of the importance of temporal factors for multisensory integration, a number of experimental paradigms have been developed for use in human subjects as a way to systematically study the temporal binding window and its associated dynamics. One of the most commonly used of these is a simultaneity judgment task, in which paired visual and auditory stimuli are presented at various SOAs and participants are asked to judge whether the stimuli occurred simultaneously or successively (Zampini et al. 2005a; Engel and Dougherty 1971; Stone et al. 2001; Stevenson et al. 2010). A distribution of responses can then be created that plots the probability of simultaneity reports as a function of SOA. This distribution yields not only the point of subjective simultaneity, defined as the peak of function (Stone et al. 2001; Zampini et al. 2005a) but, more importantly, can be used to define a "window" of time within which simultaneity judgments are highly likely. A similar approach is taken in paradigms designed to assess multisensory temporal order judgments, wherein participants judge whether stimuli within one or another modality was presented first. Similar to the simultaneity judgment task, the point of subjective simultaneity is the time point at which participants judge either stimulus to have occurred first at a rate of 50% (Zampini et al. 2003; Spence et al. 2001). Once again, this method can also be adapted to create response distributions that serve as proxies for the temporal binding window. Although the point measures (i.e., point of subjective simultaneity) derived from these studies tend to differ based on the paradigm chosen (Fujisaki et al. 2004; Vroomen et al. 2004; Zampini et al. 2003, 2005a), the span of time over which there is a high likelihood of reporting simultaneity is remarkably constant, ranging from about –100 ms to 250 ms, where negative values denote auditory-leading-visual conditions (Dixon and Spitz 1980; Fujisaki et al. 2004; Vroomen et al. 2004; Zampini et al. 2003, 2005a). The larger window size on the right side of these distributions—in which vision leads audition—appears in nearly all studies of audiovisual simultaneity perception, and has been proposed to arise from the inherent flexibility needed to process real-world audiovisual events, given that the propagation speeds of light and sound will result in SOAs only on the right side of these distributions (Dixon and Spitz 1980). Indeed, very recent efforts to model the temporal binding window within a probabilistic framework (Colonius and Diederich 2010a, 2010b) have described this asymmetry as arising from an asymmetry in Bayesian priors across SOAs corresponding to the higher probability that visual-first pairs were generated by the same external event.

11.5.2 Stimulus-Dependent Effects on the Size of the Multisensory Temporal Window

Although some have argued for an invariant size to the temporal window (see Munhall et al. 1996), there is a growing body of evidence to suggest that the size of the temporal window is very much dependent on the type of stimulus that is used (Dixon and Spitz 1980; van Wassenhove et al. 2008; Soto-Faraco and Alsius 2009). The largest distinctions in this domain have been seen when

contrasting speech versus nonspeech stimuli, in which the window for speech appears to be far larger (approximately 450 ms) when compared with the pairing of simpler stimuli such as flash-tone pairs or videos of inanimate objects, such as a hammer pounding a nail—about 250 ms (Dixon and Spitz 1980; van Atteveldt et al. 2007; van Wassenhove et al. 2007; Massaro et al. 1996; Conrey and Pisoni 2006; McGrath and Summerfield 1985). Interpretation of this seeming expansion in the case of speech has ranged from the idea that learned tolerance of asynchrony is greatest with stimuli to which we are most exposed (Dixon and Spitz 1980), to the theory that the richness of auditory spectral and visual dynamic content in speech allows for binding over a larger range of asynchrony (Massaro et al. 1996), to the view that speech window size is dictated by the duration of the elemental building blocks of the spoken language—phonemes (Crystal and House 1981).

Other studies have focused on altering the statistics of multisensory temporal relations in an effort to better characterize the malleability of these processes. For example, repeated exposure to a 250-ms auditory-leading-visual asynchronous pair is capable of biasing participants' simultaneity judgments in the direction of that lag by about 25 ms, with effects lasting on the order of minutes (Fujisaki et al. 2004; Vroomen et al. 2004). Similar recalibration effects have been noted after exposure to asynchronous audiovisual speech, as well as to visual–tactile, audio–tactile, and sensory–motor pairs (Hanson et al. 2008; Fajen 2007; Stetson et al. 2006; Navarra et al. 2005). Although the exact mechanisms underlying these changes are unknown, they have been proposed to represent a recalibration of sensory input consistent with Bayesian models of perception (Hanson et al. 2008; Miyazaki et al. 2005, 2006).

11.5.3 Can "Higher-Order" Processes Affect Multisensory Temporal Window?

In addition to these studies examining stimulus-dependent effects, other works have sought to determine the malleability of multisensory temporal processing resulting from the manipulation of cognitive processes derived from top-down networks. Much of this work has focused on attentional control, and has been strongly influenced by historical studies showing that attention within a modality could greatly facilitate information processing of a cued stimulus within that modality. This work has now been extended to the cross-modal realm, and has shown that attention to one modality can bias temporally based judgments concerning a stimulus in another modality (Zampini et al. 2005b; Spence et al. 2001; Shore et al. 2001), illustrating the presence of strong attentional links between different sensory systems.

11.6 ADULT PLASTICITY IN MULTISENSORY TEMPORAL PROCESSES: PSYCHOPHYSICAL AND NEUROIMAGING EVIDENCE

Further work in support of top-down influences on multisensory perception have focused on characterizing the plasticity that can be engendered with the use of classic perceptual learning paradigms. The first of these studies were directed outside the temporal domain, and focused on the simple question of whether perceptual learning within a single sensory modality can be improved with the use of cross-modal stimuli. In these studies, participants were trained on a motion discrimination task using either a visual cue alone or combined visual–auditory cues. Results reveal enhanced visual motion discrimination abilities and an abbreviated time course of learning in the group trained on the audiovisual version of the task when compared with those trained only on the visual version (Kim et al. 2008; Seitz et al. 2006). Similar results have been seen in the visual facilitation of voice discrimination learning (von Kriegstein and Giraud 2006), cross-modal enhancement of both auditory and visual natural object recognition (Schneider et al. 2008), and in the facilitation of unisensory processing based on prior multisensory memories (Murray et al. 2004, 2005).

More recently, our laboratory has extended these perceptual plasticity studies into the temporal realm, by attempting to assess the plasticity of the multisensory temporal binding window itself.

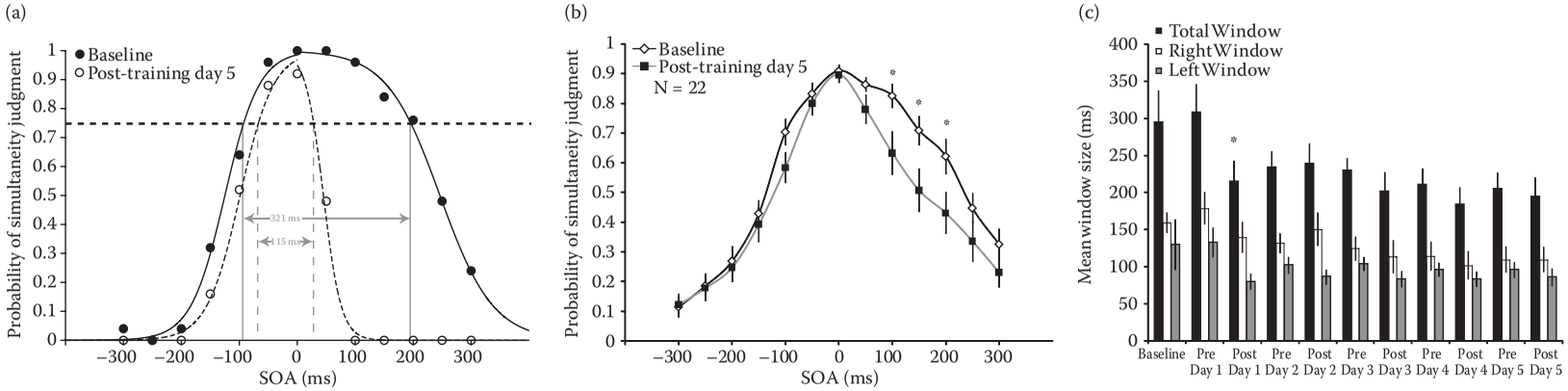

FIGURE 11.7 Training on a two-alternative forced choice simultaneity judgment forced choice task. (a) An estimate of temporal binding window is derived using a criterion set at 75% of maximum. In this representative individual case, window narrows from 321 to 115 ms after 5 days (1 h/day) of feedback training. (b) After training, a significant decrease in probability of judging nonsimultaneous audiovisual pairs to be simultaneous was found (*$P < .05$). (c) Average window size dropped significantly after first day (1 h) of training, then remained stable (*$P < .05$).

Initial efforts used a two-alternative forced choice audiovisual simultaneity judgment task in which subjects were asked to choose on a trial-by-trial basis whether a stimulus pair was synchronously or asynchronously presented (Powers et al. 2009). In the initial characterization (i.e., before training), a distribution of responses was obtained that allowed us to define a proxy measure for the multisensory temporal binding window for each individual subject (Figure 11.7). After this baseline measurement, subjects were then engaged in the same task, except that now they were given feedback as to the correctness of their judgments. Training was carried out for an hour a day over 5 days. This training regimen resulted in a marked narrowing in the width of the multisensory temporal binding window, with a group average reduction of 40%. Further characterization revealed that the changes in window size were very rapid (being seen after the first day of training), were durable (lasting at least a week after the cessation of training), and were a direct result of the feedback provided (control subjects passively exposed to the same stimulus set did not exhibit window narrowing). Additionally, to rule out the possibility that this narrowing was the result of changes in cognitive biases, a second experiment using a two-interval forced choice paradigm was undertaken in which participants were instructed to identify the simultaneously presented audiovisual pair presented within one of two intervals. The two-interval forced choice paradigm resulted in a narrowing that was similar in both degree and dynamics to that using the two-alternative forced choice approach. Overall, this result is the first to illustrate a marked experience-dependent malleability to the multisensory temporal binding window, a result that has potentially important implication for clinical conditions such as autism and dyslexia in which there is emerging evidence for changes in multisensory temporal function (Ciesielski et al. 1995; Laasonen et al. 2001, 2002; Kern 2002; Hairston et al. 2005; Facoetti et al. 2010; Foss-Feig et al. 2010).

In an effort to better define the brain networks responsible for multisensory temporal perception (and the demonstrable plasticity), our laboratory has conducted a follow-up neuroimaging study using fMRI (Powers et al. 2010). The findings revealed marked changes in one of the best-established multisensory cortical domains in humans, the posterior superior temporal sulcus (pSTS). The pSTS exhibited striking decreases in blood oxygen level dependent (BOLD) activation after training, suggestive of an increased efficiency of processing. In addition to these changes in pSTS were changes in regions of the auditory and visual cortex, along with marked changes in functional coupling between these unisensory domains and the pSTS. Together, these studies are beginning to reveal the cortical networks involved in multisensory temporal processing and perception, as well as the dynamics of these networks that must be continually adjusted to capture the ever-changing sensory statistics of our natural world as well as their cognitive valence.

Please spell out fMRI here.

11.7 DEVELOPMENTAL PLASTICITY IN MULTISENSORY REPRESENTATIONS: INSIGHTS FROM ANIMAL AND HUMAN STUDIES

In addition to this compelling emerging evidence as to the plastic potential of the adult brain for having its multisensory processing architecture shaped in an experience-dependent manner, there is a rich literature on the development of multisensory representations and the role that postnatal experience plays in shaping these events. Although the questions were first posed in the literature associated with the development of human perceptual abilities, more recent work in animal models has laid the foundation for better understanding the seminal events in the maturation of multisensory behaviors and perceptions.

11.7.1 Neurophysiological Studies into Development of Multisensory Circuits

The studies described above in adult animal models provide an ideal foundation on which to evaluate the developmental events in the nervous system that lead up to the construction of mature multisensory representations. Hence, subsequent studies focused on establishing the developmental

chronology for multisensory neurons and their integrative features in these same model structures—the subcortical SC and the cortical AES. In the SC, recordings immediately after birth reveal an absence of multisensory neurons (Wallace and Stein 1997). Indeed, the first neurons present in the SC at birth and soon after are those that are exclusively responsive to somatosensory cues. By 10 to 12 days postnatal, auditory-responsive neurons appear, setting the stage for the first multisensory neurons that are responsive to both somatosensory and auditory cues. More than a week later, the first visually responsive neurons appear, providing the basis for the first visually responsive multisensory neurons. These early multisensory neurons were found to be far different than their adult counterparts, responded weakly to sensory stimuli, and had poorly developed response selectivity, long latencies, and large receptive fields (Wallace and Stein 1997; Stein et al. 1973a, 1973b). Perhaps most importantly, these early multisensory neurons failed to integrate their different sensory inputs, responding to stimulus combinations in a manner that was indistinguishable from their component unisensory responses (Wallace and Stein 1997). Toward the end of the first postnatal month, this situation begins to change, with individual neurons starting to show the capacity to integrate their different sensory inputs. Over the ensuing several months, both the number of multisensory neurons and those with integrative capacity grow steadily, such that by 4 to 5 months after birth, the adult-like incidences are achieved (Figure 11.8).

The developmental progression in the cortex is very similar to that in the SC, except that it appears to be delayed by several weeks (Wallace et al. 2006). Thus, the first multisensory neurons do not appear in AES until about 6 weeks after birth (Figure 11.8). Like with the SC, these early multisensory neurons are reflective of the adjoining unisensory representations, being auditory–somatosensory. Four weeks or so later, we see the appearance of visual neurons and the coincident appearance of visually responsive multisensory neurons. Once again, early cortical multisensory neurons are strikingly immature in many respects, including a lack of integrative capacity. As development progresses, we see a substantial growth in the multisensory population and we see most multisensory AES neurons develop their integrative abilities.

The parallels between SC and AES in their multisensory developmental chronology likely reflect the order of overall sensory development (Gottlieb 1971), rather than dependent connectivity between the two regions because the establishment of sensory profiles in the SC precedes the functional maturation of connections between AES and the SC (Wallace and Stein 2000). Thus, a

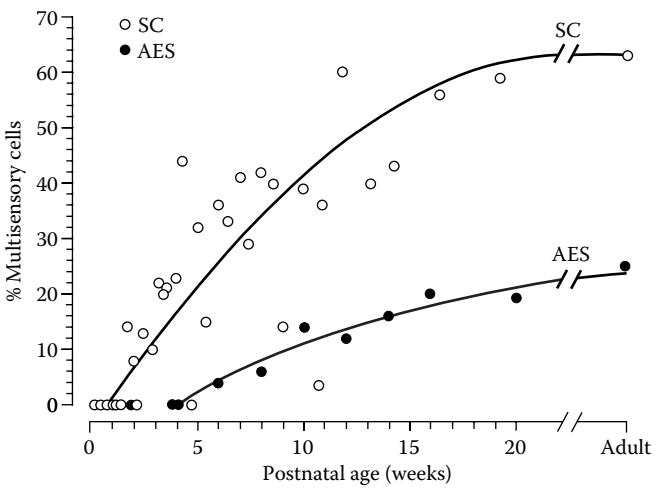

FIGURE 11.8 Development of multisensory neurons in SC (open circles) versus AES (closed circles) of cat. Development of multisensory neurons is similar between SC and AES with exceptions of onset and overall percentage of multisensory neurons. At 4 months postnatal life, percentages of multisensory neurons in both AES and SC are at their mature levels, with SC having a higher percentage than AES.

gradual recruitment of sensory functions during development appears to produce neurons capable of multisensory integration (Lewkowicz and Kraebel 2004; Lickliter and Bahrick 2004), and points strongly to a powerful role for early experience in sculpting the final multisensory state of these systems (see Section 11.7.3).

11.7.2 Development of Integrative Principles

In addition to characterizing the appearance of multisensory neurons and the maturation of their integrative abilities, these studies also examined how the integrative principles changed during the course of development. Intriguingly, the principle of inverse effectiveness appeared to hold in the earliest integrating neurons, in that as soon as a neuron demonstrated integrative abilities, the largest enhancements were seen in pairings of weakly effective stimuli. Indeed, one of the most surprising findings in these developmental studies is the all-or-none nature of multisensory integration. Thus, neurons appear to transition very rapidly from a state in which they lack integrative capacity to one in which that capacity is adult-like in both magnitude and adherence to the principle of inverse effectiveness. In the spatial domain, the situation appears to be much the same. Whereas early multisensory neurons have large receptive fields and lack integration, as soon as receptive fields become adult-like in size, neurons show integrative ability. Indeed, these processes appear to be so tightly linked that it has been suggested that they reflect the same underlying mechanistic process (Wallace and Stein 1997; Wallace et al. 2006).

The one principle that appears to differ in a developmental context is the temporal principle. Observations from the earliest integrating neurons show that they typically only show response enhancements to pairings at a single SOA (see Wallace and Stein 1997). This is in stark contrast to adults, in which enhancements are typically seen over a span of SOAs lasting several hundred milliseconds, and which has led to the concept of a temporal "window" for multisensory integration. In these animal studies, as development progresses, the range of SOAs over which enhancements can be generated grow, ultimately resulting in adult-sized distributions reflective of the large temporal window. Why such a progression is seen in the temporal domain and not in the other domains is not yet clear, but may have something to do with the fact that young animals are generally only concerned with events in the immediate proximity to the body (and which would make an SOA close to 0 of greatest utility). As the animal becomes increasingly interested in exploring space at greater distances, an expansion in the temporal window would allow for the better encoding of these more distant events. We will return to the issue of plasticity in the multisensory temporal window when we return to the human studies (see Section 11.7.4).

11.7.3 Experientially based Plasticity in Multisensory Circuits

Although the protracted timeline for the development of mature multisensory circuits is strongly suggestive of a major deterministic role for early experience in shaping these circuits, only with controlled manipulation of this experience can we begin to establish causative links. To address this issue, our laboratory has performed a variety of experiments in which sensory experience is eliminated or altered in early life, after which the consequent impact on multisensory representations is examined. In the first of these studies, the necessity of cross-modal experiences during early life was examined by eliminating all visual experiences from birth until adulthood, and then assessing animals as adults (Wallace et al. 2004; Carriere et al. 2007). Although there were subtle differences between SC and AES in these studies, the impact on multisensory integration in both structures was profound. Whereas dark-rearing allowed for the appearance of a robust (albeit smaller than normal) visual population, its impact on multisensory integration was profound—abolishing virtually all response enhancements to visual–nonvisual stimulus pairings.

A second series of experiments then sought to address the importance of the statistical relationship of the different sensory cues to one another on the construction of these multisensory

representations. Here, animals were reared in environments in which the spatial relationship between visual and auditory stimuli was systematically altered, such that visual and auditory events that were temporally coincident were always separated by 30°. When examined as adults, these animals were found to have multisensory neurons with visual and auditory receptive fields that were displaced by approximately 30°, but more importantly, to now show maximal multisensory enhancements when stimuli were separated by this disparity (Figure 11.9a). More recent work has extended these studies into the temporal domain, and has shown that raising animals in environments in which the temporal relationship of visual and auditory stimuli is altered by 100 ms results in a shift in the peak tuning profiles of multisensory neurons by approximately 100 ms (Figure 11.9b). Of particular interest was that when the temporal offset was extended to 250 ms, the neurons lost the capacity to integrate their different sensory inputs, suggesting that there is a critical temporal window for this developmental process. Collectively, these results provide strong support for the power of the statistical relations of multisensory stimuli in driving the formation of multisensory circuits; circuits that appear to be optimally designed to code the relations most frequently encountered in the world during the developmental period.

11.7.4 Development of Human Multisensory Temporal Perception

The ultimate goal of these animal model–based studies is to provide a better framework from which to view human development, with a specific eye toward the maturation of the brain mechanisms that underlie multisensory-mediated behaviors and perceptions. Human developmental studies on multisensory processing have provided us with important insights into the state of the newborn and infants brains, and have illustrated that multisensory abilities are changing rapidly in the first year of postnatal life (see Lewkowicz and Ghazanfar 2009). Intriguingly, there is then a dearth of knowledge about multisensory maturation until adulthood. In an effort to begin to fill this void, our laboratory has embarked on a series of developmental studies focused on childhood and adolescence, with a specific emphasis on multisensory temporal processes, one of the principal themes of this chapter.

These studies strongly suggest that the maturation of multisensory temporal functioning extends beyond the first decade of life. In the initial study, it was established that multisensory temporal functioning was still not mature by 10 to 11 years of age (Hillock et al. 2010). Here, children were assessed on a simultaneity judgment task in which flashes and tone pips were presented at SOAs ranging from –450 to +450 ms (with positive values representing visual-leading stimulus trials and negative values representing auditory-leading stimulus trials), allowing for the creation of a response distribution identical to what has been done in adults and which serves as a proxy for the multisensory temporal binding window (see Section 11.6). When compared with adults, the group mean window size for these children was found to be approximately 38% larger (i.e., 413 vs. 299 ms). A larger follow-up study then sought to detail the chronology of this maturational process from 6 years of age until adulthood, and identified the closure of the binding window in mid to late adolescence for these simple visual–auditory pairings (Figure 11.10; Hillock and Wallace 2011b). A final study then sought to extend these analyses into the stimulus domain with which children likely have the greatest experience—speech. Using the McGurk effect, which uses the pairing of discordant visual and auditory speech stimuli (e.g., a visual /ga/ with an auditory /ba/), it is possible to index the integrative process by looking at how often participants report fusions that represent a synthesis of the visual and auditory cues (e.g., /da/ or /tha/). Furthermore, because this effect has been shown to be temporally dependent, it can be used as a tool to study the multisensory temporal binding window for speech-related stimuli. Surprisingly, when used with children (6–11 years), adolescents (12–17 years), and adults (18–23 years), windows were found to be indistinguishable (Hillock and Wallace 2011a).Together, these studies show a surprising dichotomy between the development of multisensory temporal perception for nonspeech versus speech stimuli, a result that may reflect the powerful imperative placed on speech in young children, and reinforcing the importance of sensory experience in the development of multisensory abilities.

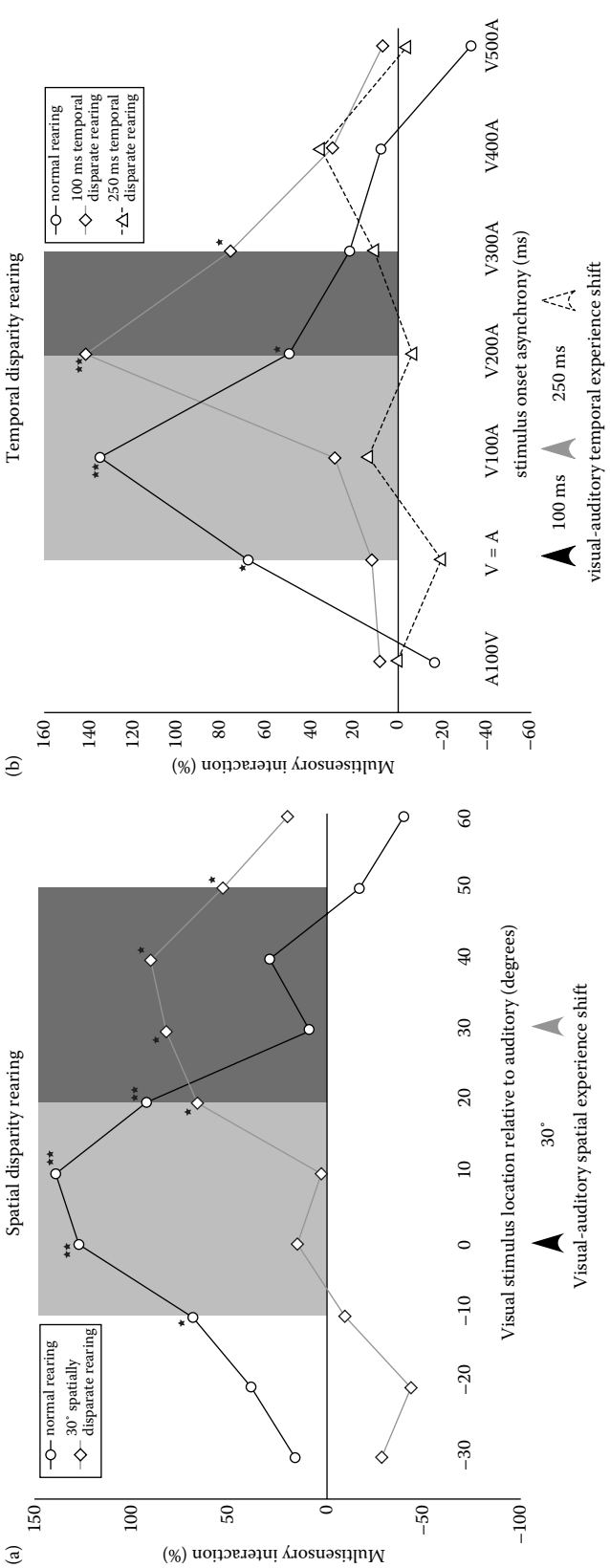

FIGURE 11.9 Developmental manipulations of spatial and temporal relationships of audiovisual stimuli. (a) Multisensory interaction is shown as a function of spatially disparate stimuli between normally reared animals and animals reared with a 30° disparity between auditory and visual stimuli. Peak multisensory interaction for disparately reared group falls by 30° from that of normally reared animals. (b) Multisensory interaction as a function of SOA in animals reared normally versus animals reared in environments with 100 and 250 ms temporal disparities. As might be expected, peak multisensory interactions are offset by 100 ms for normally reared versus the 100 ms disparate group. Interestingly, the 250 ms group loses the ability to integrate audiovisual stimuli.

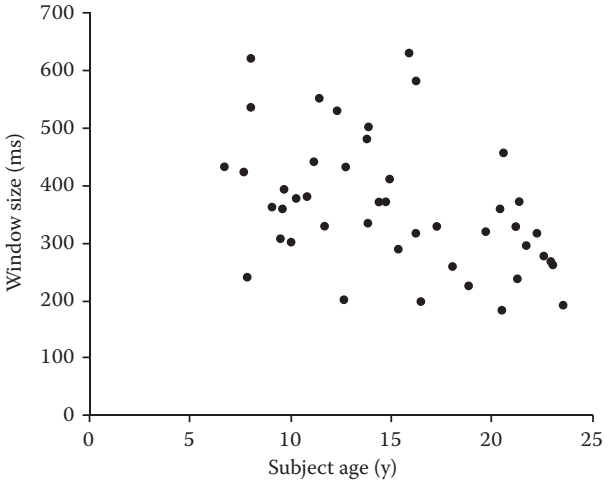

FIGURE 11.10 Temporal window size decreases from childhood to adulthood. Each data point represents a participant's window size as determined by width at 75% of maximum probability of perceived simultaneity using nonspeech stimuli. See Section 11.5.1. (Adapted from Hillock et al., Binding of sights and sounds: Age-related changes in audiovisual temporal processing, 2010, submitted for publication.)

11.8 CONCLUSIONS AND FUTURE DIRECTIONS

As should be clear from the above, substantial efforts are ongoing to bridge between the rapidly growing knowledge sets concerning multisensory processing derived from both animal and human studies. This work should not only complement each domain, but should inform the design of better experiments in each. As an example, the final series of human experiments described above begs for a nonhuman correlate to better explore the mechanistic underpinnings that result in very different timelines for the maturation of nonspeech versus speech integrative networks. Experiments in nonhuman primates, in which the critical nodes for communicative signal processing are beginning to emerge (Ghazanfar et al. 2008, 2010), can begin to tease out the relative maturation of the relevant neurophysiological processes likely to result in these distinctions.

Change to "beginning to bridge the gap (or *creating a bridge*) between the neural and the behavioral/perceptual" instead?

Although we have made great strides in recent years in building a better understanding of multisensory behavioral and perceptual processes and their neural correlates, we still have much to discover. Fundamental questions remain unanswered, providing both a sense of frustration but also a time of great opportunity. One domain of great interest to our laboratory is beginning to bridge between the neural and the behavioral/perceptual in an effort to extend beyond the correlative analyses done thus far. Paradigms developed in awake and behaving animals allow for a direct assessment of neural and behavioral responses during performance on the same task, and should more directly link multisensory encoding processes to their striking behavioral benefits (e.g., see Chandrasekaran and Ghazanfar 2009). However, even these experiments provide only correlative evidence, and future work will seek to use powerful new methods such as optogenetic manipulation in animal models (e.g., see Cardin et al. 2009) and transcranial magnetic stimulation in humans (e.g., see Romei et al. 2007; Beauchamp et al. 2010; Pasalar et al. 2010) to selectively deactivate specific circuit components and then assess the causative impact on multisensory function.

REFERENCES

Amlot, R., R. Walker, J. Driver, and C. Spence. 2003. Multimodal visual–somatosensory integration in saccade generation. *Neuropsychologia,* 41, 1–15.

Bar-Yosef, O., Y. Rotman, and I. Nelken. 2002. Responses of neurons in cat primary auditory cortex to bird chirps: Effects of temporal and spectral context. *Journal of Neuroscience,* 22, 8619–8632.

Beauchamp, M.S., A.R. Nath, and S. Pasalar. 2010. fMRI-guided transcranial magnetic stimulation reveals that the superior temporal sulcus is a cortical locus of the McGurk effect. *Journal of Neuroscience,* 30, 2414–2417.

Bell, A.H., M.A. Meredith, A.J. Van Opstal, and D.P. Munoz. 2005. Crossmodal integration in the primate superior colliculus underlying the preparation and initiation of saccadic eye movements. *Journal of Neurophysiology,* 93, 3659–3673.

Benedek, G., G. Eordegh, Z. Chadaide, and A. Nagy. 2004. Distributed population coding of multisensory spatial information in the associative cortex. *European Journal of Neuroscience,* 20, 525–529.

Calvert, G.A., and T. Thesen. 2004. Multisensory integration: methodological approaches and emerging principles in the human brain. *Journal of Physiology, Paris,* 98, 191–205.

Cardin, J.A., M. Carlen, K. Meletis, U. Knoblich, F. Zhang, K. Deisseroth, L.H. Tsai, and C.I. Moore. 2009. Driving fast-spiking cells induces gamma rhythm and controls sensory responses. *Nature,* 459, 663–667.

Carriere, B.N., D.W. Royal, T.J. Perrault, S.P. Morrison, J.W. Vaughan, B.E. Stein, and M.T. Wallace. 2007. Visual deprivation alters the development of cortical multisensory integration. *Journal of Neurophysiology,* 98, 2858–2867.

Carriere, B.N., D.W. Royal, and M.T. Wallace. 2008. Spatial heterogeneity of cortical receptive fields and its impact on multisensory interactions. *Journal of Neurophysiology,* 99, 2357–2368.

Chandrasekaran, C., and A.A. Ghazanfar. 2009. Different neural frequency bands integrate faces and voices differently in the superior temporal sulcus. *Journal of Neurophysiology,* 101, 773–788.

Ciesielski, K.T., J.E. Knight, R.J. Prince, R.J. Harris, and S.D. Handmaker. 1995. Event-related potentials in cross-modal divided attention in autism. *Neuropsychologia,* 33, 225–246.

Clark, B., and A. Graybiel. 1966. Factors contributing to the delay in the perception of the oculogravic illusion. *American Journal of Psychology,* 79, 377–388.

Colonius, H., and P. Arndt. 2001. A two-stage model for visual–auditory interaction in saccadic latencies. *Perception & Psychophysics,* 63, 126–147.

Colonius, H., and A. Diederich. 2004. Multisensory interaction in saccadic reaction time: A time-window-of-integration model. *Journal of Cognitive Neuroscience,* 16, 1000–1009.

Colonius, H., and A. Diederich. 2010a. The optimal time window of visual–auditory integration: A reaction time analysis. *Frontiers in Integrative Neuroscience,* 4, 11.

Colonius, H., and A. Diederich. 2010b. Optimal time windows of integration. Abstract Presented at 2010 International Multisensory Research Forum.

Conrey, B., and D.B. Pisoni. 2006. Auditory–visual speech perception and synchrony detection for speech and nonspeech signals. *Journal of the Acoustical Society of America,* 119, 4065–4073.

Corneil, B.D., and D.P. Munoz 1996. The influence of auditory and visual distractors on human orienting gaze shifts. *Journal of Neuroscience,* 16, 8193–81207.

Corneil, B.D., M. Van Wanrooij., D.P. Munoz, and A.J. Van Opstal. 2002. Auditory–visual interactions subserving goal-directed saccades in a complex scene. *Journal of Neurophysiology,* 88, 438–454.

Crystal, T.H., and A.S. House. 1981. Segmental durations in connected speech signals. *Journal of the Acoustical Society of America,* 69, S82–S83.

David, S.V., W.E. Vinje, and J.L. Gallant. 2004. Natural stimulus statistics alter the receptive field structure of v1 neurons. *Journal of Neuroscience,* 24, 6991–7006.

Dhamala, M., C.G. Assisi, V.K., Jirsa, F.L. Steinberg, and J.A. Kelso. 2007. Multisensory integration for timing engages different brain networks. *NeuroImage,* 34, 764–773.

Diederich, A., H. Colonius, D. Bockhorst, and S. Tabeling. 2003. Visual–tactile spatial interaction in saccade generation. *Experimental Brain Research,* 148, 328–337.

Dixon, N.F., and L. Spitz. 1980. The detection of auditory visual desynchrony. *Perception,* 9, 719–721.

Engel, G.R., and W.G. Dougherty. 1971. Visual–auditory distance constancy. *Nature,* 234, 308.

Facoetti, A., A.N. Trussardi, M. Ruffino, M.L. Lorusso, C. Cattaneo, R. Galli, M. Molteni, and M. Zorzi. 2010. Multisensory spatial attention deficits are predictive of phonological decoding skills in developmental dyslexia. *Journal of Cognitive Neuroscience,* 22, 1011–1025.

Fajen, B.R. 2007. Rapid recalibration based on optic flow in visually guided action. *Experimental Brain Research,* 183, 61–74.

Forster, B., C. Cavina-Pratesi, S.M. Aglioti, and G. Berlucchi. 2002. Redundant target effect and intersensory facilitation from visual–tactile interactions in simple reaction time. *Experimental Brain Research,* 143, 480–487.

Foss-Feig, J.H., L.D. Kwakye, C.J. Cascio, C.P. Burnette, H. Kadivar, W.L. Stone, and M.T. Wallace. 2010. An extended multisensory temporal binding window in autism spectrum disorders. *Experimental Brain Research,* 203, 381–389.

Frassinetti, F., N. Bolognini, and E. Ladavas. 2002. Enhancement of visual perception by crossmodal visuo-auditory interaction. *Experimental Brain Research,* 147, 332–343.

Frens, M.A., and A.J. Van Opstal. 1998. Visual–auditory interactions modulate saccade-related activity in monkey superior colliculus. *Brain Research Bulletin,* 46, 211–224.

Frens, M.A., A.J. Van Opstal, and R.F. van der Willigen. 1995. Spatial and temporal factors determine auditory–visual interactions in human saccadic eye movements. *Perception & Psychophysics,* 57, 802–816.

Fujisaki, W., S. Shimojo, M. Kashino, and S. Nishida. 2004. Recalibration of audiovisual simultaneity. *Nature Neuroscience,* 7, 773–778.

Furukawa, S., and J.C. Middlebrooks. 2002. Cortical representation of auditory space: Information-bearing features of spike patterns. *Journal of Neurophysiology,* 87, 1749–1762.

Ghazanfar, A.A., C. Chandrasekaran, and N.K. Logothetis. 2008. Interactions between the superior temporal sulcus and auditory cortex mediate dynamic face/voice integration in rhesus monkeys. *Journal of Neuroscience,* 28, 4457–4469.

Ghazanfar, A.A., C. Chandrasekaran, and R.J. Morrill. 2010. Dynamic, rhythmic facial expressions and the superior temporal sulcus of macaque monkeys: implications for the evolution of audiovisual speech. *European Journal of Neuroscience,* 31, 1807–1817.

Gottlieb, G. 1971. Ontogenesis of sensory function in birds and mammals. In *The biopsychology of development*, ed. E. Tobach, L.R. Aronson, and E. Shaw. New York, NY: Academic Press.

Guest, S., C. Catmur, D. Lloyd, and C. Spence. 2002. Audiotactile interactions in roughness perception. *Experimental Brain Research,* 146, 161–171.

Guitton, D., and D.P. Munoz 1991. Control of orienting gaze shifts by the tectoreticulospinal system in the head-free cat. I. Identification, localization, and effects of behavior on sensory responses. *Journal of Neurophysiology,* 66, 1605–1623.

Haider, B., M.R. Krause, A. Duque, Y. Yu, J. Touryan, J.A. Mazer, and D.A. McCormick. 2010. Synaptic and network mechanisms of sparse and reliable visual cortical activity during nonclassical receptive field stimulation. *Neuron,* 65, 107–121.

Hairston, W.D., J.H. Burdette, D.L. Flowers, F.B. Wood, and M.T. Wallace. 2005. Altered temporal profile of visual–auditory multisensory interactions in dyslexia. *Experimental Brain Research,* 166, 474–480.

Hall, W.C., and A.K. Moschovakis. 2004. *The superior colliculus: New approaches for studying sensorimotor integration*. Boca Raton, FL: CRC Press.

Hanson, J.V., J. Heron, and D. Whitaker. 2008. Recalibration of perceived time across sensory modalities. *Experimental Brain Research,* 185, 347–352.

Harrington, L.K., and C.K. Peck. 1998. Spatial disparity affects visual–auditory interactions in human sensorimotor processing. *Experimental Brain Research,* 122, 247–252.

Hershenson, M. 1962. Reaction time as a measure of intersensory facilitation. *Journal of Experimental Psychology,* 63, 289–293.

Hillock, A.R., and M.T. Wallace. 2011a. Changes in the multisensory temporal binding window persist into adolescence. In preparation.

Hillock, A.R., and M.T. Wallace. 2011b. A developmental study of the temporal constraints for audiovisual speech binding. In preparation.

Please update this reference.

Hillock, A.R., A.R. Powers 3rd, and M.T. Wallace. 2010. Binding of sights and sounds: Age-related changes in audiovisual temporal processing. *(Submitted).*

Hughes, H.C., P.A. Reuter-Lorenz, G. Nozawa, and R. Fendrich. 1994. Visual–auditory interactions in sensorimotor processing: saccades versus manual responses. *Journal of Experimental Psychology. Human Perception and Performance,* 20, 131–53.

Hughes, H.C., M.D. Nelson, and D.M. Aronchick. 1998. Spatial characteristics of visual–auditory summation in human saccades. *Vision Research,* 38, 3955–63.

Kavounoudias, A., J.P. Roll, J.L. Anton, B. Nazarian, M. Roth, and R. Roll. 2008. Proprio-tactile integration for kinesthetic perception: An fMRI study. *Neuropsychologia,* 46, 567–575.

Kayser, C., C.I. Petkov, and N.K. Logothetis. 2008. Visual modulation of neurons in auditory cortex. *Cerebral Cortex,* 18, 1560–74.

Kayser, C., N.K. Logothetis, and S. Panzeri. 2010. Visual enhancement of the information representation in auditory cortex. *Current Biology,* 20, 19–24.

Kern, J.K. 2002. The possible role of the cerebellum in autism/PDD: Disruption of a multisensory feedback loop. *Medical Hypotheses,* 59, 255–260.

Kim, R.S., A.R. Seitz, and L. Shams. 2008. Benefits of stimulus congruency for multisensory facilitation of visual learning. *PLoS One,* 3, e1532.

King, A. J. 2004. The superior colliculus. *Current Biology,* 14, R335–R338.

Krueger, J., M.C. Fister, D.W. Royal, B.N. Carriere, and M.T. Wallace. 2008. A comparison of spatiotemporal receptive fields of multisensory superior colliculus neurons in awake and anesthetized cat. *Society for Neuroscience Abstract*, 457.17.

Please update this reference.

Krueger, J., D.W. Royal, M.C. Fister, and M.T. Wallace. 2009. Spatial receptive field organization of multisensory neurons and its impact on multisensory interactions. *Hearing Research.*

Laasonen, M., E. Service, and V. Virsu. 2001. Temporal order and processing acuity of visual, auditory, and tactile perception in developmentally dyslexic young adults. *Cognitive, Affective & Behavioral Neuroscience,* 1, 394–410.

Laasonen, M., E. Service, and V. Virsu. 2002. Crossmodal temporal order and processing acuity in developmentally dyslexic young adults. *Brain and Language,* 80, 340–354.

Lakatos, P., C.M. Chen, M.N. O'Connell, A. Mills, and C.E. Schroeder. 2007. Neuronal oscillations and multisensory interaction in primary auditory cortex. *Neuron,* 53, 279–292.

Lewkowicz, D.J., and K.S. Kraebel. 2004. The value of multisensory redundancy in the development of intersensory perception. In *The Handbook of Multisensory Processes,* ed. G.A. Calvert, C. Spence, and B.E. Stein. Cambridge, MA: MIT Press.

Lewkowicz, D.J., and A.A. Ghazanfar. 2009. The emergence of multisensory systems through perceptual narrowing. *Trends in Cognitive Sciences,* 13, 470–478.

Lickliter, R., and L.E. Bahrick. 2004. Perceptual development and the origins of multisensory responsiveness. In *The Handbook of Multisensory Processes*, ed. G.A. Calvert, C. Spence, and B.E. Stein. Cambridge, MA: MIT Press.

Lovelace, C.T., B.E. Stein, and M.T. Wallace. 2003. An irrelevant light enhances auditory detection in humans: a psychophysical analysis of multisensory integration in stimulus detection. *Brain Research Cognitive Brain Research,* 17, 447–453.

Macaluso, E., N. George, R. Dolan, C. Spence, and J. Driver. 2004. Spatial and temporal factors during processing of audiovisual speech: A PET study. *NeuroImage,* 21, 725–732.

Machens, C.K., M.S. Wehr, and A.M. Zador. 2004. Linearity of cortical receptive fields measured with natural sounds. *Journal of Neuroscience,* 24, 1089–1100.

Manabe, K., and H. Riquimaroux. 2000. Sound controls velocity perception of visual apparent motion. *Journal of the Acoustical Society of Japan,* 21, 171–174.

Massaro, D.W., M.M. Cohen, and P.M. Smeele. 1996. Perception of asynchronous and conflicting visual and auditory speech. *Journal of the Acoustical Society of America,* 100, 1777–1786.

McGrath, M., and Q. Summerfield. 1985. Intermodal timing relations and audio-visual speech recognition by normal-hearing adults. *Journal of the Acoustical Society of America,* 77, 678–685.

Meredith, M.A., J.W. Nemitz, and B.E. Stein. 1987. Determinants of multisensory integration in superior colliculus neurons. I. Temporal factors. *Journal of Neuroscience,* 7, 3215–3229.

Meredith, M.A., and B.E. Stein, 1983. Interactions among converging sensory inputs in the superior colliculus. *Science,* 221, 389–391.

Meredith, M.A., and B.E. Stein 1985. Descending efferents from the superior colliculus relay integrated multisensory information. *Science,* 227, 657–659.

Meredith, M.A., and B.E. Stein 1986. Spatial factors determine the activity of multisensory neurons in cat superior colliculus. *Brain Research,* 365, 350–354.

Middlebrooks, J.C., and E.I. Knudsen. 1984. A neural code for auditory space in the cat's superior colliculus. *Journal of Neuroscience,* 4, 2621–2634.

Middlebrooks, J.C., L. Xu, A.C. Eddins, and D.M. Green. 1998. Codes for sound-source location in nontonotopic auditory cortex. *Journal of Neurophysiology,* 80, 863–881.

Miyazaki, M., D. Nozaki, and Y. Nakajima. 2005. Testing Bayesian models of human coincidence timing. *Journal of Neurophysiology,* 94, 395–399.

Miyazaki, M., S. Yamamoto, S., Uchida, and S. Kitazawa. 2006. Bayesian calibration of simultaneity in tactile temporal order judgment. *Nature Neuroscience,* 9, 875–877.

Molholm, S., W. Ritter, M.M. Murray, D.C. Javitt, C.E. Schroeder, and J.J. Foxe. 2002. Multisensory auditory–visual interactions during early sensory processing in humans: A high-density electrical mapping study. *Brain Research. Cognitive Brain Research,* 14, 115–128.

Duplicate entry for Munhall et al. 1996 was deleted.

Munhall, K.G., P. Gribble, L. Sacco, and M. Ward. 1996. Temporal constraints on the McGurk effect. *Perception & Psychophysics,* 58, 351–362.

Munoz, D.P., and D. Guitton. 1991. Control of orienting gaze shifts by the tectoreticulospinal system in the head-free cat: II. Sustained discharges during motor preparation and fixation. *Journal of Neurophysiology,* 66, 1624–1641.

Munoz, D.P., D. Guitton, and D. Pelisson. 1991a. Control of orienting gaze shifts by the tectoreticulospinal system in the head-free cat: III. Spatiotemporal characteristics of phasic motor discharges. *Journal of Neurophysiology,* 66, 1642–1666.

Munoz, D.P., D. Pelisson, and D. Guitton. 1991b. Movement of neural activity on the superior colliculus motor map during gaze shifts. *Science,* 251, 1358–1360.

Murray, M.M., C.M. Michel, R. Grave De Peralta, S., Ortigue, D., Brunet, S. Gonzalez Andino, and A. Schnider. 2004. Rapid discrimination of visual and multisensory memories revealed by electrical neuroimaging. *NeuroImage,* 21, 125–135.

Murray, M.M., J.J. Foxe, and G.R. Wylie. 2005. The brain uses single-trial multisensory memories to discriminate without awareness. *NeuroImage,* 27, 473–478.

Nagy, A., G. Eordegh, and G. Benedek. 2003. Spatial and temporal visual properties of single neurons in the feline anterior ectosylvian visual area. *Experimental Brain Research,* 151, 108–114.

Navarra, J., A. Vatakis, M. Zampini, S. Soto-Faraco, W. Humphreys, and C. Spence. 2005. Exposure to asynchronous audiovisual speech extends the temporal window for audiovisual integration. *Brain Research. Cognitive Brain Research,* 25, 499–507.

Noesselt, T., J.W. Rieger, M.A. Schoenfeld, M. Kanowski, H. Hinrichs, H.J. Heinze, and J. Driver. 2007. Audiovisual temporal correspondence modulates human multisensory superior temporal sulcus plus primary sensory cortices. *Journal of Neuroscience,* 27, 11431–11441.

Pandey, P.C., H. Kunov, and S.M. Abel. 1986. Disruptive effects of auditory signal delay on speech perception with lipreading. *Journal of Auditory Research,* 26, 27–41.

Pasalar, S., T. Ro, and M.S. Beauchamp. 2010. TMS of posterior parietal cortex disrupts visual tactile multisensory integration. *European Journal of Neuroscience,* 31, 1783–1790.

Populin, L.C. 2005. Anesthetics change the excitation/inhibition balance that governs sensory processing in the cat superior colliculus. *Journal of Neuroscience,* 25, 5903–5914.

Powers 3rd, A.R., A.R. Hillock, and M.T. Wallace. 2009. Perceptual training narrows the temporal window of multisensory binding. *Journal of Neuroscience,* 29, 12265–12274.

Powers 3rd, A.R., M.A. Hevey, and M.T. Wallace. 2010. Neural correlates of multisensory perceptual learning. In preparation.

Qin, L., J.Y. Wang, and Y. Sato. 2008. Representations of cat meows and human vowels in the primary auditory cortex of awake cats. *Journal of Neurophysiology,* 99, 2305–2319.

Romei, V., M.M. Murray, L.B. Merabet, and G. Thut. 2007. Occipital transcranial magnetic stimulation has opposing effects on visual and auditory stimulus detection: implications for multisensory interactions. *Journal of Neuroscience,* 27, 11465–11472.

Rouger, J., S. Lagleyre, B. Fraysse, S. Deneve, O. Deguine, and P. Barone. 2007. Evidence that cochlear-implanted deaf patients are better multisensory integrators. *Proceedings of the National Academy of Sciences of the United States of America,* 104, 7295–7300.

Rowland, B.A., S. Quessy, T.R. Stanford, and B.E. Stein. 2007. Multisensory integration shortens physiological response latencies. *Journal of Neuroscience,* 27, 5879–5884.

Royal, D.W., B.N. Carriere, and Wallace. M.T. 2009. Spatiotemporal architecture of cortical receptive fields and its impact on multisensory interactions. *Experimental Brain Research,* 198, 127–136.

Schneider, T.R., A.K. Engel, and S. Debener. 2008. Multisensory identification of natural objects in a two-way crossmodal priming paradigm. *Experimental Psychology,* 55, 121–132.

Schorr, E.A., N.A. Fox, V. van Wassenhove, and E.I. Knudsen. 2005. Auditory–visual fusion in speech perception in children with cochlear implants. *Proceedings of the National Academy of Sciences of the United States of America,* 102, 18748–18750.

Seitz, A.R., R. Kim, and L. Shams. 2006. Sound facilitates visual learning. *Current Biology,* 16, 1422–1427.

Sekuler, R., A.B. Sekuler, and R. Lau. 1997. Sound alters visual motion perception. *Nature,* 385, 308.

Shams, L., Y. Kamitani, and S. Shimojo. 2000. Illusions. What you see is what you hear. *Nature,* 408, 788.

Shams, L., Y. Kamitani, and S. Shimojo. 2002. Visual illusion induced by sound. *Brain Research Cognitive Brain Research,* 14, 147–152.

Shore, D.I., C. Spence, and R.M. Klein. 2001. Visual prior entry. *Psychological Science,* 12, 205–212.

Soto-Faraco, S., and A. Alsius. 2009. Deconstructing the McGurk–MacDonald illusion. *Journal of Experimental Psychology. Human Perception and Performance,* 35, 580–587.

Soto-Faraco, S., A. Kingstone, and C. Spence. 2003. Multisensory contributions to the perception of motion. *Neuropsychologia,* 41, 1847–1862.

Sparks, D.L. 1986. Translation of sensory signals into commands for control of saccadic eye movements: Role of primate superior colliculus. *Physiological Reviews,* 66, 118–171.

Sparks, D.L., and Groh, J.M. 1995. The superior colliculus: A window for viewing issues in integrative neuroscience. In *The Cognitive Sciences,* ed. Gazzaniga, M.S. Cambridge, MA: MIT Press.

Spence, C., D.I. Shore, and R.M. Klein. 2001. Multisensory prior entry. *Journal of Experimental Psychology. General,* 130, 799–832.

Stanford, T.R., S. Quessy, and B.E. Stein. 2005. Evaluating the operations underlying multisensory integration in the cat superior colliculus. *Journal of Neuroscience,* 25, 6499–6508.

Stein, B.E., and M.A. Meredith 1993. *The Merging of the Senses.* Cambridge, MA: MIT Press.

Stein, B.E., and M.T. Wallace. 1996. Comparisons of cross-modality integration in midbrain and cortex. *Progress in Brain Research,* 112, 289–299.

Stein, B.E., E. Labos, and L. Kruger. 1973a. Determinants of response latency in neurons of superior colliculus in kittens. *Journal of Neurophysiology,* 36, 680–689.

Stein, B.E., E. Labos, and L. Kruger. 1973b. Sequence of changes in properties of neurons of superior colliculus of the kitten during maturation. *Journal of Neurophysiology,* 36, 667–679.

Stein, B.E., W.S. Huneycutt, and M.A. Meredith. 1988. Neurons and behavior: The same rules of multisensory integration apply. *Brain Research,* 448, 355–358.

Stein, B.E., M.A. Meredith, W.S. Huneycutt, and L. McDade. 1989. Behavioral indices of multisensory integration: Orientation to visual cues is affected by auditory stimuli. *Journal of Cognitive Neuroscience,* 1, 12–24.

Stein, B.E., N. London, L.K. Wilkinson, and D.D. Price. 1996. Enhancement of perceived visual intensity by auditory stimuli: A psychophysical analysis. *Journal of Cognitive Neuroscience,* 8, 497–506.

Stetson, C., X. Cui, P.R. Montague, and D.M. Eagleman. 2006. Motor-sensory recalibration leads to an illusory reversal of action and sensation. *Neuron,* 51, 651–659.

Stevenson, R.A., N.A. Altieri, S. Kim, D.B. Pisoni, and T.W. James. 2010. Neural processing of asynchronous audiovisual speech perception. *NeuroImage,* 49, 3308–3318.

Stone, J.V., N.M. Hunkin, J. Porrill, R. Wood, V. Keeler, M. Beanland, M. Port, and N.R. Porter. 2001. When is now? Perception of simultaneity. *Proceedings of the Royal Society of London. Series B. Biological Sciences,* 268, 31–38.

Sumby, W.H., and I. Pollack. 1954. Visual contribution to speech intelligibility in noise. *Journal of the Acoustical Society of America,* 26, 212–215.

Ter-Mikaelian, M., D.H. Sanes, and M.N. Semple. 2007. Transformation of temporal properties between auditory midbrain and cortex in the awake Mongolian gerbil. *Journal of Neuroscience,* 27, 6091–6102.

van Atteveldt, N.M., E. Formisano, L. Blomert, and R. Goebel. 2007. The effect of temporal asynchrony on the multisensory integration of letters and speech sounds. *Cerebral Cortex,* 17, 962–794.

van Wassenhove, V., K.W. Grant, and D. Poeppel. 2007. Temporal window of integration in auditory–visual speech perception. *Neuropsychologia,* 45, 598–607.

van Wassenhove, V., D.V. Buonomano, S. Shimojo, and L. Shams. 2008. Distortions of subjective time perception within and across senses. *PLoS One,* 3, e1437.

Von Kriegstein, K., and A.L. Giraud. 2006. Implicit multisensory associations influence voice recognition. *PLoS Biology,* 4, e326.

Vroomen, J., M. Keetels, B. De Gelder, and P. Bertelson. 2004. Recalibration of temporal order perception by exposure to audio-visual asynchrony. *Brain Research. Cognitive Brain Research,* 22, 32–35.

Wade, N.J., and R.H. Day. 1968. Development and dissipation of a visual spatial aftereffect from prolonged head tilt. *Journal of Experimental Psychology,* 76, 439–443.

Wallace, M.T., and B.E. Stein 1996. Sensory organization of the superior colliculus in cat and monkey. *Progress in Brain Research,* 112, 301–311.

Wallace, M.T., and B.E. Stein. 1997. Development of multisensory neurons and multisensory integration in cat superior colliculus. *Journal of Neuroscience,* 17, 2429–2444.

Wallace, M.T., and B.E. Stein 2000. Onset of cross-modal synthesis in the neonatal superior colliculus is gated by the development of cortical influences. *Journal of Neurophysiology,* 83, 3578–3582.

Wallace, M.T., and B.E. Stein 2001. Sensory and multisensory responses in the newborn monkey superior colliculus. *Journal of Neuroscience,* 21, 8886–8894.

Wallace, M.T., M.A. Meredith, and B.E. Stein 1992. Integration of multiple sensory modalities in cat cortex. *Experimental Brain Research,* 91, 484–488.

Wallace, M.T., L.K. Wilkinson, and B.E. Stein 1996. Representation and integration of multiple sensory inputs in primate superior colliculus. *Journal of Neurophysiology,* 76, 1246–1266.

Wallace, M.T., T.J. Perrault Jr., W.D. Hairston, and B.E. Stein. 2004. Visual experience is necessary for the development of multisensory integration. *Journal of Neuroscience,* 24, 9580–9584.

Wallace, M.T., B.N. Carriere, T.J. Perrault Jr., J.W. Vaughan, and B.E. Stein 2006. The development of cortical multisensory integration. *Journal of Neuroscience,* 26, 11844–11849.
Wang, X., T. Lu, R.K. Snider, and L. Liang. 2005. Sustained firing in auditory cortex evoked by preferred stimuli. *Nature,* 435, 341–346.
Xu, L., S. Furukawa, and J.C. Middlebrooks. 1999. Auditory cortical responses in the cat to sounds that produce spatial illusions. *Nature,* 399, 688–691.
Ye, C.Q., M.M. Poo, Y. Dan, and X.H. Zhang. 2010. Synaptic mechanisms of direction selectivity in primary auditory cortex. *Journal of Neuroscience,* 30, 1861–1868.
Zampini, M., D.I. Shore, and C. Spence. 2003. Audiovisual temporal order judgments. *Experimental Brain Research,* 152, 198–210.
Zampini, M., S. Guest, D.I. Shore, and C. Spence. 2005a. Audio-visual simultaneity judgments. *Perception & Psychophysics,* 67, 531–544.
Zampini, M., D.I. Shore, and C. Spence. 2005b. Audiovisual prior entry. *Neurosci Letters,* 381, 217–22.

Published in final edited form as:
J Comp Neurol. 2011 January 1; 519(1): 64–74. doi:10.1002/cne.22504.

Organization of somatosensory cortex in the northern grasshopper mouse (*Onychomys leucogaster*), a predatory rodent

Diana K. Sarko[1], **Duncan B. Leitch**[2,3], **Isabelle Girard**[4], **Robert S. Sikes**[5], and **Kenneth C. Catania**[3]

[1] Vanderbilt University, Department of Hearing and Speech Sciences, 7110 MRB III, Nashville, TN, 37232

[2] Vanderbilt University, Neuroscience Graduate Program, VU Station B, Box 35-1634, Nashville, TN, 37235-1634

[3] Vanderbilt University, Department of Biological Sciences, VU Station B, Box 35-1634, Nashville, TN, 37235-1634

[4] University of Wisconsin-Stevens Point, Department of Biology, Stevens Point, WI 54481

[5] University of Arkansas, Little Rock, Department of Biology, 2801 S. University Ave., Little Rock, AR 72204

Abstract

Northern grasshopper mice (*Onychomys leucogaster*) are among the most highly carnivorous rodents in North America. Because predatory mammals may have specialization of senses used to detect prey, we investigated the organization of sensory areas within grasshopper mouse neocortex and quantified the number of myelinated axons in grasshopper mouse trigeminal, cochlear, and optic nerves. Multiunit electrophysiological recordings combined with analysis of flattened sections of neocortex processed for cytochrome oxidase were used to determine the topography of primary somatosensory cortex (S1) and the location and size of both the visual and auditory cortex in adult animals. These findings were then related to the distinctive chemoarchitecture of layer IV visible in flattened cortical sections of juvenile grasshopper mice labeled with the serotonin transporter (SERT) antibody, revealing a striking correspondence between electrophysiological maps and cortical anatomy.

Keywords

S1; trigeminal; somatosensory; visual; forepaw; evolution; predator

Introduction

The northern grasshopper mouse (*Onychomys leucogaster*) is a small nocturnal mammal that inhabits short-grass prairies and semi-desert regions primarily in the western United States (Fig. 1A). Grasshopper mice differ from other rodents in being the most highly carnivorous genus of rodent in North America, with animal matter composing up to 89% of their diet (Horner et al., 1964;Landry, 1970). They occasionally prey on other small mammals such as

Correspondence to: Diana Sarko, Vanderbilt University, Department of Hearing and Speech Sciences, 7110 MRB III, Nashville, TN, 37232, Phone: (615) 936-7108, Fax: (615) 936-0212, diana.sarko@vanderbilt.edu.

pocket mice, deer mice, voles, and even cotton rats three times their weight (Horner et al., 1964;Ruffer, 1968;McCarty, 1978;Timberlake and Washburne, 1989). As might be expected, grasshopper mice exhibit behavioral and morphological adaptations commensurate with a predatory lifestyle including low population densities and large home ranges (Bailey and Sperry, 1929;Blair, 1953;Egoscue, 1960;Ruffer, 1968).

Studies of grasshopper mice also indicate that they are comparatively aggressive and resistant to the inhibitory effects of novel or aversive stimuli from prey (Timberlake and Washburne, 1989; Langley, 1994). Grasshopper mice have developed a resistance to the toxins from certain prey items such as Arizona bark scorpion venom (Rowe and Rowe, 2008) and are reported to be tenacious predators (Timberlake and Washburne, 1989; Langley, 1994). Whereas most animals learn to avoid noxious prey, grasshopper mice persistently attack insects with formidable defenses, enabling them to exploit prey that are avoided by other species. These behaviors include an impressive repertoire of tactics specific to the prey's defenses. For instance, the southern grasshopper mouse species (*Onychomys torridus*), subdues chemically-toxic stink beetles by forcing the caudal end of the beetle into the dirt and quickly biting off the head, thus avoiding their chemical spray (Eisner and Meinwald, 1966). Scorpions are disarmed by first immobilizing the stinger and then consuming the cephalothorax (Langley, 1981). Preying on lubber grasshoppers requires an initial attack aimed at the powerful legs that could otherwise injure the grasshopper mouse (Whitman et al., 1986). In the case of vertebrate prey, such as the horned lizard, vulnerable points such as the eyes are attacked to avoid the spiny scales (Frank, 1989). Small mammalian prey are often killed by an incisor bite aimed at the base of the skull (Bailey and Sperry, 1929) and occasionally grasshopper mice even strangle prey (Egoscue, 1960).

Grasshopper mice first diverged from *Peromyscus* (deer mice) in the late Miocene, approximately 6 million years ago, appearing in their present form in the middle Pliocene (Hibbard, 1968; McCarty, 1978). Fossil records of dentition suggest that grasshopper mice retained an omnivorous lifestyle until the radiation of deer mice and concurrent onset of competition for resources, at which point transition to a carnivorous lifestyle became evident in the Pleistocene (Carleton and Eshelman, 1979). Grasshopper mice appear to have developed numerous specializations for predation including: long claws that aid in seizure of prey with the forepaws; well-developed jaw muscles allowing strong bite force and a wide gape for consuming larger prey; modified dentition with shortened incisors and molars that are less adapted for grinding plant matter (Fig. 1B); and a modified stomach optimized for increased digestion of insects (Bailey and Sperry, 1929; Horner et al., 1964; Landry, 1970; Satoh and Iwaku, 2006). Here we investigate their central nervous system to explore potential neural correlates of the transition to carnivory. An additional goal is to provide data for comparative studies aimed at determining features of cortical organization common to mammals and features that may be unique to specific lineages or lifestyles. Using multiunit electrophysiological recordings we delineated the topography and orientation of neocortical sensory areas in the grasshopper mouse with a focus on primary somatosensory cortex. We relate these findings to modules and barrels in S1 and provide evidence for a least one additional somatosensory area in lateral cortex. In addition, we identify an auditory area and primary visual cortex (V1). Finally, we counted myelinated axons within the trigeminal, optic, and cochlear cranial nerves in order to assess the relative importance of somatosensation, vision, and audition in grasshopper mice.

Materials and Methods

Animals

Adult northern grasshopper mice (*Onychomys leucogaster*; n=9) from laboratory colonies at the University of Arkansas, Little Rock and the University of Wisconsin, Stevens Point were pair-housed and provided free access to food (rodent chow supplemented with mealworms and wax worms) and water in a 14/10-hour light/dark cycle at 68-77°F. Additionally, 3 pups were obtained from an adult breeding pair and sacrificed at P7, P9 and P13 (weights of 6.5, 6.9, and 9.0 g, respectively) to examine the timeline of serotonin transporter (SERT) expression in the neocortex. The skull of one additional adult grasshopper mouse was cleaned, sputter-coated with gold, and imaged using a Tescan Vega-II scanning electron microscope (Tescan USA Inc.) to illustrate cranial and dental features (Fig. 1B). All research procedures were approved by the Institutional Animal Care and Use Committee at Vanderbilt University.

Electrophysiology

A surgical plane of anesthesia was induced with an i.p. injection of 15% urethane in distilled water (1 g/kg) in adult grasshopper mice. Additional injections of 10% ketamine (15 mg/kg, i.p.) were given as needed. Body temperature was maintained with a heating pad and hot water bottles. Animals were secured by a head post with dental cement, and the left hemisphere of the cerebral cortex was exposed by craniotomy with the dura removed. The brain was protected with liquid silicon and a digital photograph of the cortical surface was taken. Tungsten microelectrodes (1.0 MΩ at 1 kHz) placed perpendicular to the cortical surface were used to perform multiunit electrode recordings in layer IV of the cortex. Neuronal responses were amplified and delivered to an oscilloscope and speaker. Selected electrode penetration sites were marked with electrolytic lesions (10 μA while withdrawing electrode at 50 μm/sec) to serve as anatomical landmarks.

Receptive fields of neurons at each penetration site were mapped by stimulating the teeth, vibrissae, and body surface. Mapping of receptive fields focused on cutaneous stimulation of the animal's body using calibrated monofilaments (von Frey hairs - synthetic hairs for quantitative mechanical stimulation of skin receptors). Responses to periodontal receptors of the teeth were evoked by light touch (using von Frey hairs) or light taps. Moving beams of light were used to identify visual responses. A series of clicks was used to evaluate auditory responses, although specific frequencies were not defined. Specific retinotopy and tonotopy of visual and auditory cortex respectively were not explored.

After each recording procedure was complete, grasshopper mice were given an overdose of sodium pentobarbital (at least 120 mg/kg, i.p.) and perfused transcardially with 0.01 M phosphate-buffered saline (PBS, pH 7.2) followed by 4% paraformaldehyde in 0.01 M PBS (pH 7.2). For each specimen the brain was removed and postfixed overnight. The cortex was separated and flattened, then cryoprotected in 30% sucrose/PBS, and a freezing microtome was used to cut sections at 50 μm parallel to the cortical surface.

Cortical immunohistochemistry and histochemistry

For each specimen, following sectioning, the left hemisphere was processed for the metabolic enzyme cytochrome oxidase (Wong-Riley, 1979) to reveal sensory areas. The right hemisphere of each juvenile specimen was processed using the anti-5-HT transporter antibody (SERT; rabbit polyclonal, 1:1000; Calbiochem/EMD Biosciences, La Jolla, CA, USA; isotype IgG; catalog number PC177L). The immunogen was a synthetic peptide corresponding to amino acids 602-622 of rat 5-HT transporter, and the specificity of this antibody has been determined by immunoblotting analysis using rat brain extracts of the

cortex, hypothalamus, midbrain, and hindbrain, which specifically detected a single band (Calbiochem/EMD Biosciences, La Jolla, CA, USA). This protein has been shown to recognize the serotonin (5-HT) transporter in the cortex, raphe nuclei, hypothalamus, and spinal cord of rats (Coccaro and Murphy, 1990; Blakely et al., 1994; Zhou et al., 1996; Boylan et al., 2000) and staining specificity has been previously characterized in rats (Coccaro and Murphy, 1990; Blakely et al., 1994; Zhou et al., 1996; Boylan et al., 2000), mice (Eagleson et al., 2007; Hoerder-Suabedissen et al., 2008), humans (Verney et al., 2002), vervet monkeys (Way et al., 2007), chimpanzees and rhesus macaques (Raghanti et al., 2008). Staining is completely eliminated by pretreatment of antibody with Serotonin (5-HT) Transporter Control Peptide (Calbiochem/EMD Biosciences, La Jolla, CA, USA; catalog number PP87) at a concentration of 5 μg/ml. Controls for the specificity of SERT labeling were provided by the use of preadsorption controls as well as the demonstration that labeling was characteristic of thalamocortical projection zones producing a pattern of immunoreactivity that appeared identical to that of other rodents (e.g., Eagleson et al., 2007). Negative controls omitting the primary antibody controlled for the specificity of the secondary antiserum. Sections were initially collected in tissue freezing medium and stored at -20°C for approximately 3 weeks. Briefly, as described elsewhere (Boylan et al., 2000; Eagleson et al., 2007), free-floating sections were incubated in primary antibody (anti-SERT) for 72 hours at 4°C followed by secondary incubations in biotin-SP-conjugated donkey anti-rabbit IgG (1:1000, Jackson ImmunoResearch, West Grove, PA, USA) for 1 hour at room temperature and processed by using the Vectastain ABC histochemical method (Vector Labs, Burlingame, CA, USA). Sections were treated for 4 minutes at room temperature in 0.5% 3′3′-diaminobenzidine (DAB) with 0.05% H_2O_2. The sections were washed, mounted onto gelatin-subbed slides, dehydrated with alcohols, cleared with CitriSolve (Fisher), and coverslipped in DPX (Fisher).

Cortical area measurement

Grayscale images of histological sections were acquired with a Zeiss AxioCam HRc camera (Zeiss, Jena, Germany) mounted onto a Zeiss Axioskop microscope and using Zeiss Axiovision 4.5 software. Images were imported into the public domain program ImageJ, version 1.33, for morphometric analysis. Figures were prepared using Adobe Photoshop CS3 (Adobe Systems Incorporated, San Jose, CA, USA) and adjusted to optimize contrast. Neocortical areas were measured using optimal tangential sections reacted for SERT or CO. Only those sections with the entire posteromedial barrel subfield (PMBSF) or primary visual area (V1) present were analyzed. The PMBSF and forelimb areas of S1, as well as area V1, were measured in representative sections with the clearest outline in flattened cortical sections from juvenile specimens (P7 and P9) reacted for SERT. Forelimb area is reported as a percentage of S1 both including and excluding oral/intraoral modules because these latter areas may have been excluded from previous analyses. Flattened cortical sections from adult specimens processed for cytochrome oxidase were also measured for PMBSF and V1 area.

Nerve processing and axon quantification

Following perfusion portions of the optic (n=4), trigeminal (n=4) and cochlear nerves (n=3) (~1 mm for each) were excised and placed in 2.5% glutaraldehyde in 0.1 M PBS, pH 7.4, for at least one hour. Each sample was washed twice with 0.2 M PBS, pH 7.4, for 10 minutes and postfixed for 2 hours with OsO_4 in 0.1 M PBS, pH 7.4. Samples were then washed twice in 0.1M PBS followed by dehydration in a graded series of ethanol washes culminating in three changes of 100% ethanol. Individual samples were then placed on a rotator overnight in a 1:1 mixture of EMBed812 (EM Sciences) to 100% propylene oxide. This was followed by placement in 100% EMBed812 resin for 2 hours. Finally, samples were polymerized in an oven at 70°C overnight. Samples were sectioned with a diamond

knife (Diatome US, Hatfield, PA, USA) on a Reichert Ultracut E ultramicrotome at 0.5 μm. Sections were transferred to glass slides, stained with 1% toluidine blue, and coverslipped.

Optimal cross-sections of each nerve were imaged at 100× as described above. Images were imported into Adobe Photoshop CS3 (Adobe Systems Incorporated, San Jose, CA, USA) and montaged to create a composite image of the entire nerve. Axons were then counted manually (see Figure 4).

Results

Histochemical and immunohistochemical characterization

Because serotonin immunoreactivity presents a transient postnatal pattern in the primary sensory cortical areas of rats, mice, and hamsters that matches the distribution of thalamocortical axon terminals (Fujimiya et al., 1986; D'Amato et al., 1987; Rhoades et al., 1990; Bennett-Clarke et al., 1993; Boylan et al., 2000) we first used immunohistochemistry to determine the developmental time course of expression of the serotonin transporter (SERT) on thalamocortical afferents in the primary sensory areas of the cortex. SERT expression was present at P7 and P9 but became barely discernible at P13 (Fig. 2), a time course intermediate between that of mice (Fujimiya et al., 1986) and rats (D'Amato et al., 1987; Boylan et al., 2000). The labeling of thalamocortical afferents allowed us to clearly delineate the boundaries of primary sensory areas in flattened preparations of neocortex. Subsequent electrophysiological recordings revealed how the different modules visible in S1 corresponded to representations of various body parts (Fig. 3). SERT labeling also corresponded well with flattened cortical preparations sectioned through layer IV and processed for cytochrome oxidase, differentiating regions of chronically high metabolic activity and thus distinguishing primary sensory areas (Wong-Riley et al., 1979). Characteristic CO-densely regions were present for the head, trunk, and limb representations within S1, including prominent barrels within the head representation and a large forelimb representation relative to the hindlimb. Far lateral cortex also contained multiple modular representations of oral structures including the tongue, lower and upper incisor, and intraoral regions.

We quantified the area of V1 along with the area of a well-defined portion of S1, the posteromedial barrel subfied (PMBSF), to allow comparisons with other species (e.g., see Kaskan et al., 2005). Total neocortical area in juvenile grasshopper mice (n = 2) was 36.70 ± 0.32 mm^2, with V1 occupying 4.26 ± 0.54 mm^2 (approximately 12%) and PMBSF of S1 occupying 0.90 ± 0.08 mm^2 (approximately 5%). Total neocortical area in adult grasshopper mice (n = 4) was 58.31 ± 1.44 mm^2, with V1 occupying 8.47 ± 0.46 mm^2 (approximately 15%) and PMBSF occupying 2.98 ± 0.10 mm^2 (approximately 5%). To further assess the dedication of neural resources across the primary sensory modalities the optic, trigeminal, and cochlear nerves were sectioned and the number of axons within each was quantified (see Fig. 4). The trigeminal nerve was by far the largest in absolute size, but contained only one third the number of myelinated axons (24,105) found in the thinner optic nerve (78,646). The cochlear nerve was the smallest, containing only 5,887 myelinated axons.

Multiunit electrophysiological recordings: primary somatosensory cortex

Recordings were made from nine adult grasshopper mice for a total of 564 electrode penetration sites with strong responses to light stimulation of the skin, fur, whiskers and periodontium. Primary somatosensory cortex (S1) was identified as a complete and systematic representation of the contralateral body surface. The somatotopic map for S1 was orderly and continuous in each case with a single representation of each body part present.

Figure 5 shows the recording data from a representative case with 68 electrode penetrations from which responses were recorded while stimulating the body, face, and periodontium (additional cases can be seen in supplemental Figures 1-4). These recordings delineated a complete map of the contralateral face and body surface with responses to stimulation of the skin surface and pelage fur, whiskers, incisors, tongue, and intraoral region. Within S1 the orientation of the body representation was inverted such that the hindlimb and tail were located medially and the face and oral structures were located laterally. The somatotopic organization of the body representation is shown with receptive fields illustrated for a progression of selected penetration sites (Fig. 5; note that numerical and alphabetical order does not necessarily reflect temporal progression during recordings). Penetration sites 1-3 delineate the location of the hindlimb representation (site 1, located medially) relative to the trunk (site 2) and the forelimb (site 3). The digits were located rostrally within the forelimb representation and there was a rostral-to-caudal progression from the thumb to more distal digit representations (Fig 5, sites 4-7), respectively, as has been shown in other rodents (Dawson and Killackey, 1987;Henry et al., 2006).

The forepaw representation appeared to be relatively large in grasshopper mouse S1. This was primarily evident during electrophysiological mapping. Of the 564 recording sites across 9 animals, 91 responded to forelimb stimulation and 69 were specific to the forepaw. Also, despite the otherwise broad receptive fields characteristic of S2/PV, recording sites responsive to the forepaw alone were found in several instances (see below). In the flattened cortex preparations labeled for SERT, the forelimb representation occupied 17.5% of S1 in the P7 grasshopper mouse (19% with oral/intraoral modules excluded) and 15.5% of total S1 in a P9 grasshopper mouse (17.2% with oral/intraoral included).

Electrode penetrations further lateral in cortex responded to stimulation of the head beginning with the chin, followed by the lower lip and tongue, the intraoral region, and the upper lip and upper incisor as the electrode was moved more laterally (Fig 5, sites 8-15). Site 15 responded to stimulation of both the upper and lower incisor and might correspond to the mixed incisor representation found in rat S2 (Remple et al., 2003). This sequence continued to a penetration site responsive to stimulation of the nose (site 16) and a rostrocaudal sequence of individual whiskers (sites 17-19). A separate pair of penetrations (sites A-B) illustrates the orientation of the vibrissae representation, with a ventrally located vibrissa on the mystacial pad (site A) represented medial to a dorsally located vibrissa (site B) of the mystacial pad. Two additional sites in this case responded more broadly and weakly to tactile stimulation of the forepaw (site a) and whiskers (site b) and likely represent S2 or PV based on response properties, location, and histochemical staining characteristics (see next section). Finally, a relatively large cortical area responded strongly to visual stimuli and a more lateral area of the cortex responded to auditory stimuli. The overall somatotopy of the body representation in S1 was investigated in 8 additional mapping cases. Four of these cases are illustrated in supplemental Figures 1-4.

Additional somatosensory areas

Along the caudolateral extent of S1, responses to stimulation of the body surface were weaker and associated with larger receptive fields. Recordings identified at least one additional representation of the contralateral body surface composed of a smaller, mirror-image of S1 and sharing a common border at the midline representation of the face and snout. Within this area, the face representation was located rostromedially and the limbs and trunk were located caudolaterally. Four cases (Figs. 5; supplemental Figs. 1, 3 and 4) provided evidence for additional somatosensory areas lateral to S1, however the most complete map is shown in Fig. 6 (showing S2/PV; for the complete case see supplemental Fig. 4). Receptive fields for the whiskers generally encompassed the entire mystacial field (e.g., Fig. 5 site b) and receptive fields for the body often included limbs and trunk (Fig. 6

site b) or almost the entire contralateral body surface (Fig. 6 sites e-f). Although this area was darkly labled in SERT-processed sections from juveniles, it did not contain barrels typical of the S1 representation of whiskers and forepaw pads.

The overall somatotopy in this region suggests that many of the electrode penetrations were located in S2 (e.g., Sur et al., 1981; Krubitzer et al., 1986). The facial representation was organized such that rostral surfaces of the periphery were represented more rostrally (e.g. supplemental Fig. 3, sites a-b) whereas the forelimb representation was located lateral to the face representation (Fig. 5 sites a-b; Fig. 6 sites a-b) and at some sites the receptive fields were restricted to the forepaw (e.g. Fig. 5 site a; also see supplemental Fig. 3, site c). As the electrode was moved more caudally, the trunk, hindlimb, and tail representations were identified (Fig. 6 sites b-f).

Visual and auditory areas

Although receptive fields were not mapped, strong visual and auditory responses were obtained from a number of cortical areas. Large areas of neocortex were devoted to vision and a smaller area of cortex responded to auditory stimuli (e.g., Figs. 5). In one case (supplemental Fig. 3), cortical areas rostral and caudolateral to visually-responsive cortex responded to both auditory and visual stimuli, although auditory responses rapidly habituated.

Discussion

Using multiunit electrophysiological recordings, combined with sections of flattened neocortex, we investigated the organization of S1 and found evidence for at least one additional somatosensory area in the lateral cortex of grasshopper mice. Primary visual cortex and an auditory area were also identified based on their distinctive appearances in sections processed for cytochrome oxidase or SERT-immunolabeling and their responses to visual and auditory stimuli. In addition, myelinated axons were quantified from trigeminal, optic, and cochlear nerves. A composite showing the relative sizes of sensory areas within the neocortex as well as the topographical organization of primary somatosensory cortex is shown in Figure 7.

Primary somatosensory cortex

The neocortex of the grasshopper mouse contained a large and distinctive primary somatosensory cortex (S1) consisting of a complete somatotopic map of the contralateral body surface, as found in other rodents (Welker, 1971, 1976; Dawson and Killackey, 1987; Waters et al., 1995; Henry et al., 2006; Campi et al., 2007). S1 was easily identified in grasshopper mice based on relative location, orientation, histological characteristics, and response properties. In particular, the cortex from juveniles processed for SERT provided a striking correlation between histologically visible modules, including barrels, and the representations of different body parts (Figs. 2-3).

As in most other rodent species, the large mystacial vibrissae dominated the somatosensory representation and corresponded to a prominent barrel field visible in both CO and SERT processed sections. Smaller barrels were located more rostrally and laterally, corresponding to the microvibrissae (buccal pad) around the oral region. At the far lateral and rostral extreme of S1, responses were primarily obtained from oral structures including the lips, tongue, and teeth. This region of cortex is not always investigated during electrophysiological experiments, perhaps because of its far lateral position in the neocortex, and the difficulty localizing oral receptive fields. However recent investigations suggest that

most mammals have a relatively large representation of oral structures in this location (Manger, 1996; Jain et al., 2001; Remple et al., 2003; Kaas et al., 2006; Iyengar et al., 2007).

The forepaw representation also appeared to be a relatively large component of grasshopper mouse S1. Behavioral observations indicate that grasshopper mice initially use their forepaws to seize and manipulate fast-moving prey such as crickets. In contrast, deer mice (rodents of similar size and overlapping habitat) and hamsters seize prey with their mouth (Langley, 1994). This suggests a more specialized attack by grasshopper mice (Eisenberg and Leyhausen, 1972) that relies on the forelimb, and perhaps corresponds to a magnification of this representation relative to other rodents (Dawson and Killackey, 1987).

Additional Somatosensory Areas

Evidence for at least one additional somatosensory area was found in lateral cortex. In the most extensive case, a complete representation of the contralateral body surface (e.g. Fig. 6) was found, with the face and whiskers represented more rostromedially whereas the limbs and trunk of the body were represented caudolaterally. This area was a mirror image of S1 with a common border along the midline of the snout and vibrissae fields. As the electrode was moved laterally, across the S1 border, receptive fields became markedly larger as has been reported for both S2 and PV (Nelson et al., 1979;Carvell and Simons, 1986;Krubitzer et al., 1986;Krubitzer and Kaas, 1990;Krubitzer and Calford, 1992;Krubitzer et al., 1995;Remple et al., 2003). The larger receptive fields were consistent with the small overall size of S2 and PV compared to S1, following the principle that receptive field size is inversely proportional to area of neocortical representation (Sur et al., 1980). Because two lateral somatosensory areas (S2 and PV) are found in most small mammals, it seems likely that we have recorded from both S2 and PV in different cases in the present investigation. Thus we have labeled the area S2/PV to reflect this interpretation.

Visual and auditory cortex

A distinctive primary visual area (V1) was identified in flattened cortical sections (e.g., Fig. 3) and electrophysiological mapping (e.g., Fig. 5) of grasshopper mouse neocortex. Additional visual responses were obtained lateral to V1, some of which almost certainly correspond to V2 as identified in a wide range of mammals and other rodents (Rosa and Krubitzer, 1999). V2 typically occupies a band of cortex just lateral to V1 and contains a retinotopic map in a mirror image of V1. In one case areas between V1 and the auditory area responded to both visual and auditory stimuli (supplementary figure 3) and in another case there was interdigitation of somatosensory and visual stimuli (supplementary figure 4), suggesting that cortex lateral to V2 may be involved in multimodal processing and perhaps some parts of V2 and auditory cortex process multiple modalities (e.g. Campi et al., 2007). Further studies would be necessary to evaluate whether visual structures (V1 and the optic nerve) are larger than would be predicted allometrically for grasshopper mice (see Kaskan et al., 2005 and Finlay et al., 2008), and if so, whether that might be an adaptation to predation. Deer mice would be a particularly intriguing comparison as a closely related herbivorous species.

A distinctive and uniformly dark area in CO and SERT processed sections corresponded to auditory cortex, as is often reported for other species. The histochemically apparent region responded to auditory stimuli and was relatively small compared to primary somatosensory and visual areas. However auditory responses were found beyond the boundaries of this module in some cases (see supplementary data), suggesting a larger extent of cortex may be involved in auditory processing than indicated by the borders of the CO dense region.

Behavioral studies of grasshopper mouse auditory acuity have produced contradictory results. Although several studies suggest that audition is well-developed in the grasshopper mouse and important for capturing prey (Bailey and Sperry, 1929; Egoscue, 1960; Langley, 1983), sound localization tests revealed a poor discrimination threshold similar to that of other rodents (Heffner and Heffner, 1988). Despite poor discrimination thresholds, grasshopper mice appeared to make more efficient use of binaural cues than their herbivorous counterparts (Heffner and Heffner, 1988) but otherwise did not appear to have specialized levels of auditory sensitivity for predation (Heffner and Heffner, 1985). However, the repertoire of vocalizations and use of calling behaviors – particularly alarm calls – in the grasshopper mouse is thought to be extensive and critical for survival. Many of these calls exist in the ultrasonic range, which was not explored in the present study and might account for a larger area of auditory cortex than was delineated electrophysiologically.

In summary, grasshopper mouse neocortex is dominated by large visual and somatosensory areas and a smaller auditory region in lateral cortex. This is generally consistent with the volumes of afferent input quantified for selected cranial nerves, with approximately 78,600, 24,100, and 5,800 myelinated afferents found in the optic, trigeminal, and cochlear nerves respectively. Flattened sections of juvenile cortex processed for SERT reveal the precise borders of primary visual cortex, the detailed representations of individual body parts in primary somatosensory cortex, and the approximate size of an auditory area that likely includes A1 and perhaps surrounding auditory areas.

Supplementary Material

Refer to Web version on PubMed Central for supplementary material.

Acknowledgments

We thank Danielle Gauthier for excellent technical assistance and Dr. Kathie Eagleson for optimization of SERT staining in this species. Thanks also to Jan Decher for the image shown in Fig. 1A and to the Vanderbilt Department of Animal Care for their attentive oversight of the grasshopper mice.

Grant sponsor: NIH grant # DE016061 and an NSF grant# 0844743 to K.C.C.

Literature Cited

Bailey V, Sperry CC. Life history and habits of grasshopper mice, *Onychomys*. Tech Bull US Dept Agric. 1929; 145:1–19.

Beck PD, Pospichal MW, Kaas JH. Topography, architecture, and connections of somatosensory cortex in opossums: evidence for five somatosensory areas. J Comp Neurol. 1996; 366:109–133. [PubMed: 8866849]

Bennett-Clarke CA, Leslie MJ, Chiaia NL, Rhoades RW. Serotonin 1B receptors in the developing somatosensory and visual cortices are located on thalamocortical axons. Proc Natl Acad Sci USA. 1993; 90:153–157. [PubMed: 8419917]

Blair WF. Population dynamics of rodents and other small mammals. Adv Genet. 1953; 5:1–41. [PubMed: 13040131]

Blakely RD, De Felice LJ, Hartzell HC. Molecular physiology of norepinephrine and serotonine transporters. J Exp Biol. 1994; 196:263–281. [PubMed: 7823027]

Boylan CB, Bennett-Clarke CA, Chiaia NL, Rhoades RW. Time course of expression and function of the serotonin transporter in the neonatal rat's primary somatosensory cortex. Somatosens Mot Res. 2000; 17:52–60. [PubMed: 10833084]

Campi KL, Karlen SJ, Bales KL, Krubitzer L. Organization of sensory neocortex in prairie voles (Microtus ochrogaster). J Comp Neurol. 2007; 502:414–426. [PubMed: 17366609]

Carleton, MD.; Eshelman, RE. A synopsis of fossil grasshopper mice, genus *Onychomys*, and their relationship to recent species (Papers on Paleontology, No 21). Ann Arbor: Museum of Paleontology, University of Michigan; 1979. p. 45-47.

Carvell GE, Simons DJ. Somatotopic organization of the secondary somatosensory area (SII) in the cerebral cortex of the mouse. Somatosens Res. 1986; 3:213–237. [PubMed: 3749662]

Coccaro, EF.; Murphy, DL. Serotonin in major disorders (progress in psychiatry series). Amer Psych P; Washington D.C.: 1990.

D'Amato RJ, Blue ME, Largent BL, Ledbetter DJ, Molliver ME, Snyder SH. Ontogeny of the serotonergic projection to rat neocortex: transient expression of a dense innervation to primary sensory areas. Proc Natl Acad Sci USA. 1987; 84:4322–4326. [PubMed: 3473503]

Dawson DR, Killackey HP. The organization and mutability of the forepaw and hindpaw representations in the somatosensory cortex of the neonatal rat. J Comp Neurol. 1987; 256:246–256. [PubMed: 3558880]

Eagleson KL, Schlueter McFadyen-Ketchum LJ, Ahrens ET, Mills PH, Does MD, Nickols J, Levitt P. Disruption of Foxg1 expression by knock-in of Cre recombinase: effects on the development of the mouse telencephalon. Neuroscience. 2007; 148:385–399. [PubMed: 17640820]

Egoscue HJ. Laboratory and field studies of the northern grasshopper mouse. J Mammal. 1960; 41:99–110.

Eisenberg J, Leyhausen P. The phylogenesis of predatory behavior in mammals. Zeitschrift fur Tierpsychologie. 1972; 30:59–93. [PubMed: 5063891]

Eisner T, Meinwald J. Defensive secretions of arthropods. Science. 1966; 153:1341–1350. [PubMed: 17814381]

Finlay BL, Franco EC, Yamada ES, Crowley JC, Parsons M, Muniz JA, Silveira LC. Number and topography of cones, rods and optic nerve axons in New and Old World primates: implications for the evolution of retinal development. Vis Neurosci. 2008; 25:289–299. [PubMed: 18598400]

Fujimiya M, Kimura H, Maeda T. Postnatal development of serotonin nerve fibers in the somatosensory cortex of mice studied by immunohistochemistry. J Comp Neurol. 1986; 246:191–201. [PubMed: 3082945]

Frank, DH. Diss. Cornell U; 1989. Spatial organization, social behavior, and mating strategies of the southern grasshopper mouse (*Onychomys torridus*) in southeastern Arizona.

Heffner HE, Heffner RS. Hearing in two cricetid rodents: wood rat (Neotoma floridana) and grasshopper mouse (Onychomys leucogaster). J Comp Psychol. 1985; 99:275–288. [PubMed: 3899497]

Heffner RS, Heffner HE. Sound localization in a predatory rodent, the northern grasshopper mouse (*Onychomys leucogaster*). J Comp Psychol. 1988; 102:66–71. [PubMed: 3365945]

Henry EC, Remple MS, O'Riain MJ, Catania KC. Organization of somatosensory cortical areas in the naked mole-rat (*Heterocephalus glaber*). J Comp Neurol. 2006; 495:434–452. [PubMed: 16485289]

Hibbard, CW. Paleontology. In: King, JA., editor. Biology of *Peromyscus*. Special publication no 2. Amer Soc Mammal; Stillwater, Oklahoma: 1968. p. 6-26.

Hoerder-Suabedissen A, Paulsen O, Molnár Z. Thalamocortical maturation in mice is influenced by body weight. J Comp Neurol. 2008; 511:415–420. [PubMed: 18803242]

Horner BE, Taylor JM, Padykula HA. Food habits and gastric morphology of the grasshopper mouse. J Mammal. 1964; 45:513–535.

Iyengar S, Qi H, Jain N, Kaas JH. Cortical and thalamic connections of the representations of the teeth and tongue in somatosensory cortex of new world monkeys. J Comp Neurol. 2007; 501:95–120. [PubMed: 17206603]

Jain N, Qi HX, Catania KC, Kaas JH. Anatomic correlates of the face and oral cavity representations in the somatosensory cortical area 3b of monkeys. J Comp Neurol. 2001; 429:455–68. [PubMed: 11116231]

Jeon CJ, Strettoi E, Masland RH. The major cell populations of the mouse retina. J Neurosci. 1998; 18:8936–8946. [PubMed: 9786999]

Kaas JH, Qi HX, Iyengar S. Cortical network for representing the teeth and tongue in primates. Anat Rec. 2006; 288:182–190.

Kaskan PM, Franco EC, Yamada ES, Silveira LC, Darlington RB, Finlay BL. Peripheral variability and central constancy in mammalian visual system evolution. Proc Biol Sci. 2005; 272:91–100. [PubMed: 15875575]

Krubitzer LA, Calford MB. Five topographically organized fields in the somatosensory cortex of the flying fox: microelectrode maps, myeloarchitecture, and cortical modules. J Comp Neurol. 1992; 317:1–30. [PubMed: 1573055]

Krubitzer LA, Kaas JH. The organization and connections of somatosensory cortex in marmosets. J Neurosci. 1990; 10:952–974. [PubMed: 2108231]

Krubitzer L, Manger P, Pettigrew J, Calford M. Organization of somatosensory cortex in monotremes: in search of the prototypical plan. J Comp Neurol. 1995; 351:261–306. [PubMed: 7699113]

Krubitzer LA, Sesma MA, Kaas JH. Microelectrode maps, myeloarchitecture, and cortical connections of three somatotopically organized representations of the body surface in the parietal cortex of squirrels. J Comp Neurol. 1986; 250:403–430. [PubMed: 3760247]

Landry SO Jr. The rodents as omnivores. Quart Rev Biol. 1970; 45:351–372. [PubMed: 5500524]

Langley W. Effect of prey defenses on attack behavior of *Onychomys torridus*. Zeitschrift fur Tierpsych. 1981; 56:115–127.

Langley WM. Relative importance of the distance senses in grasshopper mouse predatory behavior. Anim Behav. 1983; 31:199–205.

Langley WM. Comparison of predatory behaviors of deer mice (*Peromyscus maniculatus*) and grasshopper mice (*Onychomys leucogaster*). J Comp Psychol. 1994; 108:394–400.

Manger PR, Woods TM, Jones EG. Representation of face and intra-oral structures in area 3b of macaque monkey somatosensory cortex. J Comp Neurol. 1996; 371:513–521. [PubMed: 8841906]

McCarty R. Mammalian Species, *Onchymys leucogaster*. Amer Soc Mammal. 1978; 87:1–6.

Nelson RJ, Sur M, Kaas JH. The organization of the secondary somatosensory area (SmII) of the grey squirrel. J Comp Neurol. 1979; 184:473–490. [PubMed: 422752]

Raghanti MA, Stimpson CD, Marcinkiewicz JL, Erwin JM, Hof PR, Sherwood CC. Differences in cortical serotonergic innervation among humans, chimpanzees, and macaque monkeys: a comparative study. Cereb Cortex. 2008; 18:584–597. [PubMed: 17586605]

Remple MS, Henry EC, Catania KC. Organization of somatosensory cortex in the laboratory rat (*Rattus norvegicus*): evidence for two lateral areas joined at the representation of the teeth. J Comp Neurol. 2003; 467:105–118. [PubMed: 14574683]

Rhoades RW, Mooney RD, Chiaia NL, Bennett-Clarke CA. Development and plasticity of the serotoninergic projection to the hamster's superior colliculus. J Comp Neurol. 1990; 299:151–166. [PubMed: 2172325]

Rosa MG, Krubitzer LA. The evolution of visual cortex: where is V2? Trends Neurosci. 1999; 22:242–248. [PubMed: 10354599]

Rowe AH, Rowe MP. Physiological resistance of grasshopper mice (*Onychomys* spp.) to Arizona bark scorpion (*Centruroides exilicauda*) venom. Toxicon. 2008; 52:597–605. [PubMed: 18687353]

Ruffer DG. Agonistic behavior of the northern grasshopper mouse (*Onychomys leucogaster breviauritus*). J Mamm. 1968; 49:481–487.

Satoh K, Iwaku F. Jaw muscle functional anatomy in northern grasshopper mouse, *Onychomys leucogaster*, a carnivorous murid. J Morph. 2006; 267:987–999. [PubMed: 16710844]

Sur M, Merzenich MM, Kaas JH. Magnification, receptive-field area, and “hypercolumn” size in areas 3b and 1 of somatosensory cortex in owl monkeys. J Neurophysiol. 1980; 44:295–311. [PubMed: 7411189]

Sur M, Weller RE, Kaas JH. The organization of somatosensory area II in tree shrews. J Comp Neurol. 1981; 201:121–133. [PubMed: 7276248]

Timberlake W, Washburne DL. Feeding ecology and laboratory predatory behavior toward live and artificial moving prey in seven rodent species. Animal Learning & Behavior. 1989; 17(1):2–11.

Verney C, Lebrand C, Gaspar P. Changing distribution of monoaminergic markers in the developing human cerebral cortex with special emphasis on the serotonin transporter. Anat Rec. 2002; 267:87–93. [PubMed: 11997877]

Waters RS, Li CX, McCandlish CA. Relationship between the organization of the forepaw barrel subfield and the representation of the forepaw in layer IV of rat somatosensory cortex. Exp Brain Res. 1995; 103:183–197. [PubMed: 7789426]

Way BM, Laćan G, Fairbanks LA, Melega WP. Architectonic distribution of the serotonin transporter within the orbitofrontal cortex of the vervet monkey. Neuroscience. 2002; 148:937–948. [PubMed: 17766046]

Welker C. Microelectrode delineation of fine grain somatotopic organization of (SmI) cerebral neocortex in albino rat. Brain Res. 1971; 26:259–275. [PubMed: 4100672]

Welker C. Receptive fields of barrels in the somatosensory neocortex of the rat. J Comp Neurol. 1976; 166:173–189. [PubMed: 770516]

Whitman DW, Blum MS, Jones CG. Prey specific attack behavior in the southern grasshopper mouse, *Onychomys torridus*. Anim Behav. 1986; 34:295–297.

Wong-Riley M. Changes in the visual system of monocularly sutured or enucleated cats demonstrable with cytochromes oxidase histochemistry. Brain Res. 1979; 171:11–28. [PubMed: 223730]

Zhou FC, Xu Y, Bledsoe S, Lin R, Kelley MR. Serotonin transporter antibodies: production, characterization, and localization in the brain. Brain Res Mol Brain Res. 1996; 43:267–278. [PubMed: 9037542]

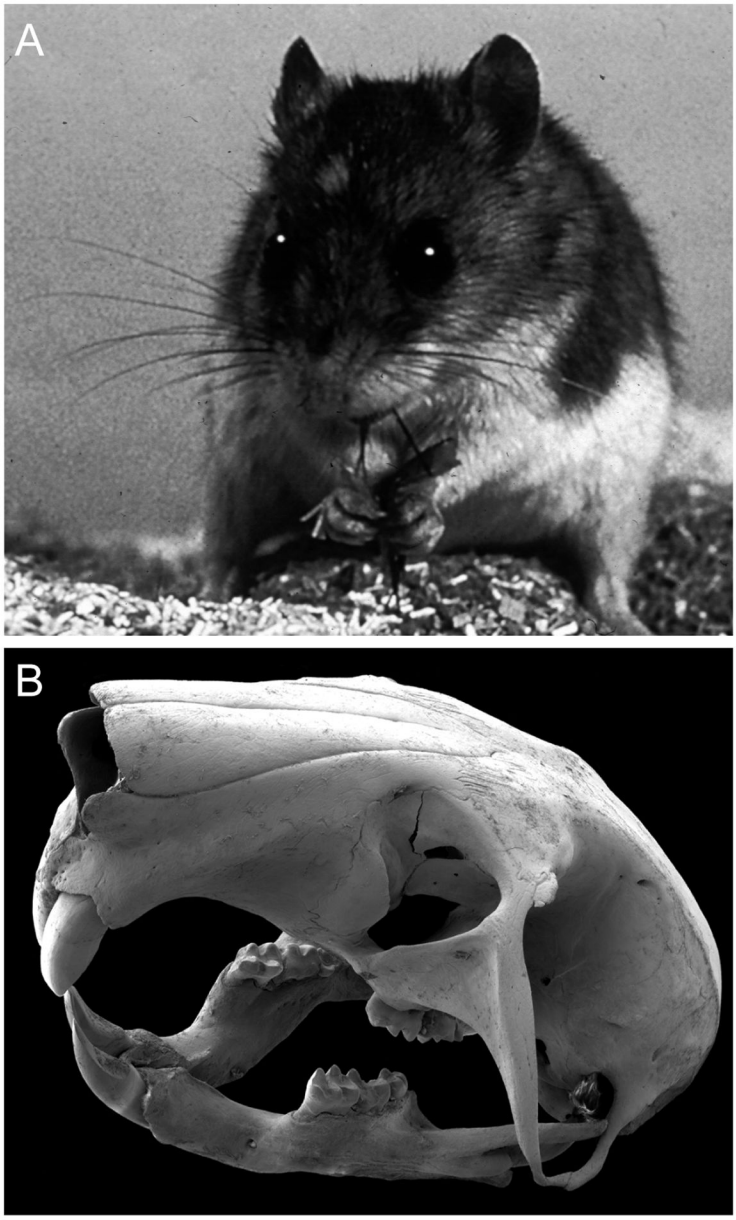

Figure 1.
The grasshopper mouse (A) is a carnivorous rodent with prominent vibrissae and long claws. B) A grasshopper mouse skull imaged using a scanning electron microscope illustrates dentition modified for carnivory. Image for A provided by Jan Decher. The black background was digitally shaded in B.

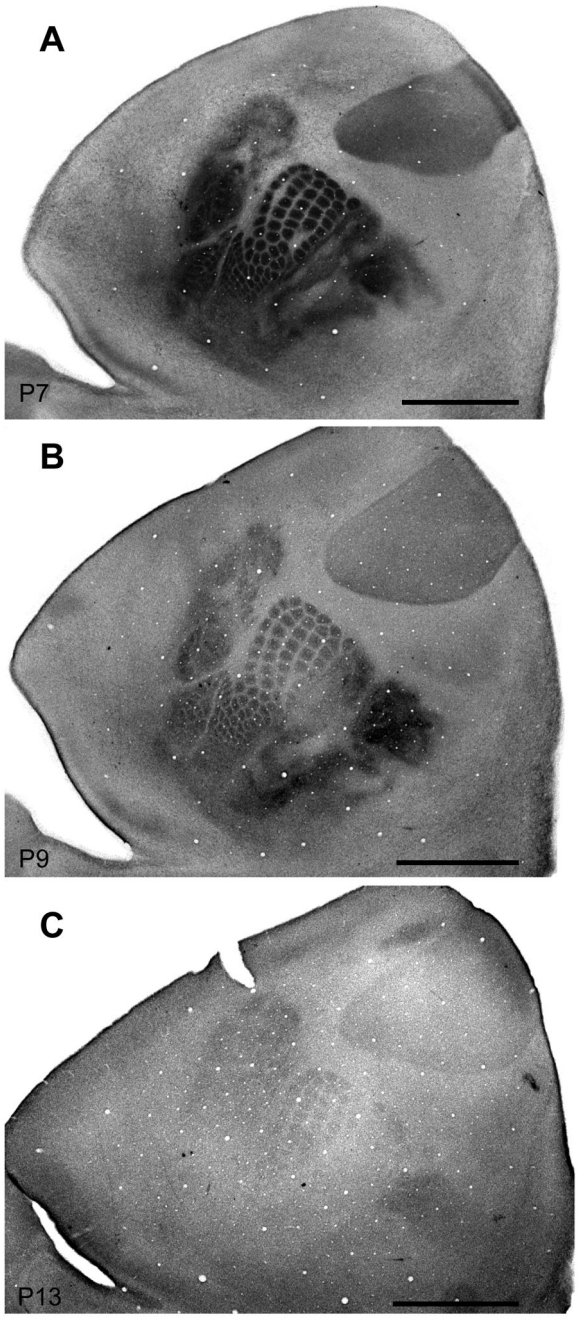

Figure 2.
Flattened cortical sections of juvenile grasshopper processed for the serotonin transporter (SERT). A-C show the time course of expression of SERT for thalamocortical afferents in the primary sensory areas. In postnatal grasshopper mice SERT expression persisted until P13 (C) when it became barely discernible, a time course similar to that of other rodents. SERT labeling also corresponded well with flattened cortex sections through layer IV that were processed for cytochrome oxidase and distinguished primary sensory areas. Scale bar = 2 mm.

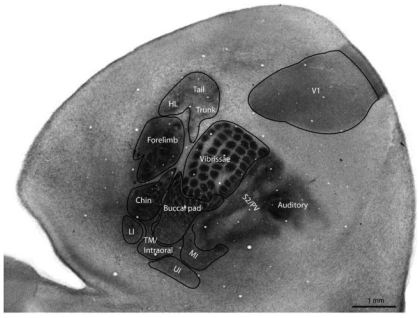

Figure 3.

Flattened cortical section from a juvenile grasshopper mouse (P7) labeled for primary sensory areas and for functional subdivisions within somatosensory cortex. The labeling of SERT-positive thalamocortical afferents delineated the boundaries of primary sensory areas, allowing assignment of preliminary functional representations that were subsequently confirmed through cortical recordings. HL = hindlimb, LI = lower incisor, MI = mixed incisor, PV = parietal ventral cortex, S2 = secondary somatosensory cortex, UI = upper incisor, V1 = primary visual cortex.

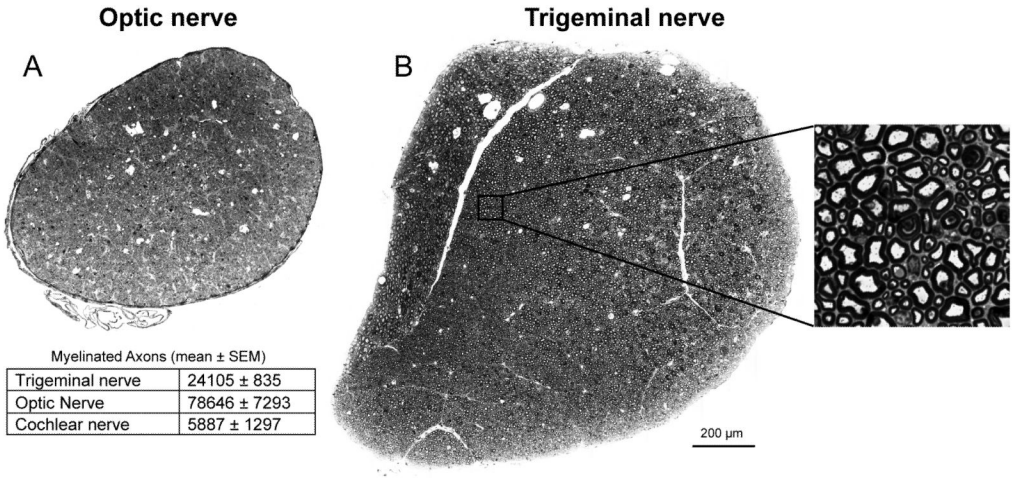

Myelinated Axons (mean ± SEM)

Trigeminal nerve	24105 ± 835
Optic Nerve	78646 ± 7293
Cochlear nerve	5887 ± 1297

Figure 4.

Semi-thin light microscopic preparations and quantification of myelinated axons in trigeminal, cochlear and optic nerves. Cross-sections of representative optic (A) and trigeminal (B) nerves from the grasshopper mouse, shown at the same scale, illustrate their relative sizes and the myelinated axons (inset).

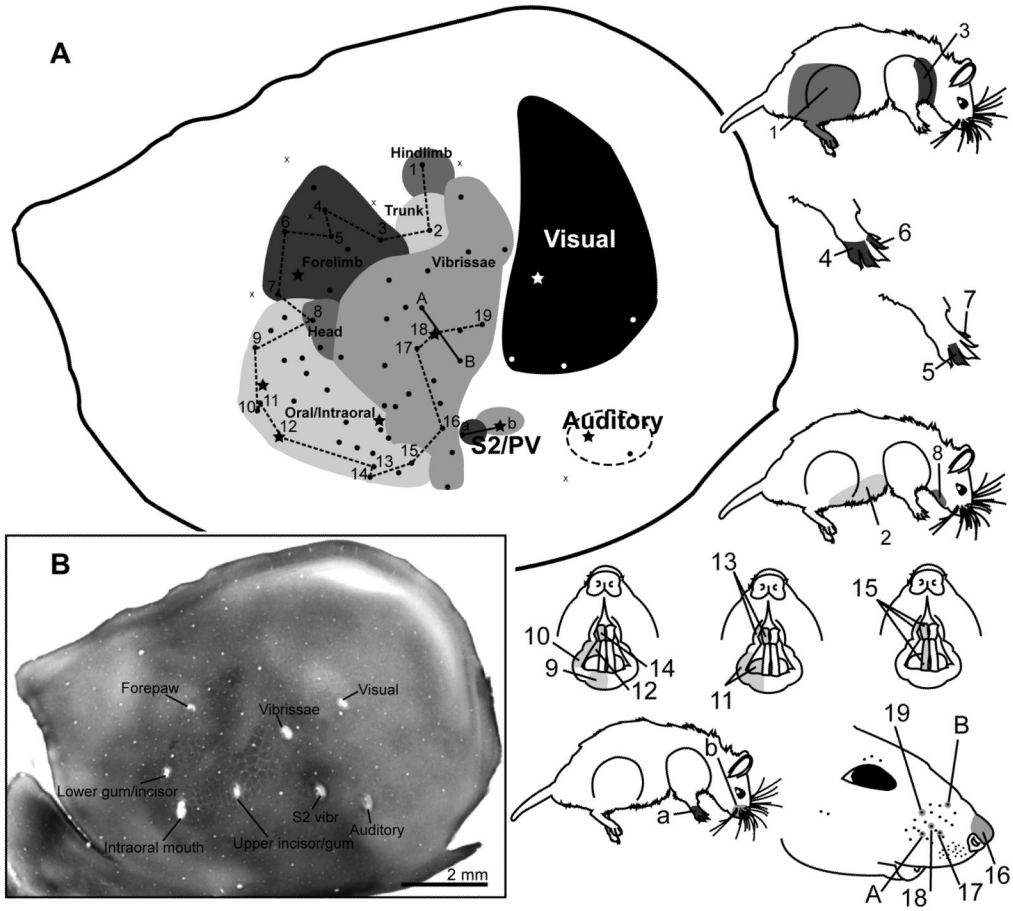

Figure 5.

Topography and chemoarchitecture of the grasshopper mouse neocortex with mapping of S1. A) Schematic of the microelectrode-derived map of cutaneous inputs to the neocortex showing representative receptive field sequences to the left. B) Locations of microlesions, labeled according to corresponding receptive fields, in a flattened cortical section processed for CO. Rostral is left, medial is up for the cortical schematic and CO section.

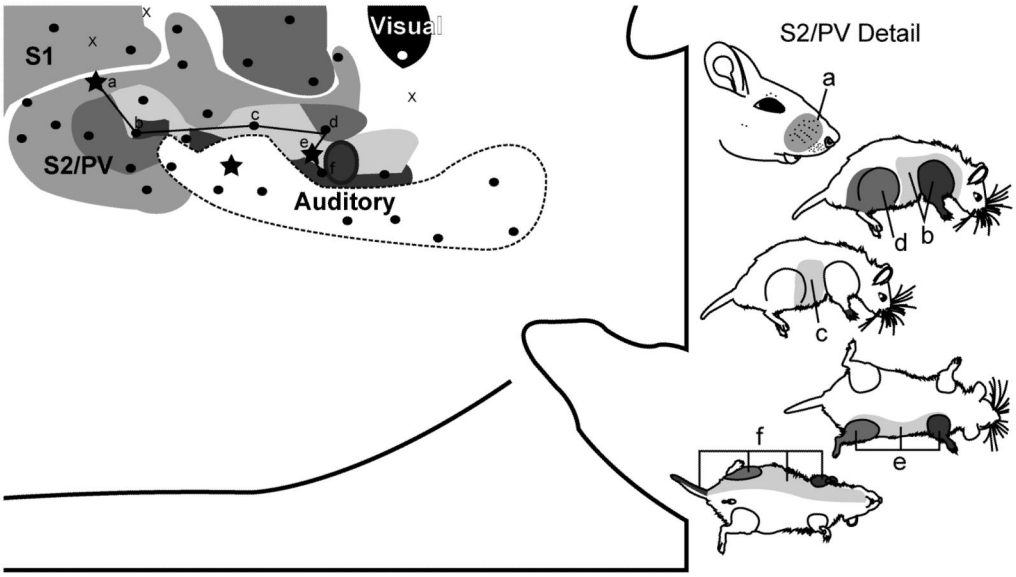

Figure 6.

Topography of the grasshopper mouse neocortex with mapping of S2/PV. The schematic of the microelectrode-derived map of cutaneous inputs to the neocortex shows a representative receptive field sequence (see supplementary Fig. 4 for complete mapping schematic). Rostral is left, medial is up for the cortical schematic.

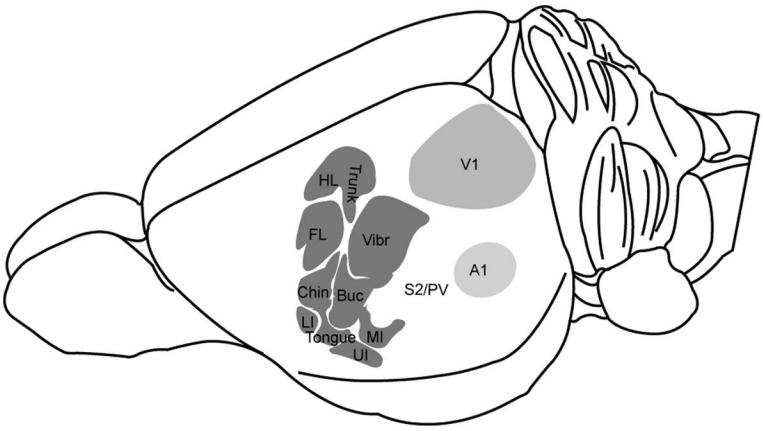

Figure 7.
Composite illustration showing the functional representations within S1 of the grasshopper mouse.

THE JOURNAL OF COMPARATIVE NEUROLOGY 504:217–237 (2007)

Adaptations in the Structure and Innervation of Follicle-Sinus Complexes to an Aquatic Environment as Seen in the Florida Manatee (*Trichechus manatus latirostris*)

DIANA K. SARKO,[1]* ROGER L. REEP,[2] JOSEPH E. MAZURKIEWICZ,[3] AND FRANK L. RICE[3]
Department of Biological Sciences, Vanderbilt University, Nashville, Tennessee 37235
Department of Physiological Sciences, University of Florida, Gainesville, Florida 32610
Center for Neuropharmacology and Neuroscience, Albany Medical College, Albany, New York 12208

ABSTRACT

Florida manatees are large-bodied aquatic herbivores that use large tactile vibrissae for several purposes. Facial vibrissae are used to forage in a turbid water environment, and the largest perioral vibrissae can also grasp and manipulate objects. Other vibrissae distributed over the entire postfacial body appear to function as a lateral line system. All manatee vibrissae emanate from densely innervated follicle-sinus complexes (FSCs) like those in other mammals, although proportionately larger commensurate with the caliber of the vibrissae. As revealed by immunofluorescence, all manatee FSCs have many types of C, Aδ and Aβ innervation including Merkel, club, and longitudinal lanceolate endings at the level of the ring sinus, but they lack other types such as reticular and spiny endings at the level of the cavernous sinus. As in non-whisking terrestrial species, the inner conical bodies of facial FSCs are well innervated but lack Aβ-fiber terminals. Importantly, manatee FSCs have two unique types of Aβ-fiber endings. First, all of the FSCs have exceptionally large-caliber axons that branch to terminate as novel, gigantic spindle-like endings located at the upper ring sinus. Second, facial FSCs have smaller caliber Aβ fibers that terminate in the trabeculae of the cavernous sinus as an ending that resembles a Golgi tendon organ. In addition, the largest perioral vibrissae, which are used for grasping, have exceptionally well-developed medullary cores that have a structure and dense small-fiber innervation resembling that of tooth pulp. Other features of the epidermis and upper dermis structure and innervation differ from that seen in terrestrial mammals. J. Comp. Neurol. 504:217–237, 2007.

Indexing terms: vibrissae; FSC; somatosensory; Merkel endings

Follicle-sinus complexes (FSCs, or vibrissae) form highly innervated tactile arrays generally found on a restricted region of the mammalian body—principally the mystacial region. However, recent evidence suggests that the Florida manatee (*Trichechus manatus latirostris*) possesses a sophisticated tactile sense through a system of FSCs distributed over the entire body (Reep et al., 2002). Manatees are large-bodied, obligate aquatic herbivores (a trait unique among marine mammals) that lack predators, do not pursue active prey, usually reside in a shallow, turbid water environment, and have greatly reduced visual systems. They appear to have reasonably developed hearing capabilities (Gerstein et al., 1999; Mann et al., 2005) but reduced sight (Bauer et al., 2003). Although little is known about the extent of their olfactory or taste

Grant sponsor: University of Florida College of Veterinary Medicine (to R.L.R.); Grant sponsor National Institutes of Health; Grant numbers: NS34692 (to F.L.R.) and RR01976 (to J.E.M).

*Correspondence to: D.K. Sarko, Department of Biological Sciences, Vanderbilt University, VU Station B, Box 35-1634, Nashville, TN 37235. E-mail: diana.sarko@vanderbilt.edu

Received 5 March 2007; Revised 29 May 2007; Accepted 12 June 2007
DOI 10.1002/cne.21446
Published online in Wiley InterScience (www.interscience.wiley.com).

capabilities, these senses also appear to be subordinate based on anatomical assessments (Levin and Pfeiffer, 2002; Mackay-Sim et al., 1985). The haptic (tactile) sense may therefore be crucial in the manatee's detection of environmental cues.

This hypothesis is supported by the distribution of sinus-type tactile hairs over the entire body, with specialized and more densely packed vibrissae on the face, in addition to the elaboration of somatosensory areas at the neuroanatomical level (Dexler, 1912; Welker et al., 1986; Johnson et al., 1986, 1987, 1994; Reep et al., 1989, 2001, 2002; Marshall and Reep, 1995; Sarko and Reep, 2007). Vibrissae are known to provide detailed textural information about objects and surfaces in an animal's immediate environment, and most mammals use vibrissae exclusively for sensory purposes such as finding prey and navigating successfully when vision is compromised, such as in low-light situations (Brecht et al., 1997; Dehnhardt et al., 1998, 2001; Dykes, 1975; Ling, 1977). Vibrissae appear to have a similar role in manatees, providing detailed sensory feedback. Whereas manatee facial vibrissae are involved in direct tactile investigation, the postfacial body is supplied with approximately 3,000 hairs, each having an independent field of deflection, forming an arrangement unique to sirenia that is proposed to be analogous to the lateral line system in fish (Reep et al., 2002). Such a system is potentially capable of conveying crucial information about water currents, the approach of other animals, and other features of the underwater environment through hydrodynamic stimulation of mechanoreceptors affiliated with postfacial FSCs (Reep et al., 2002).

Facial vibrissae are packed 30 times more densely than on the rest of the body, an attribute that should increase spatial resolution, and they can be distinguished from postfacial vibrissae by their greater rigidity due to smaller length/diameter ratios (Reep et al., 1998). The hair and bristles of the manatee face are distributed on nine distinct regions, six of which are perioral bristles (Fig. 1B): four (U1–U4) fields on each side of the upper lips and oral cavity and two (L1–L2) fields on each side of the lower lip pad (Reep et al., 1998). The nine follicle regions are distinguishable by location, number, range of length/diameter ratios, and behavioral role (Reep et al., 2001). Each of these follicles can be classified as a follicle-sinus complex (FSC), in which the follicle and its affiliated dense innervation are surrounded by a blood sinus encased within a thick connective tissue capsule (Rice et al., 1986). Manatees also have an expanded philtrum called the oral disk that contains bristle-like hairs (BLHs) that are the main tactile exploration component involved in object recognition (Fig. 1B; Reep et al., 1998). Postfacial FSCs are located on the supradisk portion of the face posterior to the orofacial ridge and on the chin in addition to the entire postfacial extent of the body (Fig. 1; Bachteler and Dehnhardt, 1999; Reep et al., 1998).

Perioral fields U2 and L1 are actively everted and used in grasping ("oripulation," a behavior unique among mammals) during feeding as well as in social behaviors (Reep et al., 2001; Marshall et al., 1998b; for videos of oripulative behavior in manatees, see http://www.marinebiology.edu/Marshall/video.htm, documented by Dr. Christopher Marshall). The eyes are often closed during feeding and tactile exploration (Marshall et al., 1998b; Bachteler and Dehnhardt, 1999), further emphasizing haptic over visual input. In the manatee, facial vibrissae serve dual and synergistic motor and sensory roles in manatee feeding and direct tactile exploration of the environment (Marshall et al., 1998a,b). The vibrissae have a high level of dexterity and perioral tactile discrimination that is also reflected in the manatee's relative tactile difference threshold of 14%, which is comparable in sensitivity to that of an Asian elephant's trunk (Bachteler and Dehnhardt, 1999). The prehensile function of facial vibrissae is present in dugongs as well but is absent in pinnipeds despite their higher tactile resolving power (Bachteler and Dehnhardt, 1999; Marshall et al., 1998b, 2003).

In an earlier study of manatee follicle innervation, the U2 fields were found to contain the largest FSCs, with the longest hair shafts, the widest ring sinuses, the thickest capsules, and the highest degree of innervation, at over 200 axons per follicle (Reep et al., 2001). L1 follicles are innervated by the second largest number of axons, at about 200 per FSC, followed by U3, U4, and L2 follicles (about 100), and finally U1 follicles, whose range overlaps that of the BLHs at 49–74. The chin and supradisk follicles exhibit the least innervation, with a range of 34–48 (Reep et al., 2001, 2002). Although the manatee's status as an endangered species precludes it from more invasive analysis, Reep et al. (2001) provided data describing general morphological features and axonal counts for each follicle type. However, silver staining did not consistently reveal the morphology of nerve endings. This limitation is

Abbreviations

A	artery
AVS	arterovenous shunt
BLH	bristle-like hair
BM	basement membrane
C	capsule
CGRP	calcitonin gene-related peptide
CS	cavernous sinus
DP	dermal papilla
DVN	deep vibrissal nerve
E	epidermis
F	follicle
FNE	free nerve ending
FSC	follicle-sinus complex
HP	hair papilla
ICB	inner conical body
L1	lower perioral field 1
LLE	longitudinal lanceolate ending
MC	Merkel cell
ME	Merkel ending
MS	mesenchymal sheath
NF or NF200	200-kDa subunit of neurofilament
NPY	neuropeptide Y
OCB	outer conical body
PGP	protein gene product 9.5
RRC	rete ridge collar
RS	ring sinus
RW	ringwulst
T	trabecula
TH	tyrosine hydroxylase
U2	upper perioral field 2
UD	upper dermis
V	vein
VC	vibrissa cortex
VM	vibrissa medulla

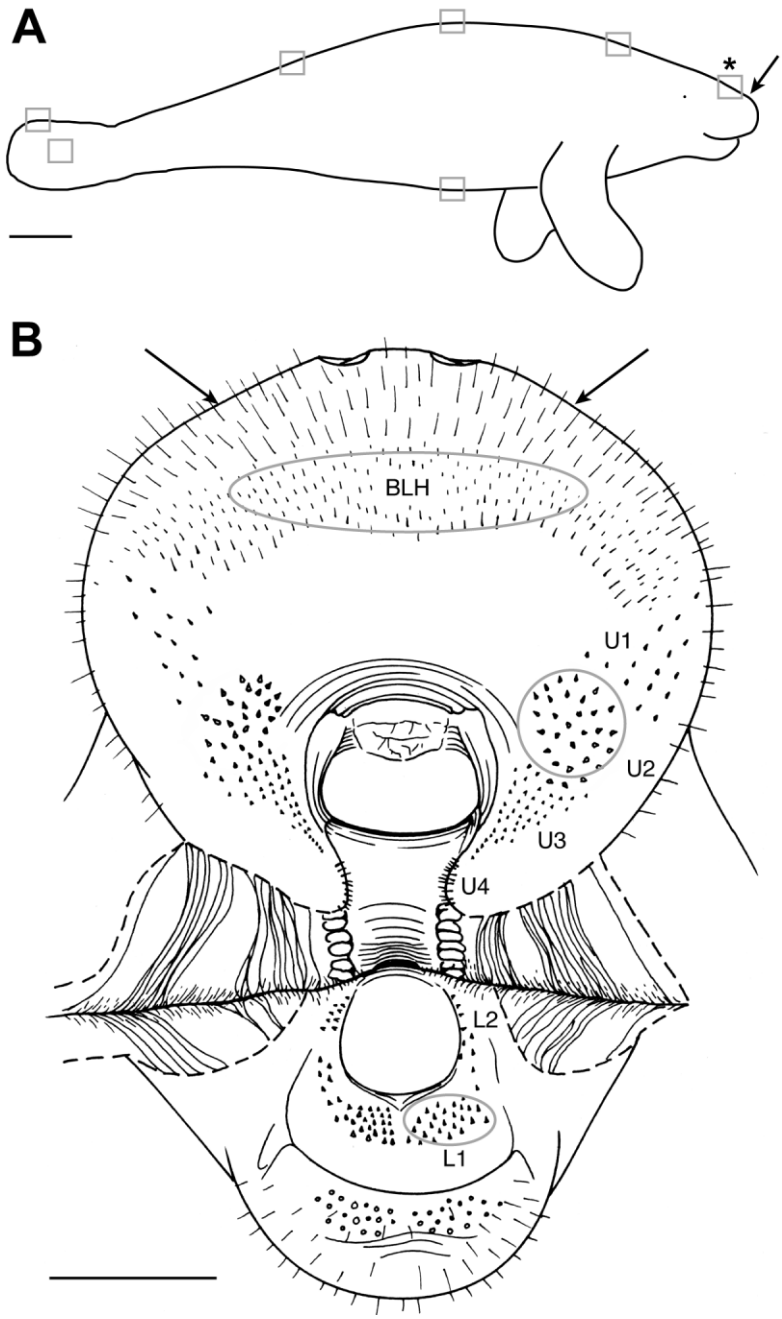

Fig. 1. Vibrissae sampling regions of the body and face. **A:** Post-facial body regions of interest include the tail (lateral edge and dorsomedial areas), ventromedial area, and rostral, central, and caudal areas of the dorsal midline. The supradisk region (asterisk) is caudal to the orofacial ridge (arrows) and is thought to contain vibrissae like those on the body. **B:** Frontal view of the manatee face with cheek muscles cut to reveal perioral follicle fields. Due to their behavioral significance, facial follicles of interest include the bristle-like hairs (BLHs), upper perioral field 2 (U2), and lower perioral field 1 (L1) follicle fields. Scale bar = 30 cm in A; 5 cm in B.

solved here through systematic immunolabeling analysis by using anti-protein gene product 9.5 (PGP), a neuronal cytoplasmic enzyme, as a standard in combination with antibodies against several other neural antigens in order to characterize functionally the innervation of manatee vibrissal FSCs. Given the varying behavioral and sensory tasks for which each manatee bristle field is specialized, we would expect to reveal similarly varying attributes in patterns of innervation, with facial vibrissae engaged in tactile behavior (the U2 and BLH follicles) exhibiting more densely distributed and varied types of nerve endings. Also, although the anatomical structure of FSCs remains relatively consistent across a wide range of species, patterns of innervation often vary considerably, pre-

TABLE 1. Specimens Used in the Study

Specimen	Sex	Length (cm)	Weight (kg)	Classification	Cause of death
TM0406	M	290	393	Adult	Watercraft
TM9728	M	295	500	Adult	Watercraft
TM0506	M	172	134	Calf	Cold stress
MNW0614	F	238	326	Subadult	Watercraft

sumably due to evolutionary pressures and concurrent behavioral demands (Dehnhardt et al., 1999; Ebara et al., 2002).

As an evolutionary outlier, the Florida manatee offers a unique opportunity to understand mammalian sensory systems better in general by examining a system of vibrissae that has assumed an expanded functional role. A systematic analysis of manatee FSCs may also elucidate their potential relationship to cortical cellular aggregates called Rindenkerne (Dexler, 1912; Reep et al., 1989; Marshall and Reep, 1995; Johnson, 1990; Johnson et al., 1994) that appear to be similar to barrels found in the somatosensory cortex of other species (Woolsey et al., 1975; Rice, 1995).

MATERIALS AND METHODS

Manatees in Florida are endangered and protected under federal law. Postmortem manatee follicle samples were acquired through the statewide manatee salvage program under Federal Fish and Wildlife Permit PRT-684532 and Institutional Animal Care and Utilization Committee (IACUC) protocol #C233. For each specimen, necropsy sheets summarizing body morphometrics, body weight, gender, likely cause of death, and condition upon recovery were obtained. Specimens are described in Table 1 and included TM0406 (adult male, euthanized after watercraft impact; three BLH and three U2 follicles sampled), TM9728 (adult male, death due to watercraft; three rostrodorsal, one dorsocentral, and one dorsocaudal follicles sampled), TM0506 (male neonate, suffered multisystemic failure due to immune suppression secondary to cold stress; two U2, two BLH, two L1, and one dorsocaudal body sampled), and MNW0614 (subadult female, death due to watercraft; three follicles from each of 10 body regions of interest sampled).

Hair follicle samples were acquired as available from seven body regions (Fig. 1A; supradisk, dorsocentral midline, rostrodorsal midline, caudodorsal midline, ventrocentral midline, dorsal tail, and tail edge) as well as from perioral fields L1, U2, and BLH (Fig. 1B), as described by Reep et al. (1998) by using a #11 scalpel blade to extract a block of tissue (roughly $5 \times 5 \times 15$ mm) surrounding the follicle of interest. Follicles were cut mediolongitudinally to facilitate fixation and placed in 4% paraformaldehyde overnight. After 24 hours of fixation, follicles were removed and placed in 0.1 M phosphate-buffered saline (PBS), pH 7.4, and 30% sucrose. Sections were cut by using a cryostat. Sections for conventional epifluorescence evaluation were then cut at 14 μm parallel to the long axis of the follicles. These sections were directly thawed onto slides subbed with chrome-alum gelatin, allowed to air dry, and immunolabeled on the slides. Follicles for confocal analysis were cut at 80 μm, and the sections were immunolabeled free-floating before being mounted on slides. After labeling, the slides were coverslipped by using either 90% glycerin in PBS or Vectashield (Vector, Burlingame, CA).

The sections were processed for single and double immunolabeling with the following primary antibodies:

1. Anti-protein gene product 9.5 (PGP; rabbit polyclonal, 1:800; UltraClone, Isle of Wright, UK; catalog number RA95101). The antigen was human PGP 9.5 protein purified from pathogen-free human brain. The antibody shows one band at 26–28 kDa on Western blot (tested in rabbits; Wilkinson et al., 1989). Anti-PGP has been found to be a universal neuronal marker in other species including rats (Fundin et al., 1997a; Rice et al., 1997), raccoons (Rice and Rasmusson, 2000), monkeys (Paré et al., 2001, 2002), naked mole-rats (Park et al., 2003), and humans (Albrecht et al., 2006). Controls for the specificity of PGP labeling were provided in these species by the use of preadsorption controls and the demonstration that labeling was limited to neuronal innervation and glia. Staining in manatee follicle sections produced a pattern of immunoreactivity that was identical to descriptions in the previous studies of other species listed above.
2. Anti-neurofilament 200-kDa subunit (NF; rabbit polyclonal, 1:800; Chemicon, Temecula, CA,; catalog number AB1982, lot number 24080051). The antigen was a highly purified bovine neurofilament polypeptide. The antibody labels phosphorylated and nonphosphorylated 200-kDa NF and shows a band at 200 kDa and bands around 170–180 kDa on Western blot (tested in rabbits; manufacturer's technical information). Immunolabeling for this protein as been localized to myelinated fibers, including Aβ and Aδ fibers, and Merkel endings in a variety of species including rats (Fundin et al., 1997a; Rice et al., 1997), raccoons (Rice and Rasmusson, 2000), monkeys (Paré et al., 2001, 2002), naked mole-rats (Park et al., 2003), and humans (Albrecht et al., 2006). Controls for the specificity of NF labeling were provided in these species by the use of preadsorption controls and the demonstration that labeling was limited to neuronal innervation and myelinated fibers. Staining in manatee follicle sections produced a pattern of immunoreactivity that was identical to descriptions in the previous studies of other species listed above.
3. Anti-calcitonin gene-related peptide (CGRP; guinea pig polyclonal, 1:400; Peninsula, San Carlos, CA; catalog number T-5027, lot number 061121). The antigen is human α-CGRP with the following sequence: H-Ala-Cys-Asp-Thr-Ala-Thr-Cys-Val-Thr-His-Arg-Leu-Ala-Gly-Leu-Leu-Ser-Arg-Ser-Gly-Gly-Val-Val-Lys-Asn-Asn-Phe-Val-Pro-Thr-Asn-Val-Gly-Ser-Lys-Ala-Phe-NH2. The antibody has 100% reactivity with human and rat α-CGRP, human CGRP (8-37), chicken CGRP, and human β-CGRP. It has 0.04% cross-reactivity with human amylin and 0% cross-reactivity with rat amylin and with human and salmon calcitonin (by enzyme-linked immunosorbent assay [ELISA]; manufacturer's technical information). Although Western blot information was not available, this protein has been localized to Merkel cells, C-fiber innervation, and vascular innervation in rats (Rosenfeld et al., 1983; Fundin et al., 1997a; Rice et al., 1997), and staining specificity has also been previously characterized in

raccoons (Rice and Rasmusson, 2000), monkeys (Paré et al., 2001, 2002), naked mole-rats (Park et al., 2003), and humans (Albrecht et al., 2006). Controls for the specificity of CGRP labeling were provided in these species by the use of preadsorption controls and the demonstration that labeling was characteristic of Merkel cells, C-fiber innervation, and vascular innervation. Staining in manatee follicle sections produced a pattern of immunoreactivity that was identical to descriptions in the previous studies of other species listed above.

4. Anti-S100 (S100, rabbit polyclonal, used neat; Biogenesis, Brentwood, NH, catalog number 8200-0184, lot number A2255). The antigen was purified bovine S100 protein. Although Western blot information was not available, this protein has been localized to brain glial cells and ependymal cells, in addition to Schwann cells of the peripheral nervous system, and the antibody has been found to have no cross-reactivity in rats (manufacturer's technical information; Moore, 1965, 1982; Stefansson et al., 1982). Controls for the specificity of S100 labeling were provided in other species including rats (Fundin et al., 1997a; Rice et al., 1997) and monkeys (Paré et al., 2001, 2002) by the use of preadsorption controls and the demonstration that labeling was limited to glia. Staining in manatee follicle sections produced a pattern of immunoreactivity that was identical to descriptions in the previous studies of other species listed above.
5. Anti-BNaC1α (BNaC; rabbit polyclonal; 1:500; gift from Dr. Jaime García-Añoveros). The antigen was N-terminus peptide MDLKESPSEGSLQPSSC (corresponding to residues 1–16 of mouse, rat, and human BNaC1α; García-Añoveros et al., 2001) and shows a band at 58.5 kDa on Western blot in rats and mice (García-Añoveros et al., 2001). This protein is associated with low-threshold mechanoreceptors (García-Añoveros et al., 2001). Controls for the specificity of BNaC labeling were provided in these species by the use of preadsorption controls and the demonstration that labeling was limited to low-threshold mechanoreceptors. Staining in manatee follicle sections produced a pattern of immunoreactivity that appeared identical to descriptions in the previous studies of other species listed above.

Manatee follicle tissue was also prepared without each primary antibody as a control for the specificity of the secondary antiserum. Western blots could not be performed on manatee tissue due to the manatee's status as an endangered species and the consequently low availability of fresh tissue samples.

All 14-μm-thick sections were first preincubated with 1% bovine serum albumin (BSA) and 0.3% Triton X-100 in 0.1 M PBS for 1 hour and then incubated with a solution of primary antibody (diluted in PBS with 4% calf serum or 1% BSA and 0.3% Triton X-100) overnight at 4°C at high humidity. Slides were then rinsed in PBS for 30 minutes and subsequently incubated in the dark at room temperature for 2 hours with Cy3- (for red fluorescence; 1:500) and Alexa488- or Cy2- (for green fluorescence; 1:250) conjugated secondary antibodies (Molecular Probes, Eugene, OR; Jackson Immunoresearch, West Grove, PA) diluted in PBS or BSA with 0.3% Triton X-100. Slides were then rinsed in PBS and either temporarily coverslipped under PBS (in the case of future double labeling) or coverslipped with 90% glycerol in PBS. Double labeling was usually accomplished by repeating the immunofluorescence procedure described above. In some cases double labeling was achieved through a single cycle of incubations beginning with a 1:1 mix of the monoclonal and polyclonal primary antibodies. To control for nonspecific labeling, incubation with primary antibody was omitted or the primary antibody was preincubated with a specific blocking peptide. The 80-μm-thick sections were processed free-floating in the same antibody dilutions as in the thinner sections. Incubations were for 2 days in primary antibodies and overnight in secondary antibodies at 4°C. Rinses were for at least 4 hours.

Sections were analyzed as follows with an Olympus Provis AX70 microscope equipped with conventional fluorescence: 1) Cy3 filters (528–553 nm excitation, 590–650 nm emission); and 2) Cy2 filters (460–500 nm excitation, 510–560 nm emission). Fluorescence images were captured with a high-resolution (1,280 × 1,024 pixels) three-chip color CCD camera (Sony, DKC-ST5) interfaced with Northern Eclipse software (Empix Imaging, Mississauga, ON). Images were deblurred by using a deconvolution program based on a 1-μm, two-dimensional nearest neighbor paradigm (Empix Imaging). Samples were imaged on a Zeiss LSM 510Meta confocal microscope (Carl Zeiss MicroImaging, Thornwood, NY) equipped with an Argon (488 nm excitation) and a green HeNe (543 nm excitation) laser. Emissions were collected by using a band pass 500–530 nm emission filter for Alexa Fluor 488. For Cy3 either a long pass 560 nm emission filter or a band pass 560–615 nm emission filter was used, depending on whether the sample was single or double labeled. Images were collected with a Plan-Neofluor 25x/0.8 Imm corr DIC lens with the pinhole set for 1 Airy Unit. Confocal image z-stacks were collected at 512 × 512 pixel x-y resolution and 1-μm steps in z. The three-dimensional (3D) red-green stereo anaglyph (Fig. 9B) and the 3D stereo pairs (Fig. 9A,D,E) were generated by using the Zeiss LM510 software. The 3D surface-rendered images (Fig. 8A–H) were produced by using the VolumeJ plug-in for ImageJ software (http://rsb.info.nih.gov/ij/).

Because the intensity of immunolabeling for the numerous antibodies used in the present study is attributed to many variables that cannot be individually quantified, this study does not attempt to quantify the relative amounts of labeled antigens. These variables include: 1) true differences in the presence and quantity of the antigen, 2) whether the antibody is monoclonal or polyclonal, 3) background labeling, 4) antibody concentration, 5) antibody efficacy, and 6) location of the antigen (i.e., membrane or cytosol). Because the labeling intensities differed between the various types of antibodies, the photomicrographs compiled for illustrative purposes were adjusted by using Northern Eclipse, Adobe Photoshop (San Jose, CA), and Microsoft PowerPoint (Redmond, WA) software so that the maximum labeling contrast and intensity were similar for each antibody.

RESULTS

The basic structure of the FSCs in each body region is shown schematically in Figure 2 (see also Figs. 3A, 5A, 6). Each of the 10 body regions examined shared many common patterns of sensory innervation affiliated with the FSCs and

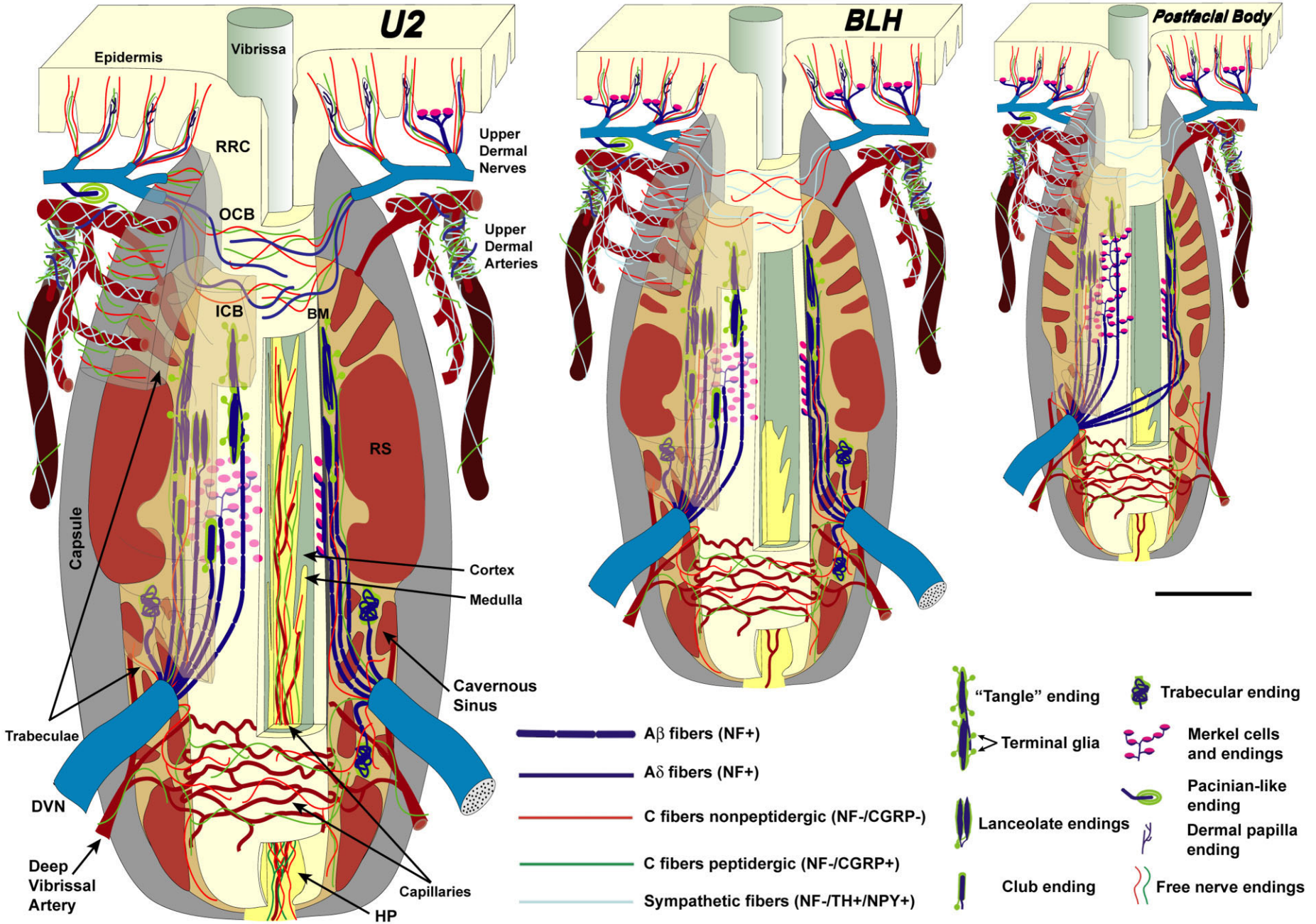

The Journal of Comparative Neurology. DOI 10.1002/cne

the adjacent skin, with a few important exceptions. The FSCs in all regions were innervated by two deep vibrissal nerves that supplied sensory endings primarily to the levels of the cavernous sinus and ring sinus and by several superficial vibrissal nerves that supplied innervation primarily to the ICB. The superficial vibrissal nerves appeared to be continuations from a plexus of small nerves that supplied the epidermis and upper dermis adjacent to the FSCs.

Innervation to the skin adjacent to the FSCs

Thin dermal papillae penetrated far into the epidermis and were laden with fine-caliber fibers (Figs. 2, 3B). Most of these fibers were NF200 negative and could be CGRP positive or negative (Fig. 7A). The other thin-caliber fibers labeled for both anti-PGP and anti-NF200 (Figs. 6B,C, 7B). In other species, NF-negative fibers—which are always thin caliber—consistently fail to label with anti-MBP (myelin basic protein), indicating that they are C fibers, whereas NF-positive fibers—which can be thin or thick caliber—consistently co-label for anti-MBP, indicating that they are Aδ and Aβ fibers, respectively (Fundin et al., 1997a; Rice and Rasmusson, 2000; Paré et al., 2001; Albrecht et al., 2006). At the mouth of the FSCs, a site referred to as the rete ridge collar (RRC), the dermal papillae curved toward the vibrissal shaft. The presumptive C fibers could be seen penetrating the epidermis, whereas the presumptive Aδ fibers appeared to ramify within the papillae. In some cases, NF-positive fibers appeared to terminate as Meissner corpuscles (Fig. 7L). Although no Merkel endings (MEs) were observed terminating at the RRC of manatee FSCs, as typically occurs in other species, MEs were visible at the base of the adjacent epidermis in all areas (Fig. 6B). A sparse distribution of presumptive Pacinian corpuscles was also observed just below the epidermis (Fig. 7M) adjacent to only U2 FSCs, whereas Pacinian corpuscles are typically located in deep dermal tissues.

The dermis surrounding the neck and capsule of each FSC contained numerous blood vessels that were densely innervated by a mixture of thin-caliber fibers that only labeled with anti-PGP (presumptive sympathetic innervation) or coexpressed CGRP immunoreactivity (Fig. 8). In other species, the vascular innervation that lacks CGRP was immunopositive for neuropeptide Y (NPY) and tyrosine hydroxylase (TH), which is indicative of sympathetic innervation (Fundin et al., 1997a; Rice and Rasmussen, 2001). However, the TH and NPY antibodies that were used failed to label manatee tissue. The CGRP-positive vascular innervation is presumably sensory and consisted of some NF-negative fibers and some NF-positive fibers that are presumptive C and Aδ fibers, respectively (Fig. 8). Some locations had excessively dense innervation suggestive of arteriovenous shunts. All of the innervation around the necks of the FSCs was supplied by numerous small nerves within the dermis. Dense peptidergic and nonpeptidergic C-fiber innervation was also intimately wrapped around the outer surface of the FSC capsule, particularly along the upper half of the capsule. This may be present in other species as well, but to a lesser extent, and has not been fully investigated.

Innervation to the inner conical body

The mouth and the neck regions together formed up to half of the total length of the FSCs, especially in the facial vibrissae (Figs. 3A, 5A). The dense connective tissue capsule had a wide site of convergence (outer conical body [OCB]) at the neck, which enclosed a less compact layer of connective tissue referred to as the inner conical body (ICB). This inner conical body is an expansion of the mesenchymal sheath, which lines the basement membrane of the vibrissal follicles. The ICB of the U2 follicles (Fig. 3C) contained a dense circumferential array of fine-caliber fibers that were mostly NF negative, with only a few NF-positive fibers present (Fig. 7C). These thin fibers presumably terminated as free nerve endings (FNEs), because no transverse lanceolate endings were observed, as is seen in terrestrial species that whisk their vibrissae (Ebara et al., 2002). In the FSCs of other body regions in the manatee, the ICBs were poorly innervated, with the few fibers being associated with some vasculature (Figs. 5E, 8).

Innervation at the ring sinus level

At the lower extent of the ICB region and the upper extent of the ring sinus, the mesenchymal sheath contained numerous gigantic, spindle-shaped nerve endings ("tangle" endings) that, of all species observed to date, are unique to the manatee (Figs. 3D, 5A,C, 6D–I). Each of these tangle endings could be as large as 300 μm long and 75 μm wide. Large-caliber fibers ascended from the deep vibrissal nerve to supply single or multiple tangle endings. The fibers and endings were positive for PGP, S100, and NF200 as well as BNaC (Fig. 7H,I), indicating that they are likely low threshold mechanoreceptors. A subregion of each ending was also CGRP positive (Fig. 7J). Typically,

Fig. 2. Schematic drawing of the structure and innervation of the U2, BLH, and postfacial vibrissal follicle-sinus complexes (FSCs) with innervation types and sensory nerve endings illustrated. The relative scales of each FSC are accurate, but innervation is presented for illustrative purposes only (see Figs. 7 and 9 for accurate scale representations). Overall morphology: The thickness of the capsule and the diameter of the vibrissa decreases progressively from the U2 to the postfacial FSC. The facial FSCs also exhibited dual innervation from the DVN at the base of the follicle whereas the DVN entered as a single bundle of axons in postfacial FSCs. Presumptive sympathetic fiber innervation is also depicted based on general characteristics in other mammals. Epidermis and RRC: The epidermis of the U2, BLH, and postfacial vibrissae contains superficially projecting dermal papillae within which are fine-caliber Aδ and C fibers. The base of the epidermis adjacent to each FSC is innervated by Merkel endings. The U2 FSC has a particularly pronounced invagination of the RRC. OCB and ICB: The U2 FSC exhibits a dense network of circumferential free nerve endings whereas the BLH and postfacial FSCs exhibit only fine-caliber and sympathetic innervation. Novel "tangle" endings are located in the facial and postfacial FSCs. RS: Dense Merkel networks were present in FSCs from each body region, but Merkel cells lacking visible innervation predominated in facial FSCs. Less densely distributed longitudinal lanceolate endings were also observed at this level for each type of FSC, and club-like endings were observed in close association with the rudimentary ringwulst in facial FSCs. CS: The trabeculae in FSCs from each body region contained fine-caliber innervation with presumptive free nerve endings. Only the facial FSCs were innervated by unique endings embedded in the trabeculae. Reticular and spiny endings were notably absent. HP: Dense fine-caliber innervation was present in the rigid U2 follicle within the medulla that extended to an extremely superficial extent. This innervation was very sparse in the BLH and postfacial vibrissae, and the medulla of each extended less superficially. For abbreviations, see list. Scale bar = 1 mm.

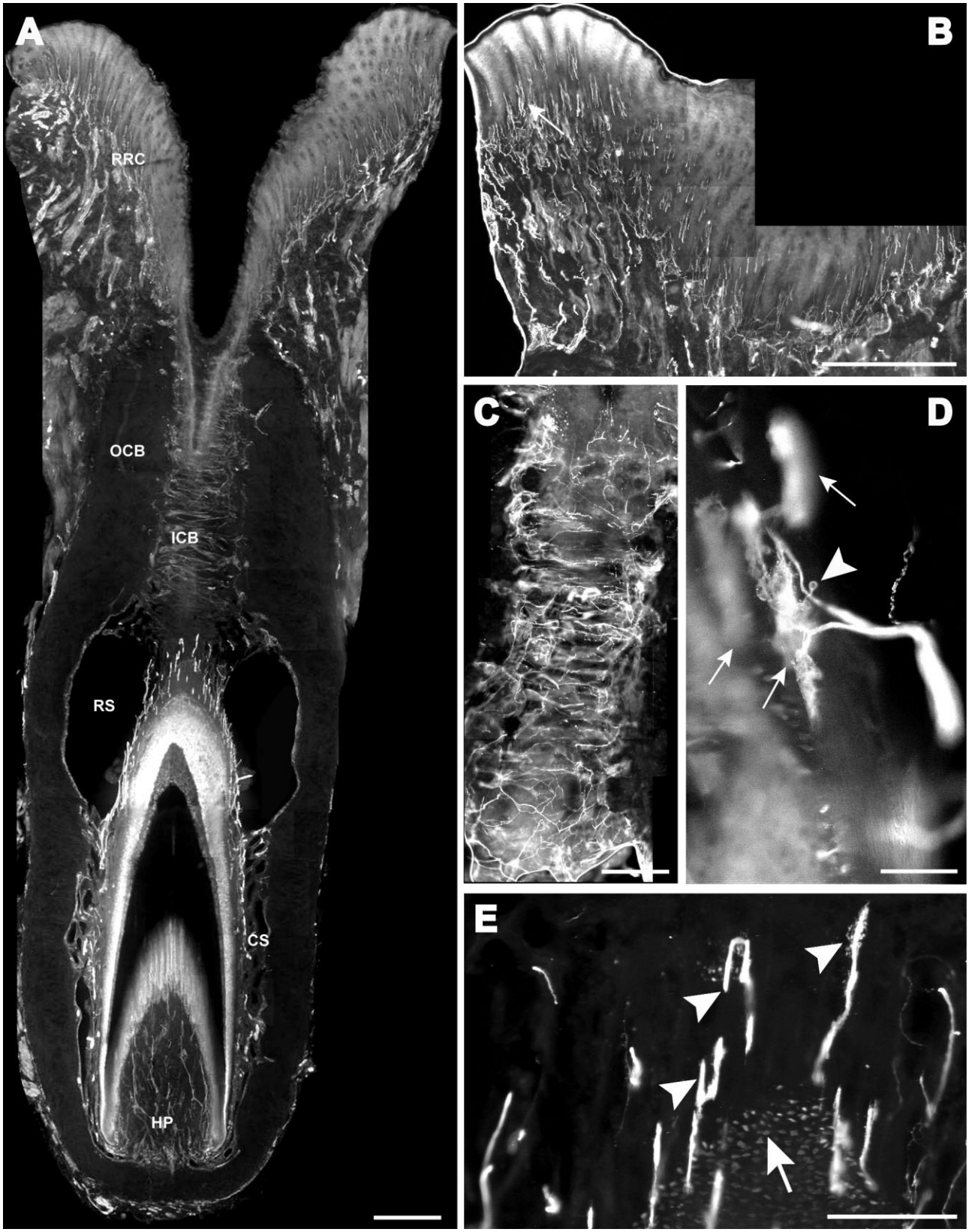

Fig. 3. Characterization of upper perioral field 2 (U2) follicle innervation. **A:** A longitudinal U2 section stained for PGP is shown grazing the follicle just prior to the central axis of the vibrissa to reveal various combinations of innervation at different levels of the FSC (specimen TM0406). **B:** Magnified RRC and epidermal region further off the central axis showing a dense distribution of C- and Aδ-fiber projections (arrow) within dermal papillae and extending into the epidermis (vibrissa is to the right). **C:** Magnification of circumferential FNEs at the ICB level (same plane of section as A). **D:** Magnification of a representative "tangle" ending located on the border of the lower ICB region and abutting the mesenchymal sheath (plane of section along the central axis). The source axon branches to form three mechanoreceptors (arrows), one of which is associated with a terminal glia (arrowhead). **E:** A dense distribution of Merkel cells (arrow) and representative LLE morphologies (arrowheads) including a bifurcated ending, hooked formation, and studded blade-like termination (same plane of section as A). For abbreviations, see list. Scale bar = 1 mm in A,B; 250 μm in C–E.

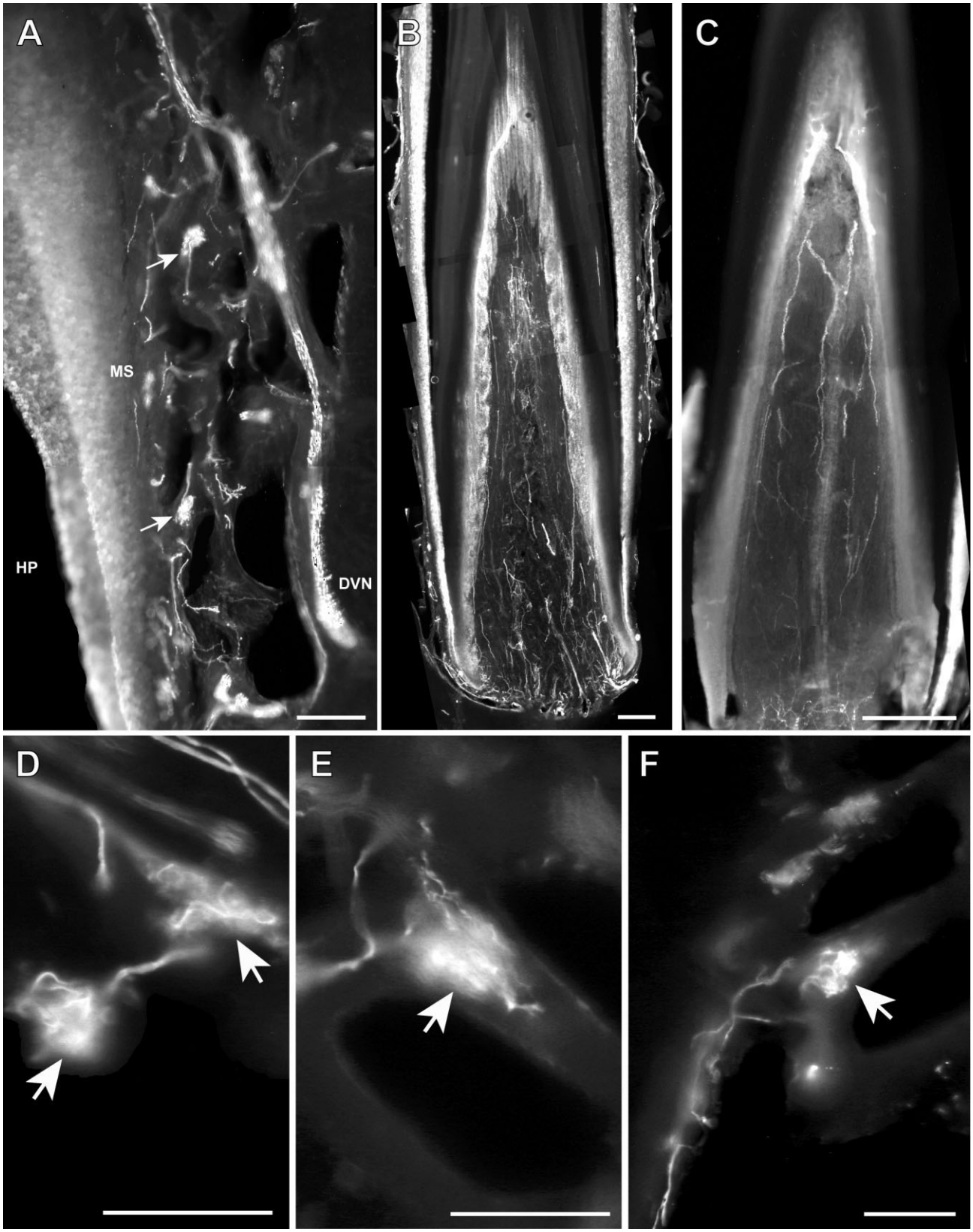

Fig. 4. Innervation of the cavernous sinus and the medulla of the hair papilla in facial FSCs. **A:** Extensive innervation along and within the trabeculae of the lower cavernous sinus in a U2 FSC (specimen TM0406). Within the trabeculae, unique endings (arrows) are supplied by large-caliber fibers, and the deep vibrissal nerve (DVN) is seen continuing to the ring sinus. The hair papilla (HP) and mesenchymal sheath (MS) are also visible. **B,C:** A dense network of small-caliber axons and presumptive FNEs proceeding to a remarkably superficial extent in the medulla of a U2 follicle (B; specimen TM0406) and an L1 follicle (C; specimen MNW0614). Magnified views show details of unique trabecular endings seen in a supradisk follicle (D; specimen MNW0614, arrow) a U2 follicle (E; specimen TM0406, arrow) and a BLH follicle (F; specimen TM0406, arrow). Scale bar = 600 μm in A; 1 mm in B,C; 200 μm in D–F.

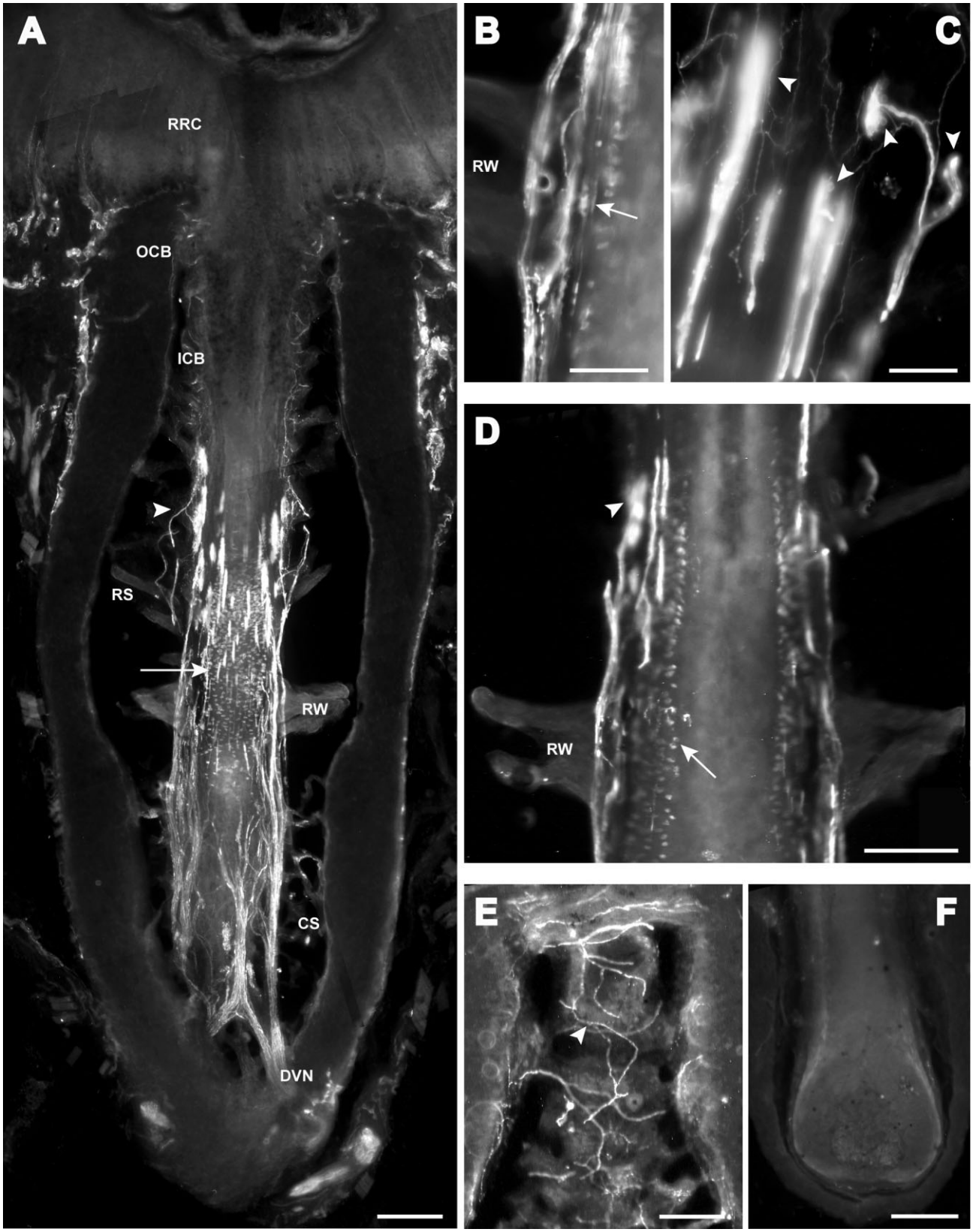

Fig. 5. Sensory innervation present in bristle-like hairs (BLHs). **A:** A longitudinal section of a BLH just off the central vibrissal axis stained for protein gene product 9.5 reveals characteristic innervation, including "tangle" endings at the lower ICB/upper RS level (arrowhead), in addition to LLEs (arrow) and MCs (magnified in D) at the RS level. **B:** Tangle endings parallel to a club-like ending (arrow) against the basement membrane at the ringwulst level are shown further from the central vibrissal axis. **C:** Tangle endings (arrowheads) with associated Schwann cells at the superficial extent of the RS (plane of section along central vibrissal axis). **D:** Merkel cells lacking visible innervation (arrow) in addition to tangle endings (arrowhead) at the upper RS level (plane of section well before or after the central vibrissal axis). **E:** Sympathetic innervation of the vascularized inner conical body (plane of section well before or after the central vibrissal axis). **F:** A dermal hair shaft medulla lacking the extensive FNE innervation seen in U2 follicles (plane of section along the central axis). For abbreviations, see list. Scale bar = 1 mm in A; 300 μm in B,C; 600 μm in D–F.

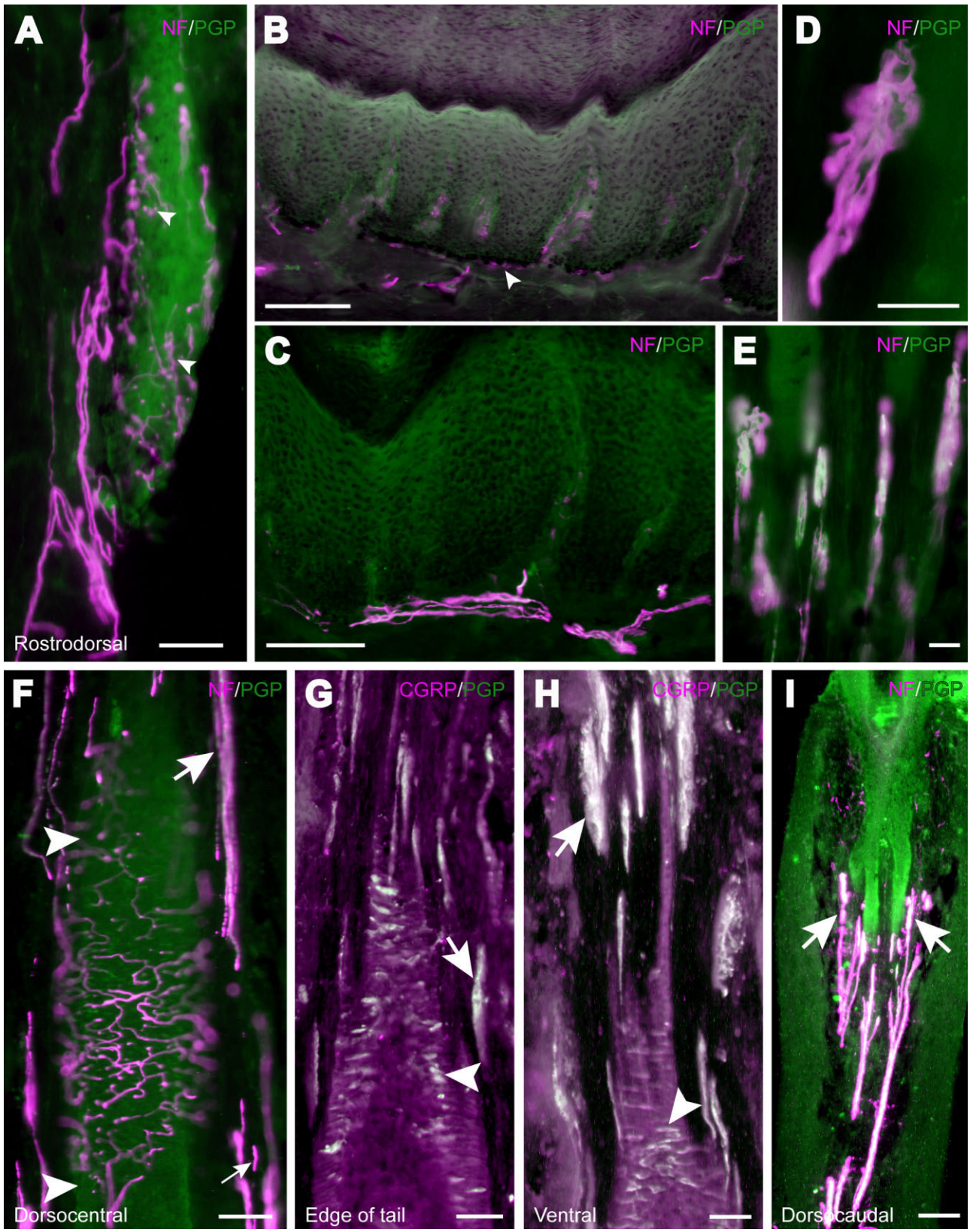

Fig. 6. Representative postfacial FSC innervation includes dense networks of MEs along with LLEs and "tangle" endings. **A:** A dorsorostral postfacial FSC (TM9728) shows characteristic Merkel innervation (arrowheads) at the RS level. **B,C:** Details shown for epidermal innervation (MEs shown with arrowhead; superficial is up) and tangle endings (**D,E**; dorsocentral postfacial hair, specimen TM9728 for B–E) at the upper RS/lower ICB level. **F:** A dorsocentral postfacial FSC (TM9728) exhibits the presence of LLEs (small arrow), large-caliber fibers leading to tangle endings (large arrow), and a particularly extensive network of MEs (between arrowheads) at the RS and ICB levels. **G–I:** Follicle-sinus complexes from the edge of the tail (G; MNW0614), ventral body (H; MNW0614), and dorsocaudal body (I; TM9728) reveal tangle endings and Merkel innervation (arrows and arrowheads, respectively) at the RS and ICB levels. All planes of the sections shown are located well before or after the central axis of the vibrissae. For abbreviations, see list. Scale bar = 1 mm in A; 600 μm in B,C; 150 μm in D,E; 750 μm in F,I; 500 μm in G,H.

the largest caliber cutaneous fibers have been classified as Aβ fibers. However, these fibers were the thickest of all encountered and might reasonably be classified as Aα or Aαβ (Burgess and Perl, 1973). At and above the level where the tangle endings were located, trabeculae radiated from the mesenchymal sheath to the capsule. Confocal imaging revealed that each ending abutted the basement membrane of the follicle and contained an intricate tangle of NF-positive fibers within a PGP-positive cytoplasmic envelope (Figs. 9D,F–H, 10A,B). The surface was studded with numerous S100-positive cells that are likely terminal glia (Figs. 3D, 7I).

At the ring sinus (RS) level, the FSCs in all regions had a dense, uniform distribution of Merkel cells (MCs) in the outer root sheath completely surrounding the follicles. The innervation to the MCs is supplied by Aβ fibers that would be the largest caliber in the FSCs of other species but are not are not as large as those that terminate as tangle endings. Each fiber branches extensively to form numerous endings that ramify over large territories of the follicle surface. Surprisingly, most of the Merkel cells in the facial FSCs lacked innervation (Figs. 3E, 5A,D). In contrast, extensive networks of Merkel endings were found in postfacial FSCs (Figs. 6F, 9B), innervating most of the MCs (Fig. 6A,F–I). Supradisk FSCs, thought to be morphologically similar to postfacial FSCs (Reep et al., 2001), possessed attributes that were intermediate between the facial and postfacial characteristics. The most noteworthy of these included sensory endings located within the connective tissue of the cavernous sinus (Fig. 4D; discussed below and found only in facial FSCs) in addition to a well-innervated Merkel network at the RS level (Fig. 10D) characteristic of postfacial FSCs.

Widely spaced longitudinal lanceolate endings (LLEs) were present in the mesenchymal sheath at the level of the RS but did not form a dense palisade as seen in other species (Figs. 3A, 5A). In contrast to tangle endings, the LLEs were significantly smaller, appeared to be associated with only one or two terminal glia, and were supplied by a smaller caliber Aβ fiber. The majority of LLEs appeared to be unbranched (Fig. 9C). They could have several morphologies: a studded blade form; a smooth blade; and a curved hook ending (Fig. 3E). Whereas the lanceolate endings and most of the Merkel endings were located above an expansion of the mesenchymal sheath referred to as the ringwulst, club-like endings that were morphologically simple, unbranched stumps of Aβ fibers were located in the mesenchymal sheath at the level of the rudimentary ringwulst (Figs. 5B, 10D). The mesenchymal sheath of the ring sinus also contained a sparse distribution of thin-caliber fibers that lacked morphologically distinct terminals and therefore presumably formed FNEs. All of the innervation observed at the ring sinus level was supplied by the deep vibrissal nerve.

Innervation at the cavernous sinus level

In the region of the cavernous sinus, numerous trabeculae spanned the space between the mesenchymal sheath and the capsule. Both the mesenchymal sheath and the trabeculae contained numerous thin-caliber fibers, some of which labeled only with anti-PGP; others that co-labeled only with CGRP; and others that co-labeled with anti-NF200. None of the thin-caliber fibers had morphologically distinct terminals and, thus, presumably formed FNEs. The trabeculae in only the facial vibrissae contained a second type of nerve ending that appears to be unique to aquatic mammals and has not been previously described in detail. These endings contained a dense cluster of neurofilament (Figs. 4, 9A) and labeled for PGP, S100, and NF200 as well as for BNaC, indicating that they were also likely low threshold mechanoreceptors (Figs. 7E,F, 10C), although the axons appeared to be among the smaller caliber Aβ fibers. Low CGRP activity was also detected (Fig. 7G). The endings measured approximately 150 μm long and 150 μm wide. Representative endings of the novel "tangle" ending and trabecular ending groups were reconstructed by using confocal imaging to confirm the 3D structural morphology and to ensure that the unusual structure was not simply a result of an aberrant plane of section through the FSC. The unique endings present in the trabeculae of the facial FSCs were notably absent in the postfacial FSCs examined. No reticular or spiny endings, normally distributed at or near the CS basement membrane of follicles in other mammalian FSCs, were observed in any of the FSCs in the manatee.

Innervation to the vibrissal medulla

An especially striking feature that was unique to the U2 and L1 follicles was an extensive medulla of the hair papilla that was permeated by extensive thin-caliber innervation far denser than that observed in any other species to date (Fig. 4B,C). In most of the manatee vibrissae, a dermal papilla was present strictly at the base of the vibrissa and contained a few thin-caliber fibers that were NF negative, some of which were CGRP negative and some of which were CGRP positive. In contrast, the dermal papillae of the U2 and L1 follicles became a pronounced medullary core that extended nearly to the exit of the vibrissa from the follicle. This core had numerous blind channels extending well into the cortex of the vibrissa, resembling the dentine tubules within teeth. The medulla contained numerous thin-caliber fibers, most of which penetrated into and ended within the channels. This innervation consisted of both NF-positive and NF-negative fibers (Fig. 7K), and the NF-negative fibers could be CGRP positive or negative. These thin-caliber fibers lacked morphological specializations, indicating that they

Fig. 7. Immunolabeling attributes of innervation. **A,B:** Dermal papillae projecting into the epidermis at the RRC level contain C- and Aδ-fiber innervation (CGRP-positive/NF-negative and NF-positive fibers, respectively). Thin-caliber fibers are shown that include NF-positive and CGRP-positive fibers intertwined (A; closely approximate green and red arrowheads, respectively) versus fibers colabeled for PGP and NF (B; yellow arrowhead). Additional fibers in B label only for PGP (green arrowhead). **C:** Circumferential free nerve endings at the ICB level of a U2 FSC reveal mostly fine-caliber fibers (PGP+, green arrowhead) interspersed among Aδ fibers (NF+/PGP+, yellow arrowhead). **D:** Largely uninnervated MCs (CGRP+, red arrowhead) interspersed among MEs (NF+, green arrowhead) at the RS level. **E–G:** Unique endings along the trabeculae of the CS stain positively for BNaC, PGP, S100, NF, and lightly for CGRP (arrows). **H–J:** Novel "tangle" endings also stain positively for BNaC, PGP, S100, and NF and lightly for CGRP (arrowheads). **K:** Presumptive FNEs within the medulla of a U2 follicle hair shaft include mostly fine-caliber fibers (PGP+/NF−, green arrowhead) interspersed among Aδ (NF+/PGP+, yellow arrowhead) fibers. **L:** Meissner's corpuscles (arrowheads) were sparsely distributed at the level of the epidermis. **M:** Pacinian ending found at the base of the epidermis. **N:** An example of vascular supply associated with NF-positive innervation. For abbreviations, see list. Scale bar = 300 μm in A–D; 150 μm in E–K,N; 75 μm in L,M.

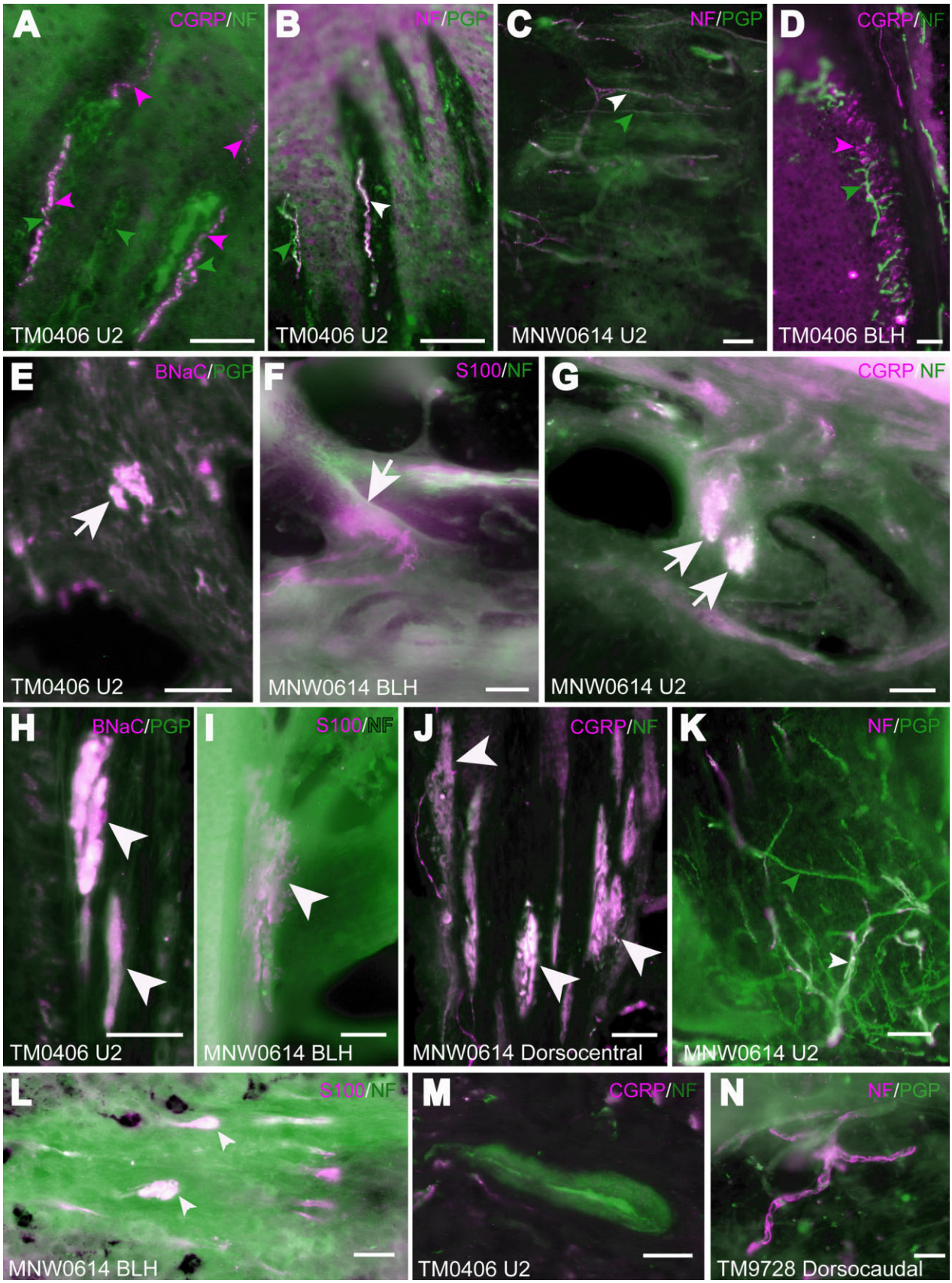
A
CGRP/NF
TM0406 U2
B
NF/PGP
TM0406 U2
C
NF/PGP
MNW0614 U2
D
CGRP/NF
TM0406 BLH
E
BNaC/PGP
TM0406 U2
F
S100/NF
MNW0614 BLH
G
CGRP/NF
MNW0614 U2
H
BNaC/PGP
TM0406 U2
I
S100/NF
MNW0614 BLH
J
CGRP/NF
MNW0614 Dorsocentral
K
NF/PGP
MNW0614 U2
L
S100/NF
MNW0614 BLH
M
CGRP/NF
TM0406 U2
N
NF/PGP
TM9728 Dorsocaudal

Figure 7

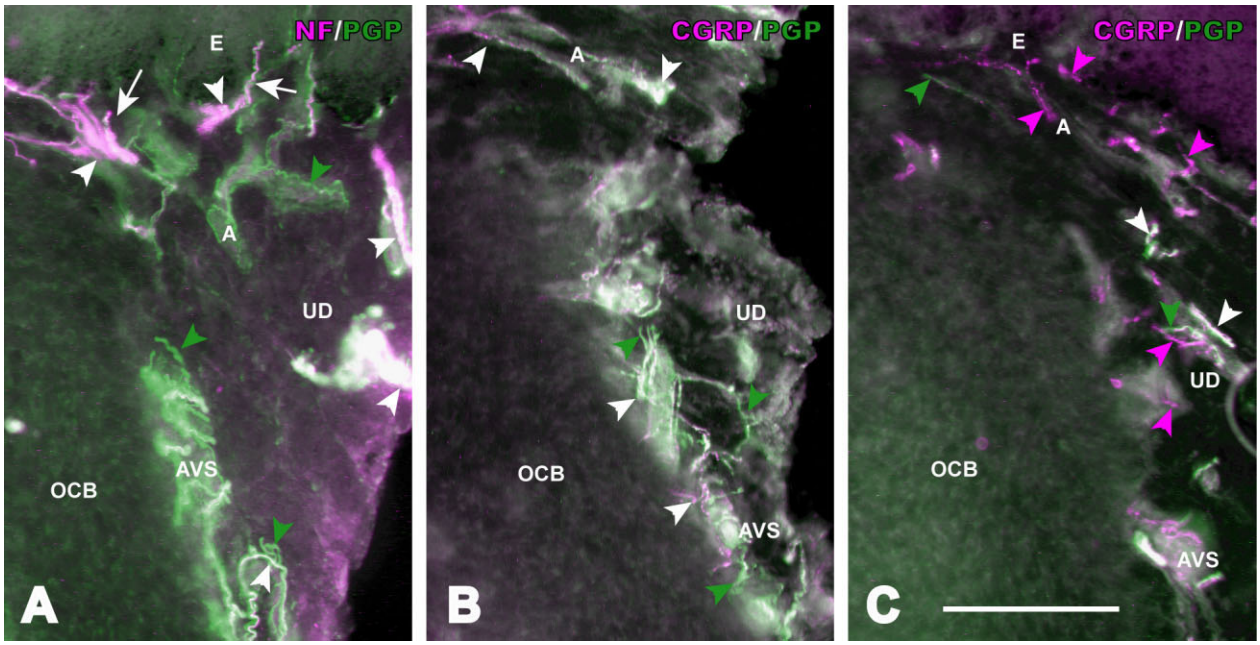

Fig. 8. Extensive innervation associated with the upper dermal vasculature adjacent to the superficial end of FSCs. **A:** A large proportion of axons in the upper dermal nerves (arrows) that supply the epidermis are double labeled with anti-NF and anti-PGP (yellow arrowheads). Small upper dermal arteries and arteriovenous shunts are innervated by a mixture of axons that label with anti-NF and anti-PGP (yellow arrowheads) and only with anti-PGP (green arrowheads). NF-positive axons are presumptive Aδ-fibers, and NF-negative axons are presumptive C-fibers. **B:** The vascular innervation also contains axons that colabel for CGRP and PGP (yellow arrowheads) or PGP alone (green arrowheads). **C:** Immunolabeling for CGRP and NF reveals a contingent of fibers that colabel for CGRP and NF (yellow arrowheads) and others that label only for CGRP (red arrowheads) or only NF (green arrowheads; presumptive Aδ-fibers) alone. For abbreviations, see list. Scale bar = 250 μm in C (applies to A–C).

terminated as free nerve endings. All of the innervation to the dermal papilla of the medulla entered through the base of the follicle independent of the deep vibrissal nerves. The medulla of the hair papilla in other facial vibrissae (e.g., BLH follicles; Fig. 5F) lacked the substantial small-caliber fiber innervation seen in the U2 and L1 vibrissae. Although presumptive FNEs were visible within the CS of postfacial vibrissae, no pronounced innervation was present within the medulla of the hair papilla.

DISCUSSION

Manatee vibrissae: overall comparative structure

The facial and postfacial vibrissae of manatees emanate from encapsulated blood-filled sinus complexes (Reep et al., 2002), making them true vibrissae (Rice et al., 1986). Although the FSCs are large, their relative length in proportion to the length and caliber of the hairs is relatively short in comparison with those of other species (Rice et al., 1986; Reep et al., 1998). The facial hairs are keratinized and unusually rigid, including the region close to the hair papilla. In contrast, rat and cat vibrissae are soft near the hair papilla and the deep half of the CS and gradually become more rigid near the upper end of the CS (Ebara et al., 2002). The CS of both manatees and smaller species has an extensive trabecular network that spans the space between the mesenchymal sheath and the sinus capsule. The neck of the FSC at the level of the OCB and ICB regions is very long and may contribute to the facial vibrissae being rigidly maintained within the FSC. In smaller species it is likely that the deep end of the vibrissa is more flexible, with the smaller neck of the FSC acting as a fulcrum against which the hair shaft can lever within the FSC. Thus the trabeculae of the CS in smaller species is likely to function more in lateral stabilization than for the manatee, in which the hair shaft is rigidly anchored at the base and neck of the FSC.

The ringwulst of manatee vibrissae extends straight out from the mesenchymal sheath rather than hanging down from its point of attachment as in other species. As has been seen in other species, each of the morphological specializations within the FSC appears to be accompanied by a unique set of innervation, suggesting that these complementary anatomical adaptations provide a means of extracting complex data from the environment.

Facial musculature involved in exploratory and prehensile vibrissal behaviors

Previous experiments in the manatee have shown that infraorbital branches of the maxillary nerve innervate the upper bristle pad, whereas the inferior alveolar branch of the mandibular nerve supplies sensory innervation to the vibrissae of the lower pad of the manatee face. The dorsal and ventral buccal branches of the facial nerve also terminate on the superficial facial musculature and are likely to contribute to bristle eversion and feeding behavior movements (Reep et al., 1998). The U2 follicles are supplied specifically by the M. levator nasolabialis muscles

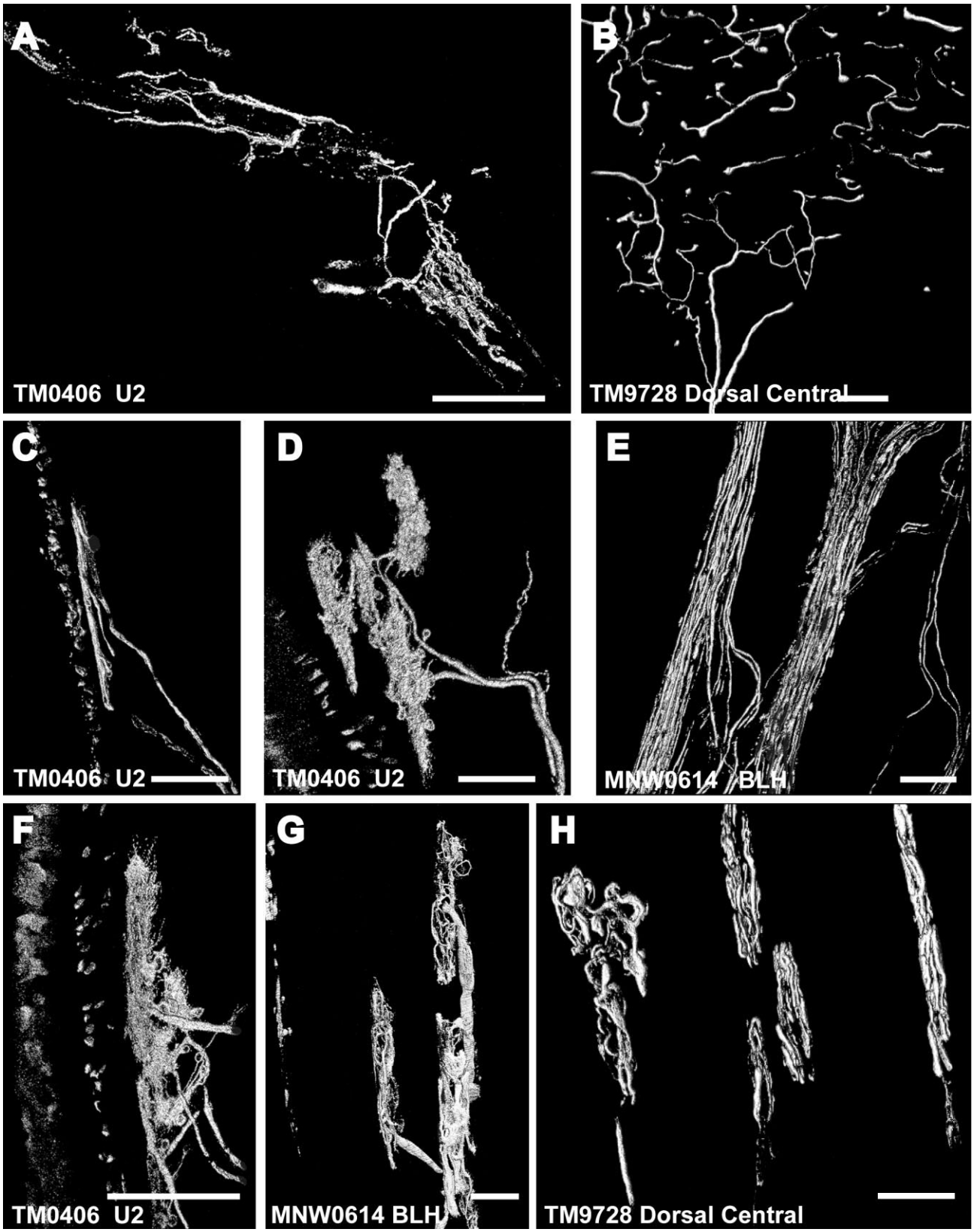

Fig. 9. Confocal surface reconstructions showing the three-dimensional structure of representative FSC innervation and novel mechanoreceptors present in the ICB, RS, and CS regions. **A:** A trabecular ending within the CS (same ending shown in Fig. 4E). **B:** Extensive Merkel ending network in a dorsocentral postfacial FSC shows the completeness of innervation (also shown in Fig. 6F). **C:** The morphology of a lanceolate ending near Merkel cells at the RS level can be compared with the larger, more intricate "tangle" ending (**D**) in the lower ICB/upper RS level of a U2 FSC (also seen in Fig. 3D). **E:** Reconstruction of a DVN penetrating the cavernous sinus and containing multiple axons of different calibers. **F–H:** Examples of tangle endings found in the upper RS/lower ICB level of U2 (F), BLH (G), and dorsocentral postfacial FSCs (H; also shown in Figs. 2–6E). Scale bar = 150 μm in A–H.

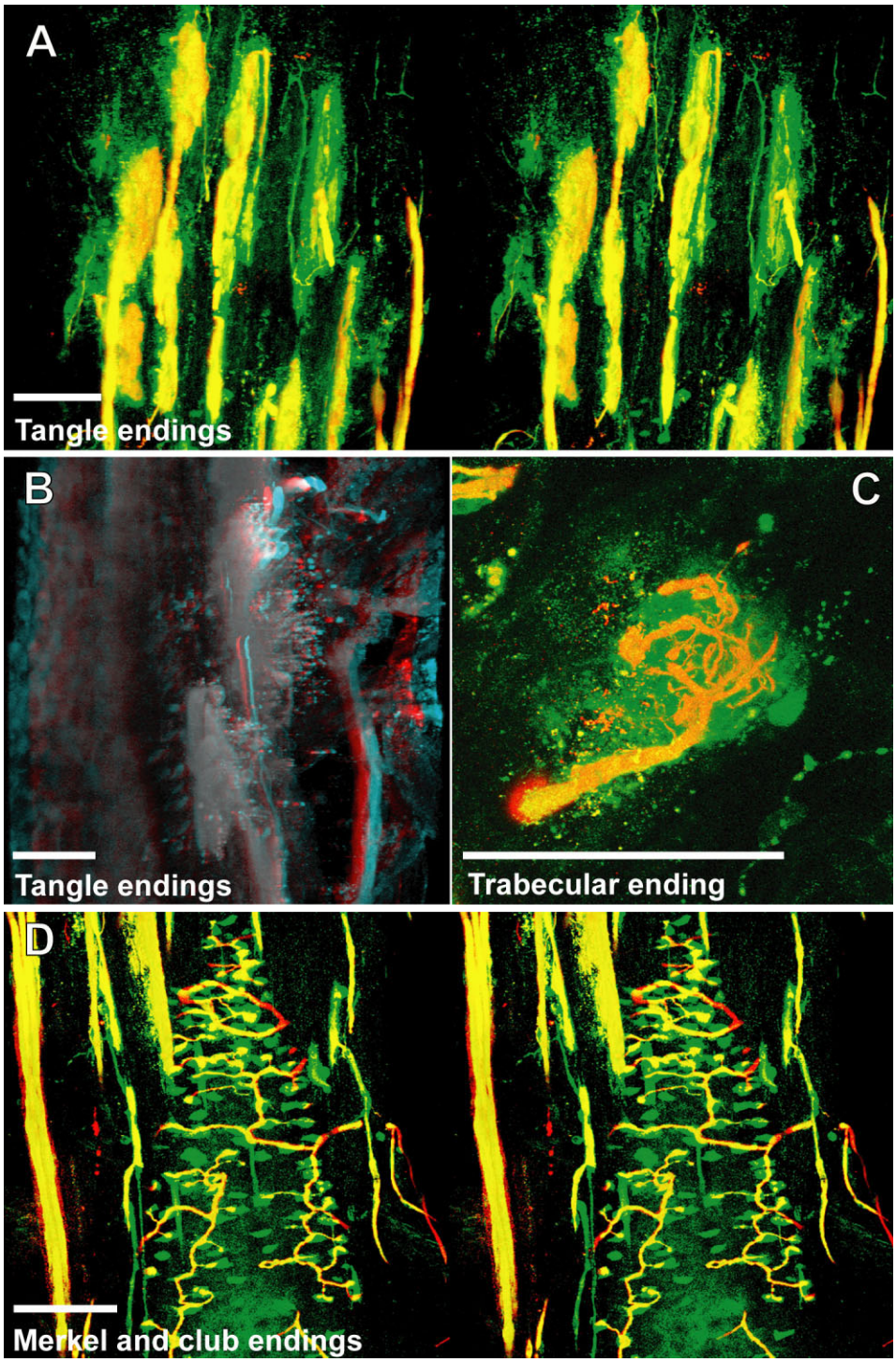

Fig. 10. Confocal three-dimensional images of novel endings stained for neurofilament (NF) and protein gene product 9.5 (PGP). **A:** Stereo pair depicting a group of "tangle" endings. **B:** A three-dimensional image (red/green anaglyph) of two tangle endings with shared innervation. **C:** A single-optical section shows a trabecular ending in detail. Red depicts NF-positive endings within a green PGP-positive cytoplasmic meshwork. **D:** A stereo pair showing Merkel innervation and closely associated club-like endings. Scale bar = 250 μm in A,B; 300 μm in C; 500 μm in D.

(Marshall et al., 1998b), making them homologous to mystacial vibrissae, and although U2 follicles are not moved individually, the left and right U2 fields can act independently from each other (Marshall et al., 1998a). The L1 follicles are supplied by mental branches of the inferior alveolar nerve (Reep et al., 1998) and are protruded by

mentalis muscle contraction (Marshall et al., 1998b), making them homologous to mental vibrissae. At rest, the U2 vibrissae are retracted within skin folds and are everted by volume displacement through contraction of the M. levator nasolabialis and the circular M. buccinatorius muscles during manipulative behaviors (Marshall et al., 1998a,b). When presented with a novel object, manatees generally touch the object with the oral disk (involving the BLH follicles) first in a side-to-side sweeping motion and then grasp the object between the bilateral U2 follicle fields, but the BLH follicles are not actively moved (Marshall et at., 1998a).

Sensory innervation of the rete ridge collar and epidermis

A high density of thin, tapering dermal papillae curve toward the vibrissae at the mouth of the FSC and penetrate throughout an extremely thick epidermis (Fig. 2). In contrast, other species generally lack papillae in nonglabrous skin and exhibit a relatively thin epidermis. Numerous peptidergic and nonpeptidergic C fibers enter the papillae and extend in a straight, unbranched manner far into the overlying epidermis and perpendicular to its surface. Little innervation was present between the papillae, but the papillae were very closely spaced resulting in a high density of innervation to the epidermis. Thin-caliber NF-positive fibers also penetrate most papillae but appear to branch within the papilla without extending into the epidermis. Although our attempts at labeling for MBP were unsuccessful, such thin-caliber NF-positive axons in other species consistently colabel for MBP, indicating that they are likely Aδ fibers. Some of these endings resemble Meissner corpuscles, suggesting that they may be a thin-caliber, low-threshold mechanoreceptor (Light and Perl, 1979). Occasional clusters of Merkel cells and innervation are located at the base of the epidermis between papillae, and these appear to be widely spaced over the epidermis.

Throughout the upper dermis and particularly at the RRC a dense vascular network extends that is well innervated with dense sympathetic innervation and, to a somewhat lesser extent, CGRP-positive sensory innervation. Thin NF-positive innervation was also present as in other species (Fundin et al., 1997a; Rice and Rasmusson, 2000; Cannon et al., 2007). Thick-walled, especially well-innervated locations appeared to be arteriovenous shunts, and there appears to be an extensive network for regulating blood flow to the epidermis potentially as a thermal regulatory mechanism (Figs. 7N, 8). Occasional Pacinian-like corpuscles were also seen much like those present among arterial networks in the glabrous skin of monkeys (Fig. 7M; Paré et al., 2002), but these were located at a surprisingly superficial extent at the base of the epidermis in the manatee, which may be related to the manatees' extensive superficial vascular network.

As seen in other species, innervation accompanies the arteries that penetrate and supply the sinuses at both the deep and superficial end of the FSCs. This suggests that there is a capacity to regulate the relative pressure within the FSC, which may alter mechanical-neural transducing properties. Interestingly, especially dense fine-caliber innervation is located in close proximity surrounding the sinus capsule, particularly at the superficial half. Although not noted previously, this innervation is located to a lesser extent in other species (Rice, unpublished observations). The extensiveness of this innervation in the manatee suggests that the pressure within the FSCs may be an especially important component for tactile sensation within an aquatic environment. Indeed, Dehnhardt et al. (1999) proposed that a more extensive vascular supply and vibrissal sinus system in aquatic mammals may compensate for the high thermal conductivity and specific heat of water. Given the manatee's poor level of thermoregulation and apparent reliance on somatosensation in navigation and foraging, this adaptation could prove to be crucial for proper stimulus detection within the FSCs because the sensitivity of mechanoreceptors has been found to decrease at lower temperatures (Inman and Peruzzi, 1961; Ishiko and Loewenstein, 1961; Necker, 1983; Green et al., 1979; Bolanowski et al., 1988).

Sensory nerve endings of the inner conical body and ring sinus

Merkel endings are thought to be low threshold, slowly adapting mechanoreceptors capable of detecting compression stimuli and directionality (Iggo, 1963, 1966; Iggo and Muir, 1969; Munger et al., 1971; Gottschaldt et al., 1973; Johansson et al., 1982a,b; Johansson and Vallbo, 1983; Rice et al., 1986; Lichtenstein et al., 1990). Given the dense distribution of MEs in the outer root sheath of both facial and postfacial FSCs, it seems that manatee FSCs are heavily invested in detecting directionality of hair deflection (Burgess and Perl, 1973; Rice et al., 1986). A commitment of nerve endings to this task would support our proposal that manatees use tactile hairs to detect hydrodynamic stimuli in a manner analogous to the lateral line system present in fish (Reep et al., 2002). In microchiropteran bats, "touch domes" along the wings are heavily invested with Merkel cells and FNEs that appear to detect air flow and aid in navigation and maneuvering (Zook, 2005, 2007; Zook and Fowler, 1986) in much the same way that manatee postfacial vibrissae might perceive water flow.

Merkel endings in the manatee were found at the level of the RS in both facial and postfacial FSCs as well as in the RRC only in postfacial and BLH FSCs. The presence of Merkel endings at two different levels, both the RRC and RS positions, may indicate that the MEs are involved in extracting different features of a stimulus at these locations (Rice et al., 1997; Ebara et al., 2002). At the RS level, MEs are situated in the external root sheath between the inner root sheath and the basement membrane, a location that makes them susceptible to small-angle deflections of the follicle (Gottschaldt et al., 1973; Rice et al., 1986), whereas MEs of the RRC are in a location that presumably lends itself to detection of large-angle deflections of a vibrissa (Rice et al., 1986). By extension, the postfacial and BLH FSCs of the Florida manatee appear to be specialized for the complete range of deflection intensities, whereas perioral facial FSCs may be more receptive to small-angle hair deflections. Although the significance of most MCs at the RS level of facial vibrissae lacking visible innervation remains uncertain, it is possible that these MCs experience a high turnover rate.

The presence of club-like endings at the attachment site of the ringwulst indicates that this region is sensitive to mechanical perturbations as well. It seems logical that blood in the RS may exert a retarding effect on the movement of the ringwulst relative to the hair shaft, which may in turn exert a force on the club endings (Ebara et al., 2002).

Lanceolate endings are thought to be low-threshold, rapidly adapting stretch receptors that encode dynamic properties of vibrissal deflection such as acceleration and deceleration (Burgess and Perl, 1973; Gottschaldt et al., 1973; Tuckett, 1978; Tuckett et al., 1978; Rice et al., 1986, 1997; Lichtenstein et al., 1990). Although the majority of the longitudinal lanceolate afferents gave rise to a single blade-like termination at the RS level in the U2 facial FSCs, a subset of LLEs exhibited a forked termination or a morphological variation including the studded and hook endings observed. A curved "shepherd's crook" morphology was also observed in LLEs along the mesenchymal sheath at the RS level of the cat and guinea pig (Rice et al., 1986). It is possible that the morphological variations of the LLEs have common inherent physiological properties but may transduce slightly different aspects of mechanosensory perception. The relatively wide spacing and low density of distribution of the LLEs in the mesenchymal sheath of all follicles examined suggests that velocity detection is of lesser importance in both the facial and postfacial FSCs.

The "tangle" endings observed at the lower inner conical body/upper ring sinus level and present in all manatee FSCs examined appear to be novel in that, to the best of our knowledge, sensory endings of this morphology and immunological characterization have not been observed at this level in the FSCs of any other species. Tangle endings consisted of one or more exceptionally large endings abutting the basement membrane and supplied by a single large Aβ fiber. Each ending consisted of thick tangles of NF-positive processes embedded in a matrix of PGP-positive cytoplasm and associated with S100-positive terminal glia. The endings are concentrated in the mesenchymal sheath at the level of the upper ring sinus trabeculae and may be involved in directionality detection associated with deflection of the hair shaft against the upper trabeculae. These endings are also BNaC positive and therefore are likely low-threshold mechanoreceptors.

Merkel cell-neurite complexes and lanceolate endings appear to be responsive to a wide frequency range and may be used to detect sounds when a vibrissa is deflected at the proper frequency (Gottschaldt and Vahle-Hinz, 1981; Hyvärinen, 1989, 1995; Stephens et al., 1973), a capability that would support cortical analysis of the Florida manatee that indicates extensive overlap between auditory and somatosensory areas (Sarko and Reep, 2007). The presence of tangle endings in manatee FSCs may be a means of extending the range of frequency detection. In fact, the primary auditory cortex appears to be occupied exclusively by cluster cortex areas that feature Rindenkerne, or "cortical nuclei" located in layer VI, thought to be analogous to barrels seen in a variety of species and potentially representative of individual vibrissae (Dexler, 1912; Reep et al., 1989; Johnson et al., 1994; Marshall and Reep, 1995; Rice, 1995). Furthermore, a behavioral study that assessed the underwater audiogram of the West Indian manatee found that one manatee adjusted its responses to low-frequency (<0.4 kHz) sounds by pivoting its body roughly 45 degrees and lowering its head—a response not exhibited for higher frequencies (Gerstein and Gerstein, 1999).

This potentially indicates adjustment of perceptual focus from sound to vibrotactile stimuli. Acting as a lateral line system, the postfacial FSCs may be particularly attuned to near-field acoustic effects (involving physical displacement of underwater molecules) caused by such environmental stimuli as the presence of a conspecific. Facial FSCs might be receptive to far-field effects (involving vibration without displacement) in addition to near-field effects due to the greater maximal length and the greater range of lengths of facial follicles compared with postfacial follicles. Although the range of frequency detection is presumably narrow, low-frequency sound waves propagate much greater distances underwater (with sounds traveling over four times faster than in air) and could also facilitate communication between conspecifics.

Additional innervation found at the ICB and OCB levels includes circumferentially oriented peptidergic and nonpeptidergic FNEs. The density of distribution was far less than the well-organized, dense circumferential bundles seen in the ICB of rats and mice, and to a lesser degree in cats. In these other species, this innervation has been hypothesized to detect movement of the entire FSC relative to the skin surface during protraction of the vibrissa and is especially well developed in species that rhythmically whisk their vibrissae such as hamsters, mice, rats, and gerbils (Rice et al., 1986). Such whisking species have Aβ fiber ICB innervation that terminates as en passant circumferentially oriented lanceolate endings that are absent in nonwhisking species (Rice et al., 1986; Mosconi et al., 1993; Ebara et al., 2002). Interestingly, innervation within the manatee ICB was more extensive within U2 versus BLH FSCs (Figs. 2, 3C, 5E) despite their related roles in tactile exploration. Although U2 FSCs contained the most extensive ICB innervation of the FSC regions examined, this innervation was still significantly less dense than that present in other species like the rat and the cat (Ebara et al., 2002). The circumferential network of Aδ and C fibers present in U2 FSCs may be sensitive to mechanical displacements resulting from prehensile grasping and oripulative behavior. Additionally, given the rigidity of the U2 follicle, the ICB region may not require the intricate innervation utilized in whisking behavior. In contrast to the U2 FSCs, the BLH FSCs in the manatee are scanned against the surface of interest and deflected through contact with an object without being actively everted. In this case, the role of the BLH follicle field in finer tactile discrimination may require only a dedication of sympathetic innervation to monitor vascular supply accurately and to optimize the sensitivity of the FSC in an aquatic environment.

Cavernous sinus innervation

The innervation at the level of the cavernous sinus in the manatee differs drastically from that of other species. First, manatees lack the reticular and spiny endings (also referred to as Ruffini endings in some initial studies) that have been consistently seen in the mesenchymal sheath of other species. The distinction between spiny and Ruffini endings has been fairly recent (Rice et al., 1997; Fundin et al., 1997b; Ebara et al., 2002). In other species, spiny endings are generally widespread within the mesenchymal sheath and are embedded among collagen bundles, where they may detect stresses within the sheath parallel to the long axis of the follicle. Reticular endings abut the basement membrane of the follicle and are only located in the upper third of the CS where trabeculae originating from the capsule converge on the mesenchymal sheath. Presumably these detect tension generated perpendicular

to the long axis of the follicle and may be directionally sensitive (Ebara et al., 2002).

Second, manatees possess morphologically unique endings within the trabeculae that may only be present in aquatic species. Relatively small-caliber Aβ fibers terminate as single or multiple trabecular endings that resemble the morphology of Golgi tendon organs. Interestingly, these endings were only observed in the facial FSCs examined, i.e., U2, L1, BLH, and supradisk FSCs. Individual endings consisted of fine-caliber tangles embedded within a terminal glial matrix and were BNaC positive, indicating that they too are very likely to be low-threshold mechanoreceptors. Conceivably they may detect tension generated within the trabeculae themselves and may be responsive to tension induced by deflection of the exceptionally rigid facial vibrissae (Reep et al., 1998). Alternatively, it has been proposed that the trabeculae of the CS may function in attenuating vascular pulsations in the arterial supply entering the base of the FSC, thereby creating more uniform blood flow at the RS level (Melaragno and Montagna, 1953; Rice et al., 1986). Novel endings within the trabeculae may have evolved to provide additional sensitivity in monitoring vascular supply at this level.

Extensive innervation of the hair papilla

The medulla of the hair papilla extends to an extremely superficial extent, well into the neck of the FSC, in U2 and L1 facial vibrissae. Cats also exhibit a superficially extending medulla, but the interface between the medulla and the cortex is smooth (Ebara et al., 2002), whereas in manatees it has a jagged appearance that resembles the dentine tubules in tooth pulp (Byers, 1984; Byers and Näri, 1999). Manatee U2 and L1 vibrissae also have extensive peptidergic and nonpeptidergic C-fiber innervation within the medulla like that of tooth pulp. Although peptidergic and nonpeptidergic innervation has generally been implicated in pain and temperature sensation, this structural-neural relationship in the especially rigid manatee facial vibrissae may be a means of detecting forces transmitted by stress without actual material displacement. Thus this specialized arrangement may also be a sensory adaptation to oripulative behaviors, allowing manatees to assess the force applied to the follicles. The sensory innervation within the medulla may provide feedback in gauging the strain applied to the U2 and L1 follicles and thereby allow manatees to adjust the force applied. This system could theoretically allow manatees to balance the need to maximize the cumulative leverage of each follicle field while also minimizing force overload to individual follicles. In another marine mammal sensory specialist, the narwhal, dentinal tubules within the unusual tusk are thought to function as a hydrodynamic sensor detecting fluid flow, salinity gradients, temperature and pressure (Nweeia et al., 2005).

Marine mammal vibrissae

Vibrissal sensory nerve endings of a limited number of other marine mammals have been examined as well. Bearded seal (*Erignathus barbatus*) FSCs are thought to be extensively innervated active-touch systems adapted to benthic foraging (Marshall et al., 2006). The mystacial FSCs have an extensive upper CS comparable to that of the ringed seal but unlike the facial FSCs of the manatee, in which the upper CS is minimal. A prominent ringwulst is present at the RS level along with LLEs and an extensive ME network. Merkel innervation predominates but was not observed at the RRC level as was observed for the manatee BLH and postfacial FSCs.

Hyvärinen (1995) examined the exceptionally well-innervated mystacial vibrissae of the ringed seal (*Phoca hispida*) by using histology and electron microscopy. The length of the upper CS accounts for 60% of the vibrissa, situating the ring sinus at a low level compared with most mammals. At the RS level, LLEs were found abutting the glassy membrane, whereas MEs were found below the glassy membrane, and a prominent ringwulst was present (Hyvärinen and Katajisto, 1984; Hyvärinen, 1989). All MCs appeared to be innervated and formed a well-developed network (Hyvärinen, 1995). Hyvärinen (1995) also described numerous encapsulated end-organs in the lower CS situated within the trabeculae. Although the techniques used did not reveal the morphology of these trabecular endings, they may be similar to those that we observed in this location in the manatee. "Reticular-like" nerve endings supplied by large-caliber axons have also been described terminating inside the CS trabeculae in the FSCs of the semiaquatic Australian water rat (Dehnhardt et al., 1999). This innervation was also not described in sufficient detail to afford a direct comparison with the trabecular endings observed in manatee facial FSCs, but it may suggest convergent evolution of sensory innervation due to pressures from an aquatic lifestyle.

Through studying a range of species (including opossums, rodents, and pinnipeds) for functional variation and unifying principles of vibrissae, Brecht et al. (1997) found that mystacial macrovibrissae tend to form rows in which effective whisker length increases exponentially in the caudal direction. Each row operates as a functional unit by sampling highly overlapping spatial information perpendicular to the rostrocaudal axis. At the cortical level there also appears to be preferential connectivity between barrels within a row (Simons, 1978; Simons and Woolsey, 1979). Macrovibrissae were proposed to function in spatial orientation associated with distance detection and object location, whereas microvibrissae appeared to be optimized for object recognition (Brecht et al., 1997). By extension, the postfacial vibrissae of the manatee appear to have adopted a function analogous to that of macrovibrissae through optimization for spatial and directional sensitivity, whereas the oral disk and the BLHs in particular serve the microvibrissal role of direct tactile object recognition. Instead of the direct surface contact stimulation that macrovibrissae generally receive, manatee postfacial follicles are exposed to perturbations of the water and consequently undergo passive deflection. In terms of overall behavioral significance, as noted above, postfacial FSCs may also serve a complementary auditory function at low frequencies (Griffin, 1958; Mahler and Hamilton, 1966; Yohro, 1977; Gerstein and Gerstein, 1999; Reep et al., 2002). The perioral vibrissae appear to be more adapted to locating and recognizing food, an important task for a strict herbivore that spends 6–8 hours per day looking for food and that must eat the equivalent of approximately 10% of its body weight per day to compensate for a low metabolic rate (McNab, 1978, 1980).

ACKNOWLEDGMENTS

The authors thank Marilyn Dockum and Maggie Stoll for their excellent technical assistance. We sincerely thank Sea World, Florida and the Department of Environmental Protection Florida Marine Research Institute in St. Petersburg, Florida for providing the samples analyzed in this study as well as the accompanying necropsy information. We are also grateful to an anonymous reviewer, who added several insights that enhanced our analysis. Finally, we thank Dr. Jaime García-Añoveros for the generous gift of the BNaC antibody used here.

LITERATURE CITED

Albrecht PJ, Hines S, Eisenberg E, Pud D, Finlay DR, Connolly MK, Pare M, Davar G, Rice FL. 2006. Pathologic alterations of cutaneous innervation and vasculature in affected limbs from patients with complex regional pain syndrome. Pain 120:244–266.

Bachteler D, Dehnhardt G. 1999. Active touch performance in the Antillean manatee: evidence for a functional differentiation of facial tactile hairs. Zoology 102:61–69.

Bauer GB, Colbert DE, Gaspard JC, Littlefield B, Fellner W. 2003. Underwater visual acuity of Florida manatees. Int J Comp Psychol 16:130–142.

Bolanowski SJ, Gescheider GA, Verillo RT, Chechosky CM. 1988. Four channels mediate the mechanical aspects of touch. J Acoust Soc Am 84:1680–1694.

Brecht M, Preilowski B, Merzenich MM. 1997. Functional architecture of the mystacial vibrissae. Behav Brain Res 84:81–97.

Burgess PR, Perl ER. 1973. Cutaneous mechanoreceptors and nociceptors. In: Iggo A, editor. Handbook of sensory physiology, 2, somatosensory systems. Berlin: Springer-Verlag. p 29–78.

Byers MR. 1984. Dental sensory receptors. Int Rev Neurobiol 25:39–94.

Byers MR, Närhi MV. 1999. Dental injury models: experimental tools for understanding neuroinflammatory interactions and polymodal nociceptor functions. Crit Rev Oral Biol Med 10:4–39.

Cannon KE, Chazot PL, Hann V, Shenton F, Hough LB, Rice FL. 2007. Immunohistochemical localization of histamine H(3) receptors in rodent skin, dorsal root ganglia, superior cervical ganglia, and spinal cord: potential antinociceptive targets. Pain. 129:76–92.

Dehnhardt G, Mauck B, Bleckmann H. 1998. Seal whiskers detect water movements. Nature 394:235–236.

Dehnhardt G, Hyvärinen H, Palviainen A, Klauer G. 1999. Structure and innervation of the vibrissal follicle-sinus complex in the Australian water rat, *Hydromys chrysogaster*. J Comp Neurol 411:550–562.

Dehnhardt G, Mauck B, Hanke W, Bleckmann H. 2001. Hyrdrodynamic trail-following in harbor seals (*Phoca vitulina*). Science 293:102–104.

Dexler H. 1912. Das Hirn von *Halicore dugong*. Erxl Gegenbaurs Morphol Jahrb 45:97–190.

Dykes RW. 1975. Afferent fibers from mystacial vibrissae of cats and seals. J Neurophysiol 38:650–662.

Ebara S, Kumamoto K, Matsuura T, Mazurkiewicz JE, Rice FL. 2002. Similarities and differences in the innervation of mystacial vibrissal follicle-sinus complexes in the rat and cat: a confocal microscopic study. J Comp Neurol 449:103–119.

Fundin BT, Pfaller K, Rice FL. 1997a. Different distributions of the sensory and autonomic innervation among the microvasculature of the rat mystacial pad. J Comp Neurol 389:545–568.

Fundin BT, Silos-Santiago I, Ernfors P, Fagan AM, Aldskogius H, DeChiara TM, Phillips HS, Barbacid M, Yancopoulos GD, Rice FL. 1997b. Differential dependency of cutaneous mechanoreceptors on neurotrophins, trk receptors, and P75 LNGFR. Dev Biol 190:94–116.

García-Añoveros J, Samad TA, Žuvela-Jelaska L, Woolf CJ, Corey DP. 2001. Transport and localization of the DEG/ENaC ion channel BNaC1α to peripheral mechanosensory terminals of dorsal root ganglia neurons. J Neurosci 21:2678–2686.

Gerstein ER, Gerstein L. 1999. The underwater audiogram of the West Indian manatee (*Trichechus manatus*). J Acoust Soc Am 105:3575–3583.

Gerstein ER, Gerstein L, Forsythe S, Blue J. 1999. The underwater audiogram of the West Indian manatee (*Trichechus manatus*). J Acoust Soc Am 105:3575–3583.

Gottschaldt K-M, Iggo A, Young DW. 1973. Functional characteristics of mechanoreceptors in sinus hair follicles of the cat. J Physiol (Lond) 235:287–315.

Gottschaldt K-M, Vahle-Hinz C. 1981. Merkel cell receptors: structure and transducer function. Science 214:183–186.

Green BG, Lederman SJ, Stevens JC. 1979. The effect of skin temperature on the perception of roughness. Sensory Processes 3:327–333.

Griffin DR. 1958. Listening in the dark. New Haven, CT: Yale University Press.

Hyvärinen H. 1989. Diving in darkness: whiskers as sense organs of the ringed seal. J Zool (Lond) 218:663–678.

Hyvärinen H. 1995. Structure and function of the vibrissae of the ringed seal (*Phoca hispada* L). In: Kastelein RA, Thomas JA, Nachtigall PA, editors. Sensory systems of aquatic mammals. Woerden: De Spil Publishers. p 429–445.

Hyvärinen H, Katajisto H. 1984. Functional structure of the vibrissae of the ringed seal (*Phoca hispida* Schr.). Acta Zool Fenn 171:17–30.

Iggo A. 1963. New specific sensory structure in hairy skin. Acta Neuroveg (Wien) 24:175–180.

Iggo A. 1966. Cutaneous receptors with a high sensitivity to mechanical displacement. In: de Reuck AVS, Knight J, editors. Touch, heat and pain. London: Churchill. p 237–256.

Iggo A, Muir AR. 1969. The structure and function of a slowly-adapting touch corpuscle in hairy skin. J Physiol (Lond) 200:763–796.

Inman DR, Peruzzi P. 1961. Effects of temperature on responses of Pacinian corpuscles. J Physiol 155:280–301.

Ishiko N, Loewenstien WR. 1961 Effects of temperature on the generator and action potentials of a sense organ. J Gen Physiol 45:105–124

Johansson RS, Landstrom U, Landstrom R. 1982a. Responses of mechanoreceptive afferent units in the glabrous skin of the human hand to sinusoidal skin displacements. Brain Res 244:17–25.

Johansson RS, Landstrom U, Landstrom R. 1982b. Sensitivity to edges of mechanoreceptive afferent units innervating the glabrous skin of the human hand. Brain Res 244:27–32.

Johansson RS, Vallbo AB. 1983. Tactile sensory coding in the glabrous skin of the human hand. TINS 6:27–32.

Johnson JI. 1990. Comparative development of somatosensory cortex. In: Hones EG, Peters A, editors. Cerebral cortex: comparative structure and evolution of cerebral cortex, vol 8B. New York: Plenum Press. p 335–449.

Johnson JI, Welker W, Reep RL, Switzer RC III. 1986. Dorsal column nuclei of the aquatic herbivorous manatee (*Trichechus manatus*). Soc Neurosci Abstr 12:110.

Johnson JI, Welker W, Reep RL. 1987. The motor nuclei of the cranial nerves in manatees, *Trichechus manatus*. Anat Rec 218:A68–A68.

Johnson JI, Kirsch JA, Reep RL, Switzer RC III. 1994. Phylogeny through brain traits: more characters for the analysis of mammalian evolution. Brain Behav Evol 43:319–47.

Levin MJ, Pfieffer CJ. 2002. Gross and microscopic observations on the lingual structure of the Florida manatee *Trichechus manatus latirostris*. Anat Histol Embryol 31:278–285.

Lichtenstein SH, Carvell GE, Simons DJ. 1990. Responses of rat trigeminal ganglion neurons to movement of the vibrissae in different directions. Somatosens Mot Res 7:47–75.

Light AR, Perl ER. 1979. Spinal termination of functionally identified primary afferent neurons with slowly conducting myelinated fibers. J Comp Neurol 186:133–50.

Ling JK. 1977. Vibrissae of marine mammals. In Harrison JB, editor. Functional anatomy of marine mammals, vol 3. London: Academic Press. p 387–415.

Mackay-Sim A, Duvall D, Graves BM. 1985. The West Indian manatee, *Trichechus manatus*, lacks a vomeronasal organ. Brain Behav Evol 27:186–194.

Mahler P, Hamilton WJ. 1966. Mechanisms of animal behavior. New York: John Wiley & Sons. p 397–425.

Mann DA, Colbert DE, Gaspard JC, Casper BM, Cook ML, Reep RL, Bauer GB. 2005. Temporal resolution of the Florida manatee (*Trichechus manatus latirostris*) auditory system. J Comp Physiol A Neuroethol Sens Neural Behav Physiol 191:903–908.

Marshall CD, Reep RL. 1995. Manatee cerebral cortex: cytoarchitecture of the caudal region in *Trichechus manatus latirostris*. Brain Behav Evol 45:1–18.

Marshall CD, Clark LA, Reep RL. 1998a. The muscular hydrostat of the

Florida manatee (*Trichechus manatus latirostris*): a functional morphological model of perioral bristle use. Mar Mamm Sci 14:290–303.

Marshall CD, Clark LA, Reep RL. 1998b. The muscular hydrostat of the Florida manatee (*Trichechus manatus latirostris*) and its role in the use of perioral bristles. Mar Mamm Sci 14:290–303.

Marshall CD, Maeda H, Iwata M, Furuta M, Asano A, Rosas F, Reep RL. 2003. Orofacial morphology and feeding behaviour of the dugong, Amazonian, West African and Antillean manatees (Mammalia: Sirenia): functional morphology of the muscular-vibrissal complex. J Zool (Lond) 259:1–16.

Marshall CD, Amin H, Kovacs KM, Lydersen C. 2006. Microstructure and innervation of the mystacial vibrissal follicle-sinus complex in bearded seals, *Erignathus barbatus* (Pinnipedia: Phocidae). Anat Rec 288A:13–25.

McNab BK. 1978. Energetics of arboreal folivores: physiological problems and ecological consequences of feeding on an ubiquitous food supply. In: Montgomery GG, editor. The ecology of arboreal folivores. Washington, DC: Smithsonian Institution. p 153–162.

McNab BK. 1980 Food habits, energetics, and the population biology of mammals. Am Nat 116:106–124.

Melaragno HP, Montagna W. 1953. The tactile hair follicles in the mouse. Anat Rec 115:129–149.

Moore BW. 1965. A soluble protein characteristic of the nervous system. Biochem Biophys Res Commun 19:739–744.

Moore BW. 1982. Chemistry and biology of the S-100 protein. Scand J Immunol Suppl 9:53–74.

Mosconi TM, Rice Fl, Song MJ. 1993. Sensory innervation in the inner conical body of the vibrissal follicle-sinus complex of the rat. J Comp Neurol 328:232–251

Munger BL, Publos LM, Publos BH. 1971. The Merkel rete papilla: a slowly adapting sensory receptor in mammalian glabrous skin. Brain Res 29:47–61.

Necker R. 1983. The problem of bimodal receptors: responses to thermal stimuli. In: Horn E, editor. Multimodal convergences in sensory systems. Fortschr Zool, vol 28. Stuttgart: Gustav Fischer Verlag. p 1–16.

Nweeia MT, Eidelman N, Eichmiller FC, Giuseppetti AA, Jung YG, Zhang Y. 2005. Hydrodynamic sensor capabilities and structural resilience of the male narwhal tusk. Soc Mar Mamm Abstr, 209.

Paré M, Elde R, Mazurkiewicz JE, Smith AM, Rice FL. 2001. The Meissner corpuscle revised: a multiafferented mechanoreceptor with nociceptor immunochemical properties. J Neurosci 21:7236–7246.

Paré M, Smith AM, Rice FL. 2002. Distribution and terminal arborizations of cutaneous mechanoreceptors in the glabrous finger pads of the monkey. J Comp Neurol 445:347–359.

Park TJ, Comer C, Carol A, Lu Y, Hong HS, Rice FL. 2003. Somatosensory organization and behavior in naked mole-rats: II. Peripheral structures, innervation, and selective lack of neuropeptides associated with thermoregulation and pain. J Comp Neurol 465:104–120.

Reep RL, Johnson JI, Switzer RC, Welker WI. 1989. Manatee cerebral cortex: cytoarchitecture of the frontal region in *Trichechus manatus latirostris*. Brain Behav Evol 34:365–386.

Reep RL, Marshall CD, Stoll ML, Whitaker DM. 1998. Distribution and innervation of facial bristles and hairs in the Florida manatee (*Trichechus manatus latirostris*). Mar Mamm Sci 14:257–273.

Reep RL, Stoll ML, Marshall CD, Homer BL, Samuelson DA. 2001. Microanatomy of facial vibrissae in the Florida manatee: the basis for specialized sensory function and oripulation. Brain Behav Evol 58:1–14.

Reep RL, Marshall CD, Stoll ML. 2002. Tactile hairs on the postcranial body in Florida manatees: a mammalian lateral line? Brain Behav Evol 59:141–154.

Rice FR. 1995. Comparative aspects of barrel structure and development. In: Jones EG, Peters A, editors. Cerebral cortex: the barrel cortex of rodents. New York: Plenum Press. p 1–75.

Rice FL, Rasmusson DD. 2000. Innervation of the digit on the forepaw of the raccoon. J Comp Neurol 417:467–90.

Rice FL, Fundin BT, Arvidsson J, Aldskogius H, Johansson O. 1997. Comprehensive immunofluorescence and lectin binding analysis of vibrissal follicle sinus complex innervation in the mystacial pad of the rat. J Comp Neurol 385:149–184.

Rice FL, Mance A, Munger BL. 1986. A comparative light microscopic analysis of the sensory innervation of the mystacial pad. I. Innervation of the vibrissal follicle-sinus complexes. J Comp Neurol 252:154–174.

Rosenfeld MG, Mermod J-J, Amara SG, Swanson LW, Sawchenko PE, Rivier J, Vale WW, Evans RM. 1983. Production of a novel neuropeptide encoded by the calcitonin gene via tissue-specific RNA processing. Nature 304:129–135.

Sarko DK, Reep RL. 2007. Somatosensory areas of manatee cerebral cortex: histochemical characterization and functional implications. Brain Behav Evol 69:20–36.

Simons DJ. 1978. Response properties of vibrissa units in the rat SI somatosensory neocortex. J Neurophysiol 41:798–820.

Simons DJ, Woolsey TA. 1979. Functional organization in the mouse barrel cortex. Brain Res 165:327–332.

Stefansson K, Wollmann RL, Moore BW. 1982. Distribution of S-100 protein outside the central nervous system. Brain Res 234:309–317.

Stephens RJ, Beebe IJ, Poulter TC. 1973. Innervation of the vibrissae of the California sea lion, *Zalophus californianus*. Anat Rec 176:421–441.

Tuckett RP. 1978. Response of cutaneous hair and field mechanoreceptors in rat to paired mechanical stimuli. J Neurophysiol 41:150–156.

Tuckett RP, Horsch KW, Burgess PR. 1978. Response of cutaneous fair and field mechanoreceptors in cat to threshold stimuli. J Neurophysiol 41:138–149.

Welker WI, Johnson JI, Reep RL. 1986. Morphology and cytoarchitecture of the brain of Florida manatees (*Trichechus manatus*). Soc Neurosci Abstr 12:110.

Wilkinson KD, Lee K, Deshpande S, Duerksen-Hughes P, Boss JM, Pohl J. 1989. The neuron-specific protein PGP 9.5 is a ubiquitin carboxyl-terminal hydrolase. Science 246:670–673.

Woolsey TA, Welker C, Schwartz RH. 1975. Comparative anatomical studies of the SmI face cortex with special references to the occurrence of "barrels" in layer IV. J Comp Neurol 164:79–94.

Yohro T. 1977. Structure of the sinus hair follicle in the big-clawed shrew, *Sorex unguiculatus*. J Morphol 153:333–354.

Zook JM. 2005. The neuroethology of touch in bats: cutaneous receptors of the wing. Soc Neurosci Abstr 78.21.

Zook JM. 2007. Somatosensory adaptations of flying mammals. In: Kaas JH, Krubitzer L, editors. Evolution of nervous systems, vol 3. New York: Elsevier Press. p 215–226.

Zook JM, Fowler BC. 1986. A specialized mechanoreceptor array of the bat wing. Myotis 23–24.